DOE/ER/41006-14

Nuclear Structure Studies of Exotic Nuclei with Radioactive Ion Beams
A Final Report

Grant Period: September 1, 1996 to August 31, 2015

by

Dr. J. A. Winger

Department of Physics and Astronomy
Mississippi State University
Mississippi State, MS 39762

April 21, 2016

Prepared for

The U.S. Department of Energy
Office of Science
AWARD NO. DE-FG02-96ER41006

Key Words: Nuclear Structure, β-Decay Spectroscopy, Radioactive Ion Beams, Evolution of Nuclear Structure, Nuclear Astrophysics, Nuclear Data

Research Summary

β-decay spectroscopy provides important information on nuclear structure and properties needed to understand topics as widely varied as fundamental nuclear astrophysics to applied nuclear reactor design. However, there are significant limitations of our knowledge due to an inability to experimentally measure everything. Therefore, it is often necessary to rely on theoretical calculations which need to be vetted with experimental results. The focus of this report will be results from experimental research performed by the Principal Investigator (PI) and his research group at Mississippi State University in which the group played the lead role in proposing, implementing, performing and analyzing the experiment. This research was carried out at both the National Superconduction Cyclotron Laboratory (NSCL) at Michigan State University and the Holifield Radioactive Ion Beam Facility (HRIBF) at Oak Ridge National Laboratory. The primary emphasis of the research was the use of β-decay spectroscopy as a tool to understand the evolution of nuclear structure in neutron-rich nuclei which could then be applied to improve theory and to increase the overall knowledge of nuclear structure.

Table of Contents

Abstract **i**

Table of Contents **i**

List of Figures **vi**

List of Tables **vii**

1 Summary **1**

2 Introduction **3**

3 Experimental Methods **11**
3.1 NSCL Experiments 11
3.2 HRIBF Experiments 13

4 Results **17**
4.1 NSCL Experiments 17
4.1.1 Low-energy structure of ^{40}S through ^{40}P β decay 17
4.1.2 The β decay of ^{40,42}S and ^{43}Cl 20
4.1.3 Other NSCL β decay results 24
4.2 HRIBF Experiments 39
4.2.1 Large β-delayed neutron emission probabilities in the ^{78}Ni region 39
4.2.2 Evidence for a sub-shell closure at $N=58$ beyond ^{78}Ni 43
4.2.3 β decay of the $\pi f_{5/2}$ ground state of ^{77}Cu 48
4.2.4 β-decay study of the transitional nucleus ^{75}Cu and the structure of ^{75}Zn . . . 60
4.2.5 Research in Progress: The $A=74$ β-decay Chain 77
4.3 ADN Systematics 83

Bibliography **87**

Appendix A Acronyms **97**

List of Figures

2.1 Section of the Chart of Nuclides for neutron-rich nuclei between O and Ca. Highlighted in the figure are the two areas of deformation near ^{32}Mg and ^{44}S. Also indicated in the figure are the nuclei for which β-decay data were obtained at the NSCL. 4

2.2 Section of the Chart of Nuclides in the region near ^{78}Ni showing the limits of nuclear structure information available at the start of the research project as taken from Ref. [NNDC]. In many cases for the most neutron rich members of an isotonic chain only very limited information was know about excited states. This was especially true for those where only the isomeric state decay was known. 5

2.3 Plot of the migration of single-particle states in the proton *fp* shell due to the tensor interaction with neutrons in the $\nu g_{9/2}$ orbital as described by Otsuka *et al.*[Ots05] Indicated in the plot are possible proton shell closures. 6

2.4 Systematics of the odd-A $N=51$ isotones showing the steady drop in the $\nu s_{1/2}$ state relative to the $\nu d_{5/2}$ state. The dashed lines indicate the average of the shell-model predictions presented by Thomas *et al.*,[Tho07] indicating the failure of the current interaction to predict the continued drop in the energy of the first excited state. . . . 7

2.5 Portion of the chart of nuclides showing predicted paths for the *r-process* for three values of the neutron flux (n_n in $neutrons/cm^3$). Indicated in the plot are the waiting-point nuclei that will decay back to stability at freeze out for different values of n_n and therefore dictate the *r-process* path. Also indicated are the most neutron-rich member of each isotopic chain for which the half-life had been reported prior to research associated with this grant. Adapted from Ref. [Kra06]. 9

3.1 Particle identification (PID) plots (energy loss in Si PIN diode versus time of flight) for the A1200 set to center ^{42}S on the focal plane. Taken from [Win06] 12

3.2 Technical drawings showing the layout of the NSCL target wheel setup. On the left shows the target wheel with the β detector centered behind the implantation target. On the right is an overhead view of the system indicating the placement of the two HPGe detectors 13

3.3 Schematic layout of the HRIBF. See text for details. 14

3.4 Examples from the initial RO experiment. Figure on left shows the effect of increasing gas pressure in the ion chamber to "range out" ^{76}Ga and ^{76}Ge leaving a pure ^{76}Cu beam. Although the γ ray from ^{76}Ga is observed in both cases, at the higher pressure it comes only from the decay chain starting with ^{76}Cu. Figure on the right shows use of the ion chamber as an ion implantation tag. In this case, selection of γ rays in coincidence with the ion chamber events in a defined "gate" enhances the γ rays from this decay relative to all γ rays detected. This is apparent in the γ ray spectrum where red spectrum utilizes the gate while the balck spectrum is from all events but limiting the statistics to match that of the gated spectrum. 15
3.5 Pictures of the RO (left) and LeRIBSS (right) detector setups. 16

4.1 β-gated γ-ray singles spectrum with the A1200 set to maximize the transmitted intensity of ^{40}P. γ rays assigned to the decay of ^{40}P are labeled with their energy in keV. Single escape peaks and double escape peaks are labeled with the energy of the original γ ray followed by SEP or DEP, respectively. Three lines associated with the β-delayed neutron branch to states in ^{39}S are indicated by β-n. All other lines are labeled according to their source. 18
4.2 a) Half-life curve for the decay of the 903-keV γ ray associated with ^{40}P β decay. In the figure, circles represent data form a short timing cycle and squares a long timing cycle, where closed(open) symbols represent the time spectrum projected by gating on the γ-ray peak(background). A best fit to each data set is shown as solid lines. b) Level scheme for ^{40}S. The width of the lines is proportional to the relative intensity of the γ ray. 19
4.3 a) Decay scheme for ^{40}S. b) Half-life curve for ^{42}S. c) Half-life curve for ^{43}Cl d) Decay scheme for ^{42}S. e) Decay scheme for ^{43}Cl. 21
4.4 Half-life curves for ^{39,41}P, ^{41,43}S, and ^{44,45}Cl. 25
4.5 a) Particle identification (PID) plot for two A1200 settings. b) γ-ray spectrum for ^{39}P β decay showing the effect of a strong contaminant in the spectrum (^{42}Cl). c) γ-ray spectrum for an A1200 setting which yields nearly pure ^{41}S. The main spectrum was obtained with the wheel cycle optimize ^{41}S relative to its daughter ^{41}Cl. The inset shows a comparison of the two primary γ rays in a saturation spectrum. d) γ-ray spectrum from ^{44}Cl β decayutilizing an A1200 tune and a time cycle where it is enhanced relative to other beam components as well as its daughter. 26
4.6 Preliminary decay schemes for a) ^{39}P and b) ^{41}P. The half-lives were measured in this experiment (Fig. 4.4), as well as the $P_{\beta n}$value. 28
4.7 Preliminary decay scheme for ^{41}S. The designated spins and parities are based on a deep-inelastic collision measurement which populated the yrast states.[Oll03] Closed circles indicae definite coincidences while open circles indicate possible coincidences. 29
4.8 Preliminary decay scheme for ^{41}Cl. Spin and parity assignments come from the NNDC.[NNDC] Closed circles indicae definite coincidences while open circles indicate possible coincidences. 30
4.9 a) Preliminary decay schemes for ^{43}S. Spin and parity assignments come from the NNDC.[NNDC] Closed circles indicae definite coincidences while open circles indicate possible coincidences. The half-life was measured in this experiment (Fig. 4.4. b) $\gamma\gamma$-coincidence spectrum gated on the 329-keV γ ray. c) $\gamma\gamma$-coincidence spectrum gated on the 5786-keV γ ray. 31

4.10 Preliminary decay schemes for a) ^{44}Cl and b) ^{45}Cl. Closed circles indicae definite coincidences while open circles indicate possible coincidences. Spin and parity assignments are based on the current measurement along with comparison to other experiments[NNDC] as discussed in the text. The half-life and $P_{\beta n}$ values were measured in this experiment (Fig. 4.4). The Q_β value comes from the NNDC.[NNDC] 33
4.11 a) Half-life curve for ^{33}Al taken from the β detector. b) Half-life curve for ^{34}Al taken from the β detector. c) γ-ray spectrum for ^{33}Al β decay. 37
4.12 The γ-ray spectra recorded for the βn precursors ^{76}Cu (a), ^{77}Cu (b) and ^{78}Cu (c) and showing the decays of respective Zn isotopes used to determine the $P_{\beta n}$ values. For ^{76,77}Cu the γ-ray singles spectra taken in saturation mode are shown. For ^{78}Cu a β-gated spectrum taken using a 5.2 s MTC cycle is shown. For ^{76}Cu, the corresponding particle identification plot for the mass 76 isobars in the RO mode is shown in (d). Zinc ions are removed by the charge exchange cell while the higher-Z components of the beam (^{76}Ga and ^{76}Ge) are stopped by the ion chamber resulting in a pure ^{76}Cu beam. The partial decay scheme for ^{77}Cu indicating the significance of the 772-keV isomer in ^{77}Zn to the $P_{\beta n}$ value analysis is shown in (e). The number in parenthesis following the γ-ray energy is the measured absolute γ-ray intensity from comparison of the γ-ray peak areas to the number of implanted ^{77}Cu ions. 40
4.13 The probability of β-delayed neutron emission as a function of the energy window for this decay mode. Results of this experiment (▲) are compared to those listed in Refs. [Pfe02] (■) and to our new theoretical estimates ($\diamond$), see text. 42
4.14 Proposed decay schemes for ^{83}Ga, ^{84}Ga and ^{85}Ga (inset). The intensity for each γ ray relative to the strongest γ ray from that decay is given in square brackets. The absolute β feedings for the ^{83,84}Ga decays are based on the measured absolute branching ratio for the 1348-keV γ ray (^{83}Ga) of 28.4(10)% and the 247-keV γ ray (^{84}Ga) of 8.6(8)%, respectively. The upper limits for the ground-state β-decay feedings reflect potentially unobserved γ-ray transitions. 43
4.15 β-gated γ ray spectrum obtained with a 2.5 second MTC cycle for the $A=83$ data set (a), within 300 ms of a ^{84}Ga ion implantation (b), and within 190 ms of a ^{85}Ga ion implantation (c). ^{84}Ga ion-$\beta\gamma\gamma$ spectra gated on the 624 (d), 765 (e), and 798-keV (f) γ rays. γ rays are identified by their energy in keV or source of origin. 44
4.16 a) Systematics of the proposed $\nu 3s_{1/2}$ first excited state, the second excited state, and the $\nu 1g_{7/2}$ state relative to the $\nu 2d_{5/2}$ state for the $N=51$ isotones. The dotted and dot-dashed lines shows the theoretical predictions for the energy difference between the $\nu 2d_{5/2}$ and $\nu 3s_{1/2}$ and $\nu g_{7/2}$ single-particle states, respectively. b) Systematics of the 2_1^+ energy in the $N = 48$, 50, and 52 isotones between $Z = 28$ and 50. c) Theoretical predictions for the dependence of neutron single particle energies on proton number for the $N=50$ isotones. Also indicated are the predicted shell and sub-shell closures. 45
4.17 Saturation spectrum in coincidence with the β detectors obtained in the LeRIBSS data run with a purified ^{77}Cu beam. The γ-ray peaks assigned to ^{77}Cu are indicated by their energy with single and double escape peaks marked as SEP and DEP, respectively. Other members of the two decay chains are indicated by symbols: ^{77}Zn($\diamond$), ^{76}Zn(•), ^{77}Ga($\triangle$), ^{76}Ga(∇), and ^{77}Ge(#). 49

4.18 Portion of the γ-ray singles saturation spectrum from the LeRIBSS data run showing the presence of the 772-keV γ ray from de-excitation of ^{77}Zn^m. Also labeled in the figure are lines from the β decay of ^{228}Ac(*) in the background and the 957-keV line from ^{77}Cu β decay. 50
4.19 Proposed decay scheme for ^{77}Cu to excited states in ^{76,77}Zn. The relative intensities of the γ rays to the 505-keV transition are indicated in square brackets. Closed circles indicate $\gamma - \gamma$ coincidences seen both ways, while open circles indicate a coincidence observed only from the upper transition. Transitions and levels without strong coincidence relationships and/or other linking transitions are indicated by dashed lines. The level feedings are based on the measured absolute branching ratio for the 505-keV transition (19.1(6)%) as described in the text. All energies are in keV unless otherwise noted. 52
4.20 The β detection efficiency (β_{eff}) as a function of the effective Q value (Q_{eff}) for the LeRIBSS measurement. The solid line is from a fit to the data while the dashed lines show the $\pm 2\sigma$ limits. 53
4.21 β-gated γ-ray coincidence spectra for gates on the 114-, 505-, 957-, and 1277-keV transitions. 54
4.22 Half-life curves for the γ rays depopulating the 114- and 1277-keV levels. The data were fit in both the growth and decay portions of the curve, to optimize statistics, using a non-linear least squares fit routine. Data between 1 and 3 seconds has little effect on the fitted values, therefore the initial grow-in and decay portions determine the half-life. 55
4.23 Subset of the decay schemes of ^{77}Cu and it's daughter activities showing, in bold, the directly measured absolute branching ratios per ^{77}Cu decay. The intensities of the five γ rays were determined solely in the current experiments while $P_{\beta n}$and $P_{\beta}$for ^{77}Zn^g incorporate additional information as discussed in the text. Also shown is the β decay probability for ^{77}Zn^m as derived from the other values. Energies shown, in keV, are not to scale while the widths of the γ-ray transitions are to scale. 56
4.24 Low-energy level systematics of odd-A copper isotopes. (See text for references.) . . 60
4.25 Low-energy level systematics of odd-A Z=30 zinc (lower panel) and Z=32 germanium (upper panel) isotopes. Levels in germanium are taken from [NNDC], those in zinc from [Huh98], [Lin63], and [Ehr67]. For discussion, see text. 61
4.26 Low-energy level systematics of odd-A $N = 45$ isotones. Levels are taken from [NNDC]. For discussion, see text. 63
4.27 Saturation spectrum obtained in the LeRIBSS data run with a purified ^{75}Cu beam. The γ-ray peak, assigned to ^{75}Cu are indicated by their energy with single and double escape peaks marked as sep and dep, respectively. Other members of the two decay chains are indicated by symbols: ^{75}Zn(•), ^{75}Ga(△), ^{74}Ga(▽) 64
4.28 Part I of the proposed decay scheme for ^{75}Cu to excited states in ^{75}Zn showing low energy transitions. The relative intensities of the γ rays to the 421-keV transition are indicated in the figure. Filled circles indicate γ-γ coincidences seen both ways, whereas open circles indicate coincidences observed only from the upper transition. Transitions and levels without strong coincidence relationships and/or other linking transitions are indicated by dashed lines. The level feedings are based on an estimated absolute branching ratio of 19(4)% for the 421-keV transition, see text for details. Absolute β-decay feedings and log(ft) values are specified for some levels. The log(ft) values were calculated using mass values from Refs. [Rah07] and [Bar08]. 65

4.29 Part II of the proposed decay scheme for ^{75}Cu to excited states in ^{75}Zn showing high energy transitions. The relative intensities of the γ rays to the 421-keV transition are indicated in the figure. Filled circles indicate γ-γ coincidences seen both ways, whereas open circles indicate coincidences observed only from the upper transition. Transitions and levels without strong coincidence relationships and/or other linking transitions are indicated by dashed lines. 66
4.30 Half-life curves for γ rays depopulating the 193-, 421-, 476-, and 724-keV levels. Data were fit in both the growth and the decay portions of the curve, to optimize statistics, using a nonlinear least-squares fit routine. The average half-life value was determined from the half-live values for the 109-, 193-, 268-, 345-, 421-, 476-, 724-, and 799-keV transitions. 67
4.31 γ-ray spectra coincidence with the 109-, 193-, 268-, 345-, 421-, 476-, 724-, 799-, and 1760-keV transitions. 69
4.32 Portions of the γ-ray coincidence spectra for the 109-, 268+421+668+724+799-, 3845-, and 4785-keV transitions. 70
4.33 Different scenarios of β decay of ^{75}Cu to levels in ^{75}Zn used to determine the limits for the absolute branching ratio of the 421-keV γ ray transition. The sum relative γ-ray intensities (the actual value of 353 was normalized to 100%) to corresponding levels are represented by white arrows and absolute β intensities are shown traditionally on the left next to energy levels. (See text for details.) 71
4.34 Subset of the decay schemes of ^{75}Cu and its daughter activities used to estimate the $P_{\beta n}$value. The intensities shown are relative to the 421-keV transition. 73
4.35 Low-energy level systematics of odd-A Z=30 zinc isotopes including the lowest $1/2^-$ and $9/2^+$ states in ^{75}Zn. Energy levels in zinc are taken from [Huh98], [Lin63], [Ehr67], and the present work. For discussion, see text. 76
4.36 Preliminary decay scheme for ^{74}Cu. The half-life, Q_β, and spin/parity assignments are taken from the NNDC.[NNDC] Closed dots indicate firm coincidence relationships while open dots indicate a possible coincidence. The dashed levels indicate cases here a level is placed based on a single γ ray. New levels and γ rays are indicated by a *, with the γ rays also being color coded. 78
4.37 Preliminary decay scheme for ^{74}Zn. The half-life and Q_β are taken from the NNDC.[NNDC] The spin/parity assignments for he first three levels come from the NNDC while the designated (1^+) states are based on the current analysis. Closed dots indicate firm coincidence relationships while open dots indicate a possible coincidence. The dashed levels indicate cases here a level is placed based on a single de-exciting γ ray. New levels and γ rays are indicated by a *, with the γ rays also being color coded. 79
4.38 Preliminary decay scheme for ^{74}Ga. The half-life, Q_β, and spin/parity assignments are taken from the NNDC.[NNDC] Closed dots indicate firm coincidence relationships while open dots indicate a possible coincidence. The dashed levels and transitions are for cases which are still to be confirmed. 80
4.39 The a_1 fit parameter for the near-core (solid data) and the inflated-core (open data). The solid and dashed lines represent linear fits which are included to help guide the eye. The empty horizontal bars represent direct BE(Core+$1n_e$)-BE(Core) values, to confirm the a_1 behaviors were being properly identified. 85

List of Tables

4.1 Measured β-delayed neutron emission probabilities. Mode indicates whether the ranging-out (RO) or pass-through (PT) mode of operation was used. MTC indicates the MTC cycle beam time on or if a saturation (Sat) spectrum was being taken. Rel indicates values obtained by comparison of the relative intensities of the most intense γ rays from nuclides in β and βn branches. Abs indicates values obtained by comparison of absolute intensities of the most intense γ rays from nuclei in the βn branch to the number of ions deposited. 41

1

Summary

The study of nuclei far from stability provides information on the variation of nuclear structure and properties in cases of extreme proton and neutron numbers. In turn, both nuclear structure and nuclear properties dictate the paths followed by the explosive nucleosynthesis events (e.g., the *r-process* and the *rp-process*), as well as the control and cooling of a nuclear reactor. The need for more experimental information is very apparent on the neutron-rich side of stability where above $Z = 20$ there is still an abundance of nuclei which have yet to be studied. Unfortunately, many of these nuclei remain beyond the reach of current facilities. Consequently, theoretical models will remain a very important aspect in the study of extremely neutron-rich nuclei. These models need to be firmly vetted by comparison to experimental data closer to stability. The research presented here builds a more complete knowledge of nuclear structure by studying a small set of nuclei where we believe a complete picture of the β decay can be obtained.

For many decades β-decay spectroscopy has followed a similar pattern. An interest in a particular region of nuclei or set of isotopes led to new techniques in production or separation which resulted in a rapid increase in knowledge. In many cases this involved global surveys which sought to glean as much knowledge as quickly as possible, and involved pushing as far from stability as the technique allowed. However, these studies were often incomplete, providing only a cursory glimpse at the total β-decay picture. Consequently, initial studies can provide some baseline information on nuclei while more details measurements are needed to obtain a complete picture. Although no subset of nuclei can provide a true global picture for all nuclei, a study whose goal is to obtain the most complete picture of a particular group of nuclei may inform toward a more general picture of many nuclei. The research presented here is a combination of exploratory searches and detailed studies. The regions of interest have evolved over the years based on the availability of various radioactive nuclei for study.

The research carried out through this grant has evolved over time as different facilities have become available. Initially, the research was focussed at the NSCL where a concerted effort was put in to establish a β-decay spectroscopy program using the A1200 fragment separator to provide "clean" beams of β-decay parents. A setup designed at MSU was used for these studies. Three experiments were performed with mixed results. When the NSCL shut down to begin upgrades to the coupled cyclotron facility, the focus of the research shifted to the HRIBF. During this period the PI became more involved with UNIRIB. Most of the initial HRIBF research concerned studies of proton-rich nuclei, specifically proton-emitting nuclei. The PI was interested in this research, but was seeking opportunities to establish β-decay spectroscopy research at the HRIBF. This eventually became possible with the development of neutron-rich fission fragment beams. This resulted in a large number of experiments first using accelerated beams, but eventually evolving into research

with slow beams using LeRIBSS. With closure of the HRIBF, research was starting to shift to other facilities. However, the PI has been able to continue assisting on research at ORNL. Specifically in pushing for completion and implementation of ORISS at the NSCL, and working on several MTAS measurements.

Presented in the following chapters are descriptions of the experiments in which the MSU group provided the primary effort. Experimental techniques in general terms will be discussed while detailed results from the research will be given. In addition to the β-decay studies presented in this report, the MSU group was also involved as collaborators with other researchers in a large number of experiments where the MSU group worked in a secondary role. These experiments include studies of super-deformed nuclei and proton emitting nuclei, as well as other β-decay experiments.

In conclusion, the total production from this grant over its entire lifetime has been good. Members of the group have been involved in numerous experiment proposals which have lead to participation in 43 separate experiments, most notable 7 at the NSCL and 29 at the HRIBF. These experiments have lead to 48 refereed publications, 38 conference proceedings, and 33 presentations at conferences or workshops. Seven MSU graduate students have been involved in the research. One completed research for a masters degree, but failed to complete a thesis. A second student worked on the project for a few years, but competed a degree with another MSU faculty member due to delays in getting his experiment scheduled at the HRIBF. Two students completed masters degrees, one on NSCL research and one on HRIBF research. The later student continued on to complete a doctoral degree with two publications as a first author. There were three graduate students working on the project when it ended. Each will use a portion of this research for their Ph.D. dissertation.

2

Introduction

The study of exotic nuclei is driven by our desire to better understand nuclear structure and interactions in situations quite different from those near to stability. Indeed, many unique aspects of the nuclear force can only be studied with exotic nuclei. Although the properties of nuclei near stability can be extrapolated to nuclei near the particle drip lines, it has been found that the general trends expected are not always followed, requiring new aspects of the nuclear force to be considered.

A good example is the importance of the neutron-proton interaction in determining the structure of heavy ($A > 60$) $N = Z$ nuclei where the enhanced n-p interaction strength leads to deformation.[Lis90, Mah92] It is also possible to observe nuclei with very loosely bound valence nucleons such as in the case of ^{11}Li in which the pairing force between the last two neutrons forms a diffuse halo about a tightly bound ^{9}Li core.[Mue93] Similar effects may lead to nuclei with either proton or neutron skins where an extreme difference in the number of neutrons and protons leads to a surface layer containing only one type of nucleon.[Tan92] Furthermore, the proton-neutron interaction across major shells as well as interactions with continuum states for very neutron-rich nuclei leads to the migration of the single particle states in the ^{78}Ni region.[Ots05, Dob07] Shell and sub-shell closures are seen to appear and disappear as neutrons are added.[Jan07] For the light neutron-rich nuclei, it has been found that the neutron drip-line may extend further than suggested by most theoretical calculations [Bau07]. All of this points to the fact that we have an incomplete understanding of nuclear structure for nuclei far from stability. Better experimental data along with more precise theoretical models will be needed to gain a better picture of these exotic nuclei. Although there are many aspects of nuclear structure as well as regions to study, the research performed under this grant studied specific nuclei to help fill gaps in our knowledge of the evolution of nuclear structure. This project fits into the Department of Energy's Office of Science Strategic Plan to "(5.2) Understand the structure of nucleonic matter." The need for quality nuclear structure data to understand the evolution of nuclear structure is very evident when looking in detail at certain regions of the Chart of Nuclides.

A major question in nuclear structure physics is whether the magic numbers which appear to hold near stability remain as the drip lines are approached.[War04] Fig. 2.1 on the following page shows a portion of the Chart of the Nuclides for the proton-sd/neutron-fp region. Nuclei in the proton sd shell between the $N = 20$ and 28 shell closures (i.e., the $\nu f_{7/2}$ subshell) have been of interest to this question due to the observation of regions of deformation near the singly magic nuclei ^{32}Mg and ^{44}S. Deformation near ^{32}Mg appears to arise due to an "island of inversion" where the $2\hbar\omega$ states lie below the $0\hbar\omega$ states. A similar effect is understood to occur near ^{44}S. Both ^{32}Mg and ^{44}S indicate a break down in a magic shell, $N = 20$ and 28, respectively. The observed structure in this region depends strongly on the filling of both the proton and neutron orbitals,

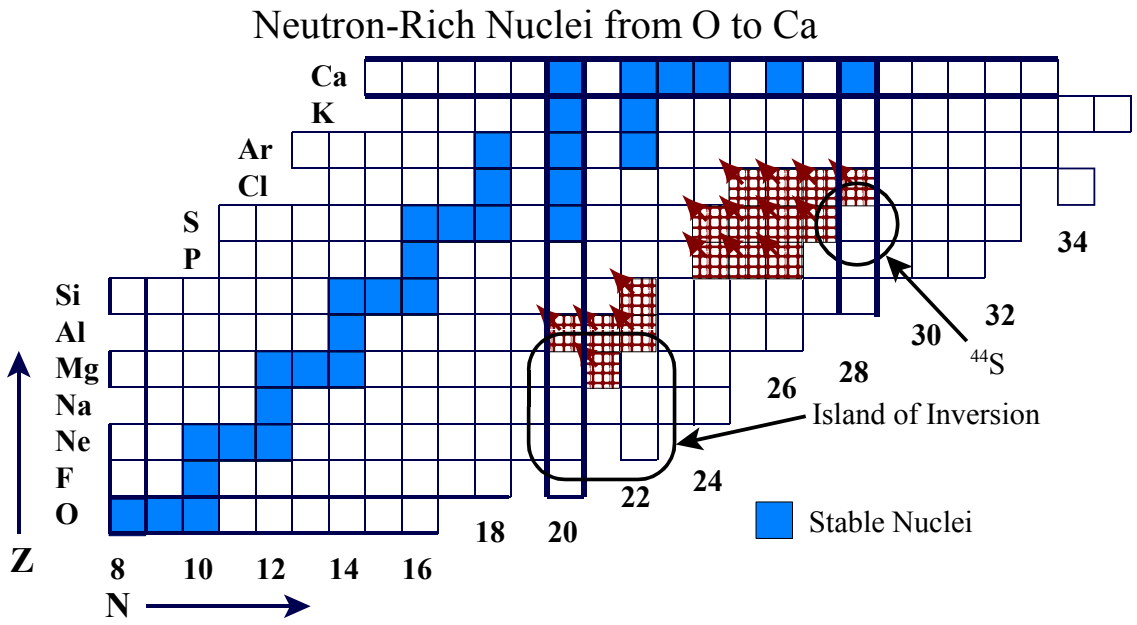

Figure 2.1: Section of the Chart of Nuclides for neutron-rich nuclei between O and Ca. Highlighted in the figure are the two areas of deformation near ^{32}Mg and ^{44}S. Also indicated in the figure are the nuclei for which β-decay data were obtained at the NSCL.

how their relative energies change as one moves away from stability, and the effects of deformation. To properly understand these effects requires knowledge of nuclear structure as it varies across the full $\nu f_{7/2}$ subshell.

A significant focus of the research presented here was on the region near doubly magic ^{78}Ni which is shown in Fig. 2.2 on the next page. The figure indicates the level of knowledge of each nuclide at about the time work on this gant began. Beyond just having basic information, many of the results were contradictory. For example, there is significant information missing about the decays of the Copper and Zinc isotopes just below $N = 50$. The decays of $^{76-78}$Cu may or may not involve isomers.[Win90, Van05] Above $N = 50$ the uncertainties increase due to a lack of solid information on absolute β decay branching ratios. A good example is ^{83}Ga for which the previously reported "evaluated" $P_{\beta n}$ value of $37 \pm 17\%$ [NNDC] was an average of the disparate experimental values of $54 \pm 7\%$,[War86] $43 \pm 7\%$,[Lun80] and $14.9 \pm 1.8\%$.[Rud93] These and other uncertainties in the reported values pointed to the need for information not only on the more exotic nuclei for which no experimental information is available, but also a need to confirm many of the β-decay properties for nuclei closer to stability. This was a primary goal of this research.

In the last two decades there has been a renewed interest in the region of nuclei near the doubly magic ^{78}Ni as advances in beam production and purification techniques have made this region more accessible to experimental studies. The extreme neutron excess in this region makes it interesting in terms of shell-model structure since we can study the effects of the neutron-proton interaction on the structure that we might assume to exist based on structure near to stability. In Fig. 2.2 on the following page we observe that for $N \leq 50$ there was a reasonable amount of information available, while for $N > 50$ very little experimental information was available. In general, the study of nuclear structure in the regions near doubly magic nuclides provides information on the strength of the shell closures and details on the interactions between individual nucleons. The structure of these

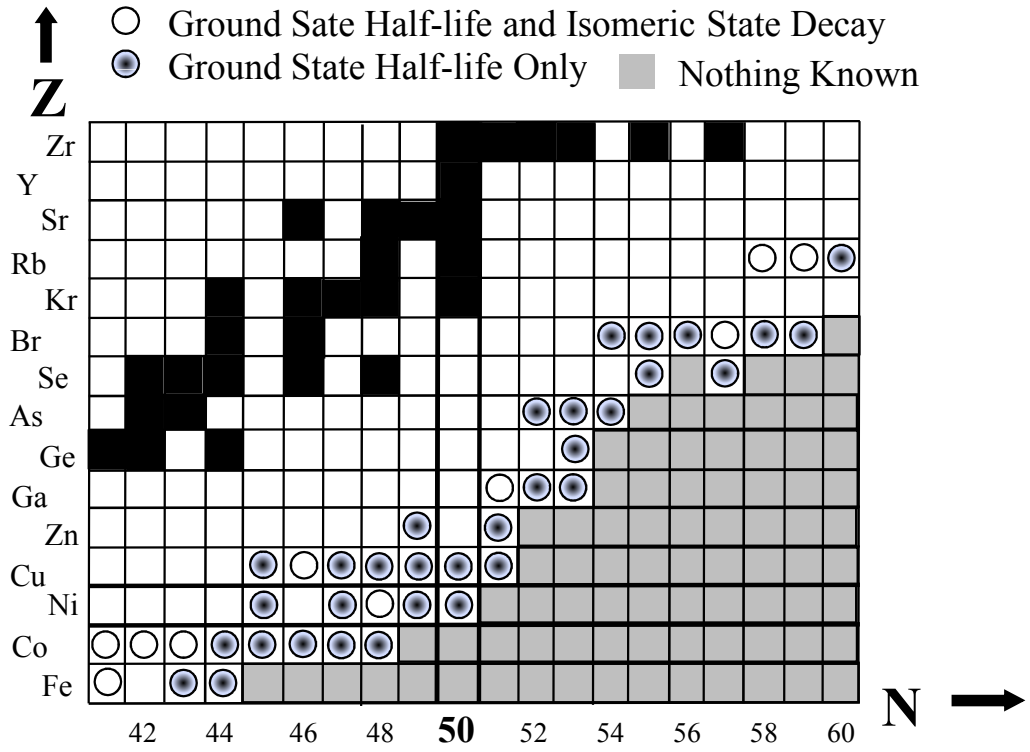

Figure 2.2: Section of the Chart of Nuclides in the region near ^{78}Ni showing the limits of nuclear structure information available at the start of the research project as taken from Ref. [NNDC]. In many cases for the most neutron rich members of an isotonic chain only very limited information was know about excited states. This was especially true for those where only the isomeric state decay was known.

nuclides can usually be well reproduced using shell-model calculations utilizing effective interactions. With an effective interaction available, it is possible to extend predictions to nuclides much further from stability which are of particular interest. However, these predictions are only as valid as the effective interaction which is based on known nuclear structure closer to stability. In order to refine the effective interactions, it is necessary to obtain additional experimental information. In addition, the assumption of closed nuclear shells must often be modified as one moves further out from stability since the magic numbers which appear to be valid near stability for some regions fail to hold up in other regions. This complexity was apparent in the interaction developed by Lisetskiy *et al.* where the single-particle energies (SPE) depend on the core which is chosen.[Lis04] The ordering of the orbitals is also very important, for example the $\pi f_{5/2}$ and $\pi p_{3/2}$ orbitals discussed in the following paragraph. Sieja and Nowacki used a large valence space shell-model calculation with a ^{48}Ca core instead of the typical ^{56}Ni core to show that excitations across the $Z=28$ shell gap are needed to explain the ground and isomeric states in the Copper isotopes.[Sie10] To better understand the way the single-particle energies change over the shell and to develop a valid interaction requires observing the evolution of states over an isotopic chain.

Otsuka *et al.* have shown in a theoretical calculation that the tensor interaction between the $\nu g_{9/2}$ state with the proton *fp* shell states reduces the spin orbit splitting resulting in the $\pi f_{5/2}$ orbital dropping below the $\pi p_{3/2}$ orbital near ^{75}Cu as shown in Fig. 2.3 on the next page.[Ots01, Ots05, Ots10] The predictions of Otsuka *et al.* are complimented by the calculations of Dobaczewski

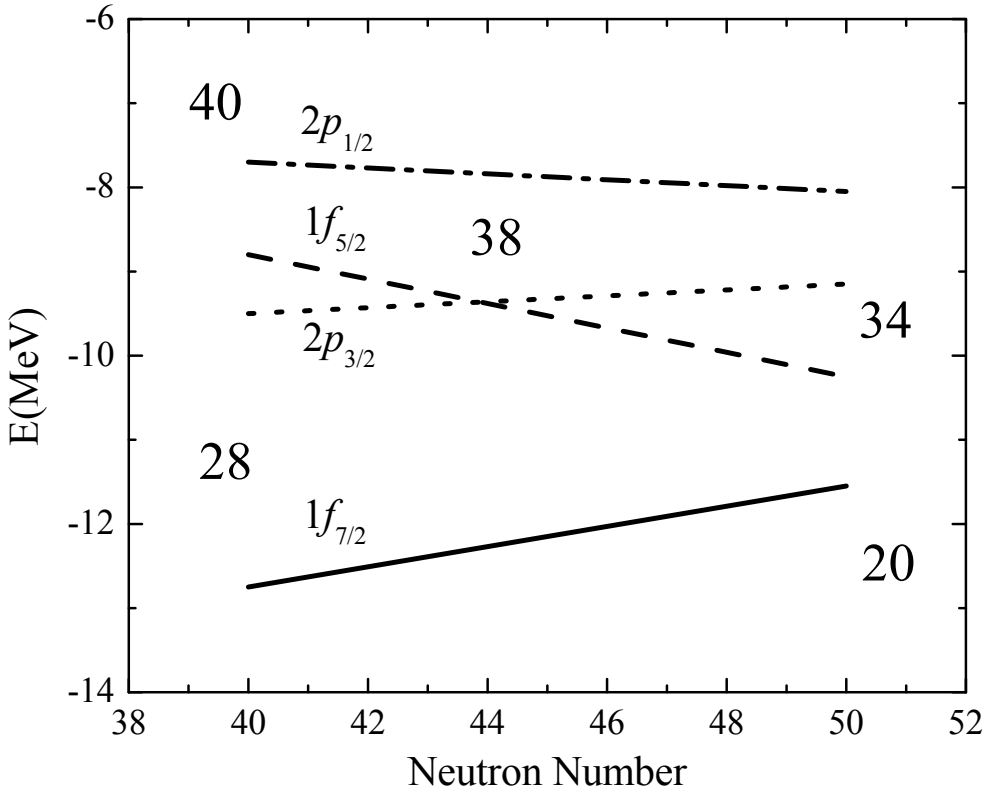

Figure 2.3: Plot of the migration of single-particle states in the proton *fp* shell due to the tensor interaction with neutrons in the $\nu g_{9/2}$ orbital as described by Otsuka *et al.*[Ots05] Indicated in the plot are possible proton shell closures.

et al. which indicate the additional importance of many-body correlations and the inclusion of coupling to continuum states to understand the structure of very neutron-rich nuclei.[Dob07] A similar effect occurs for the neutron orbitals just above $N=50$ where the migration of the neutron orbitals due to interaction between the $\pi f_{5/2}$ state with the neutron $1g$ and $2d$ states leading to a possible weakening of the $N=50$ shell gap.[Ang07b] This interaction also causes the splitting between the $\nu d_{5/2}$ and $\nu s_{1/2}$ orbitals to decrease rapidly as one approaches $Z=28$. The net effect of the migration of single-particle states is the possibility of new magic numbers such as $Z=34$ as the $\pi f_{5/2}$–$\pi p_{3/2}$ state splitting increases and $N=58$ as the $\nu d_{5/2}$ and $\nu s_{1/2}$ states become degenerate or invert. Therefore, a detailed study of the $N=51$ isotones (see Fig. 2.4 on the following page) would reveal much about the evolution of the neutron orbitals as $Z=28$ is approached. Part of the problem for the $N \geq 50$ region is that predictions for nuclei around ^{78}Ni are based on extrapolations from more complex configurations toward simpler configurations, which is the opposite of what would be desired. It would be much easier to start with the energies of the single-particle states for nuclei next to ^{78}Ni and use these to determine the energy states of nuclei with more valence nucleons. Lacking this information, we must obtain enough information on excited states in the region in order to extrapolate the effective single-particle energies back to the core. The more precise the experimental information available the better the extrapolation. Therefore, the research presented here concentrated on β-decay experiments which provided detailed information on excited states and other decay properties of nuclei in the ^{78}Ni region.

The βn emission probability ($P_{\beta n}$) increases for neutron-rich nuclei away from the line of β-

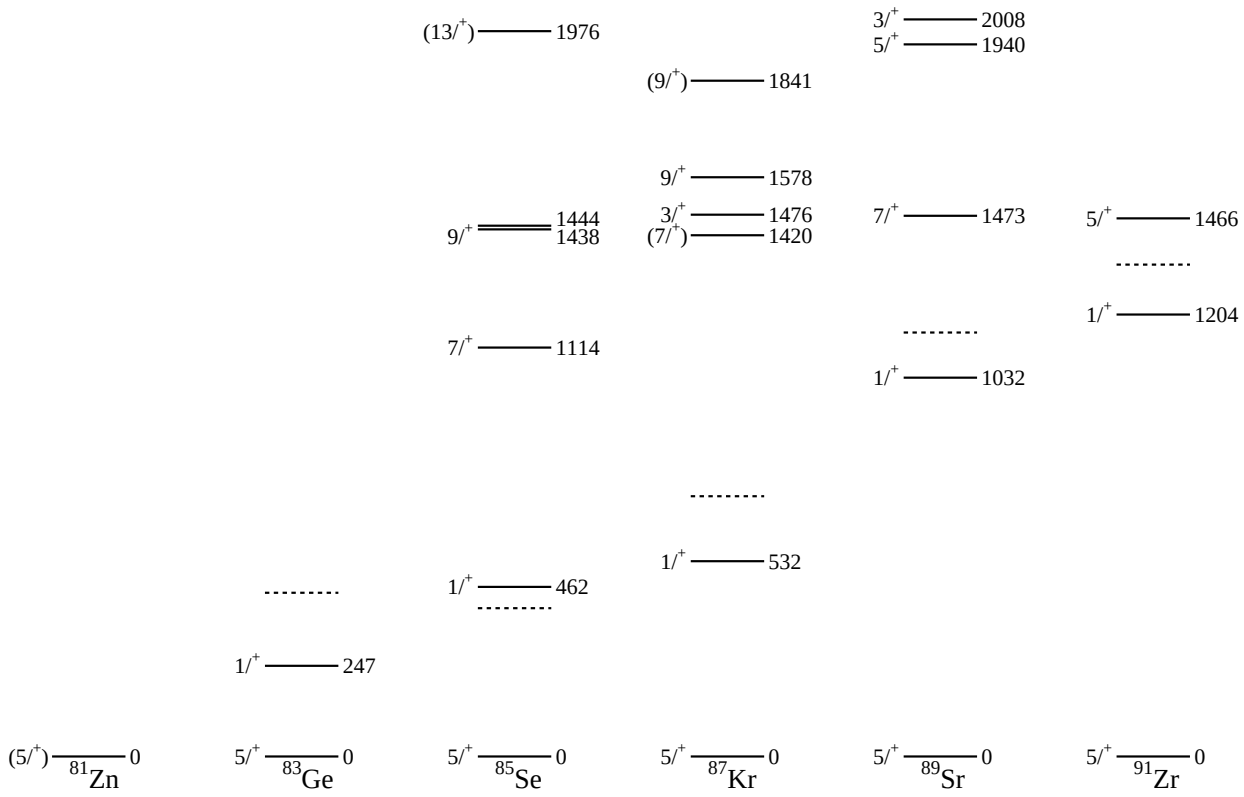

Figure 2.4: Systematics of the odd-A $N = 51$ isotones showing the steady drop in the $\nu s_{1/2}$ state relative to the $\nu d_{5/2}$ state. The dashed lines indicate the average of the shell-model predictions presented by Thomas *et al.*,[Tho07] indicating the failure of the current interaction to predict the continued drop in the energy of the first excited state.

stability primarily due to the increase in the energy window for β-decay (Q_β) and the reduction of the neutron separation energy (S_n) in the daughter activity. The properties of βn emission are also affected by details of the structure of both the parent and daughter nuclei which influence Q_β and S_n values as well as the energies of the levels primarily populated in the β decay. For example, for neutron-rich nuclei with a single neutron above the $N = 50$ nuclear-shell gap, the odd neutron will be weakly bound resulting in a low S_n value. Hence a large βn branching ratio can be expected in the decay of neutron-rich $N = 52$ isotones. The position of the proton and neutron orbitals involved in the β decay, i.e. their single-particle energies (SPE), can result in preferential feeding to states above the neutron separation energy which further enhances βn emission. This effect is particularly important when considering the decays of neutron-rich nuclei near closed shells where the allowed Gamow-Teller β transitions involve deeply bound states. Therefore, the SPE and the locations and size of shell gaps for neutron-rich nuclei are very important. Otsuka *et al.* have shown that the tensor interaction between the $\nu 1g_{9/2}$ state with the proton *fp* shell states reduces the spin-orbit splitting resulting in the $\pi 1f_{5/2}$ orbital dropping below the $\pi 2p_{3/2}$ orbital near ^{75}Cu [Ots01, Ots05]. These shell-model predictions are complemented by the mean-field calculations of Dobaczewski *et al.* which indicate the additional importance of many-body correlations and the inclusion of coupling to continuum states to understand the structure of very neutron-rich nuclei

[Dob07]. The nuclear-shell gaps known for stable nuclei can be reduced while new nuclear-shell closures may appear in very neutron-rich nuclei which can significantly affect the β-delayed neutron emission probability.

In addition to providing information on the evolution of nuclear structure, the research performed under this grant also has applications in other fields. One such field is nuclear astrophysics where data from β-decay studies are needed to understand nucleosynthesis. Nearly sixty years ago, Burbidge, Burbidge, Fowler, and Hoyle in a seminal paper in the field of nuclear astrophysics summarized a number of processes to describe nucleosynthesis in stars.[B^2FH] The goal was to explain the elemental abundances observed in nature beginning with a universe composed mainly of hydrogen and helium. In addition to long-term processes which could proceed along the line of stability, processes were also proposed which would exist much further from stability and proceed over very short time scales. These explosive processes include the rapid neutron-capture *r-process* in which a high flux of neutrons leads to the rapid capture of neutrons by seed nuclei in the iron-nickel region, and proceeds along a path of neutron-rich nuclei up to the uranium region where fission will occur. The *r-process* is the best scenario to explain the synthesis of approximately half of the nuclear species heavier than iron observed in nature. Experimental evidence in support of this process included the appearance of peaks in the elemental abundance which could be attributed to the crossing of major neutron shell gaps if the process, followed by decay back to stability, occurs much farther from stability. This occurs because the low neutron binding energy for the next neutron capture allows (γ, n) photodisintegration to break up the nucleus before another neutron can be captured, thus requiring β decays back toward stability before the process can proceed. This leads to the concept of "waiting-point nuclei", i.e. nuclei which are long-lived, in relative terms, that must β decay before the process can continue thereby delaying the processing of neutrons to reach heavier nuclei. As the neutron flux decreases with temperature, the process will terminate ("freeze out") with the remaining nuclei β decaying back to stability to produce the observed elemental abundances. The waiting-point nuclei, especially their half-lives, then define the path of the process as they will be the lowest-Z member of each isobaric chain at freeze out.[Thi07] The observed abundances will be determined not only by the nuclei occupied at freeze out, but also the various branches, including β, βn, and $\beta 2n$, followed as the activity decays back to stability. Although the general trends in the observed abundances could easily be reproduced using the experimental data and theoretical predictions available in 1957, some details were not.

Much experimental and theoretical effort has gone into improving our understanding of the *r-process* in the intervening years. The *r-process* path is determined in general by neutron separation energies (S_n) dictating the points at which equilibrium between neutron capture and photodisintegration occurs (i.e., the path) while the β decay half-lives ($t_{1/2}$) and β-delayed neutron probabilities ($P_{\beta n}$ values) set the *r-process* time scale and dictate the shape of the abundance peaks.[Kra00, Thi07] However, it is recognized that other properties, including neutron-capture cross sections ($\sigma_{n\gamma}$), are also important.[Thi07] The main problem is that the predicted path is in a region for which little experimental data is available, thus requiring theoretical models to predict the masses and β-decay properties which strongly affect the *r-process* abundance.[Kra00] Furthermore, the path taken by the *r-process* is not only dependent upon the nuclear properties, but also the physical properties (temperature T and neutron flux n_n) of the astrophysical site. Changes in T and n_n yield different abundances and time scales for the process [Kra00, Kra07] as is shown in Fig. 2.5 on the next page. This figure shows the predicted path of the *r-process* by indicating the nuclei which are predicted to be populated when the freeze-out temperature is reached. These nuclei will always be the lowest-Z member of an isobaric chain, but a waiting-point nucleus does not need to exist for each mass. After freeze out, the path back to stability will depend on the β-delayed neutron probabilities for each member of the decay chain. Using predicted properties and

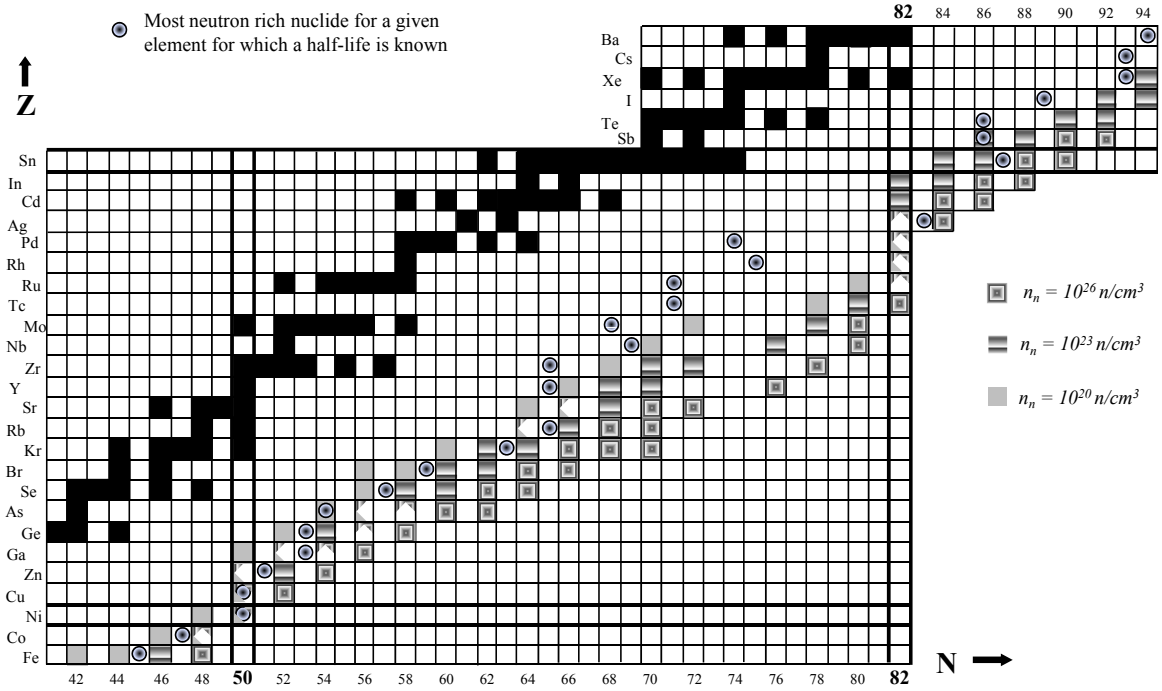

Figure 2.5: Portion of the chart of nuclides showing predicted paths for the *r-process* for three values of the neutron flux (n_n in $neutrons/cm^3$). Indicated in the plot are the waiting-point nuclei that will decay back to stability at freeze out for different values of n_n and therefore dictate the *r-process* path. Also indicated are the most neutron-rich member of each isotopic chain for which the half-life had been reported prior to research associated with this grant. Adapted from Ref. [Kra06].

comparison to observed solar system abundances revealed the need for *"shell quenching"* in order to explain abundances just above the main abundance peaks.[Kra00, Kra07] *"Shell quenching"* can be taken to mean a weakening or disappearance of the classical shells for very neutron-rich regions. Large valence space shell-model calculations suggest such a weakening of the $Z = 28$ shell gap as $N = 50$ is approached.[Sie10] In addition, comparison to elemental abundances in early generation ultra-metal-poor stars suggests that there may be two distinct *r-process* components; a "weak" *r-process* below $A \simeq 130$, and the "main" *r-process* for $A > 130$.[Kra00] Obtaining more experimental information (S_n, $t_{1/2}$, $P_{\beta n}$) for nuclei on or near the predicted *r-process* paths will aid in refining the theoretical models and calculations used to estimate the properties of nuclei further from stability and thus further refine the paths.

In recent years there has been renewed interest in developing nuclear power as an alternative electrical source to reduce the emission of greenhouse gasses.[Nuc10a, Nuc10b, Nuc10c] However, the same concerns toward nuclear energy are present today as they were 30 years ago when the construction of new nuclear reactors in the United States began to fall off. Specifically, the issues of safety, nuclear waste management, proliferation, and cost. So where does nuclear structure physics fit into this picture? The fission of nuclear fuels produces a broad range of neutron-rich radioactive products which decay back to stability by the emission of β particles, neutrons, and γ rays. Each of these contributes to the overall heat generation within the nuclear fuel (decay heat), and for β-delayed neutrons affects the overall neutron flux within the fuel. Consequently, understanding the decay properties of fission products is an important input into computer simulations used to understand current and future reactor cores. The SCALE (Standardized Computer Analysis for

Licensing Evaluation) code system used for analysis of nuclear facility design, safety, and licensing uses as input information contained in the current database of nuclear decay properties and decay schemes. The problem is that much of the information needed as input to this program may be incomplete or incorrect. In many cases, major assumptions are made about branching ratios (e.g., $P_{\beta n}$ values) and energy spectra of the β particles and γ rays being emitted. Part of the problem relates to an incomplete understanding of the energy levels fed in the daughter nuclides. As the Q_β value increases for neutron-rich nuclei, a large number of excited states are fed at high excitation energy through allowed β-decay transitions. These states will decay either by the emission of high-energy γ rays with very small intensities or by β-delayed neutron emission if they are above S_n. It is highly probable that many of the high-energy ($E_\gamma > 3$ MeV) transitions were unobserved experimentally due to their low intensity, leading to the "pandemonium" effect.[Har77] This results in incorrectly attributing the β-decay intensity to low-energy levels. Hence, any total decay heat estimates based solely on high-resolution studies of emitted γ rays may yield incorrect results. The Working Party International Nuclear Data Evaluation Cooperation (WPEC-25) was formed in response to the fact that different national and international decay data sub-libraries did not generate good estimates of decay heat without the introduction of additional data produced by means of various theoretical calculations. This group identified a list of 37 "Critical Need" isotopes which need new measurements as well as recommendations on experimental efforts required to address the need for decay heat analysis.[WPEC] Furthermore, imprecise data may contribute to inaccuracies in theoretical modeling and extrapolations which can lead to unnecessary or erroneous requirements in operation of fission reactors [Dan02] as well as nuclear waste handling and transmutation.[Gud00]

It is apparent that the study of low-energy nuclear structure through β decay can provide important information for a broad range of disciplines. The following chapters will discuss the research performed under this grant to address some of these issues.

3

Experimental Methods

The use of β decay to provide information on excited nuclear states has been around for many decades, with the same basic setup being used. This setup includes a source to provide radioactive nuclei to be studied and a set of detectors to measure emitted β particles, γ rays, *etc.* There are two primary issues which need to be addressed in any of these experiments:

1. How to obtain a source where the nuclide of interest is not totally dominated by other decays.
2. How to maximize the detection efficiency while still have the desired energy resolution.

A side issue related to the first point is how to remove unwanted sources from the detector system once the nuclides of interest have decayed.

The research performed under this grant utilized two distinct methods for source preparation. At the National superconducting Cyclotron Laboratory at Michigan State University (NSCL) projectile fragmentation of a ^{48}Ca beam on a ^{9}Be target was used to produce the nuclides of interest, while at the Holifield Radioactive Ion Beam Facility at Oak Ridge National Laboratory (HRIBF) proton-induced fission of ^{238}U was used to produce fission products which were extracted using the Isotope Separator On-Line (ISOL) technique). Both methods have there advantages and disadvantages. For projectile fragmentation, the process is fast and chemically insensitive allowing production of even the shortest lived nuclei of any chemical species. However, the resulting beam must be stopped prior to the measurement being made and generally does not allow production of a single species source. The ISOL method can produce single species sources if a sufficiently high resolution mass separator is available. However, the ISOL technique requires use of a ion source which is chemically selective and introduces lag times which limit studies of very short-lived nuclei. The following sections look into how each method was utilized in this research.

3.1 NSCL Experiments

Experiments at the NSCL utilized projectile fragmentation of ^{48}Ca at 70 or 80 MeV/u on a thick beryllium target to produce the desired beams. The projectile fragmentation process is not selective, producing a wide range of nuclei. The A1200 was used to isolate the nuclides of interest. An example of the selection provided by the A1200 is shown in Fig. 3.1 on the following page. By tuning the first half of the A1200 to select a particular nuclide, a slice is made in momentum space letting through a number of different nuclides. The selection is then improved by use of a degrader wedge to change the momentum space and then use the second half of the A1200 to center the nuclide of interest at the A1200 focal plane. As seen in the Fig. 3.1, the result is not a pure beam.

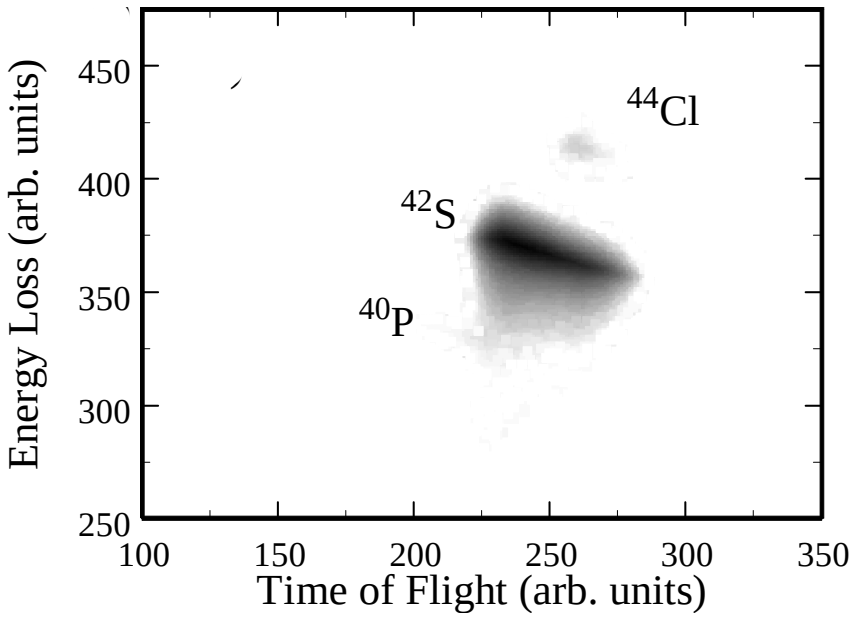

Figure 3.1: Particle identification (PID) plots (energy loss in Si PIN diode versus time of flight) for the A1200 set to center ^{42}S on the focal plane. Taken from [Win06]

However, the beam contains only one member of a mass chain. Hence, a clean decay spectrum for that mass chain can be obtained. This was sufficient for the NSCL studies where β-delayed neutron emission was not yielding daughters in the mass chains of the other beam components. Therefore, these were considered clean beams. Because only one member of the mass chain was separated , it was possible to directly measure the ground-state or unobserved feeding by using a saturation spectrum in which a comparison of the parent decay to known decays in their daughters or granddaughters was made.

The separated beam was then transported to the S2 vault where a detector station was placed to perform the measurement. Due to the energy of the beam, a non-active method for stopping the beam was devised in which the beam was implanted into a thin aluminium target. In order to increase the thickness of the target for stopping the beam while limiting the thickness of material through which the emitted β particles would need to pass, the target was held at a 45° angle relative to the beam direction as seen in Fig. 3.2 on the next page. In addition, a thin aluminum degrader was placed upstream of the target to allow slowing of the beam before the target to insure that the beam could not pass through the implantation target. Nine separate targets were arranged on a movable wheel attached to a stepper motor. This allowed movement of a target from the implantation position to a shielded location. (A $\frac{3}{8}$ inch thick iron plate served as a shield for β particles emitted from sources within the shielded area.) This system allowed data to be taken as the beam was being collected followed by a period where the fall off in activity was observed in order to measure the half-life. The source could then be moved out of the way in order to remove buildup of daughter and granddaughter nuclei.

A thin plastic scintillator positioned behind the implantation target was used to detect β particles. A second β detector mounted to the side of the implantation target (not shown in Fig. 3.2 on the following page) was used in two experiments, but it provided very little gain in the overall efficiency for the measurements. Two Hyper Pure Ge (HPGe) detectors, mounted as shown, were used

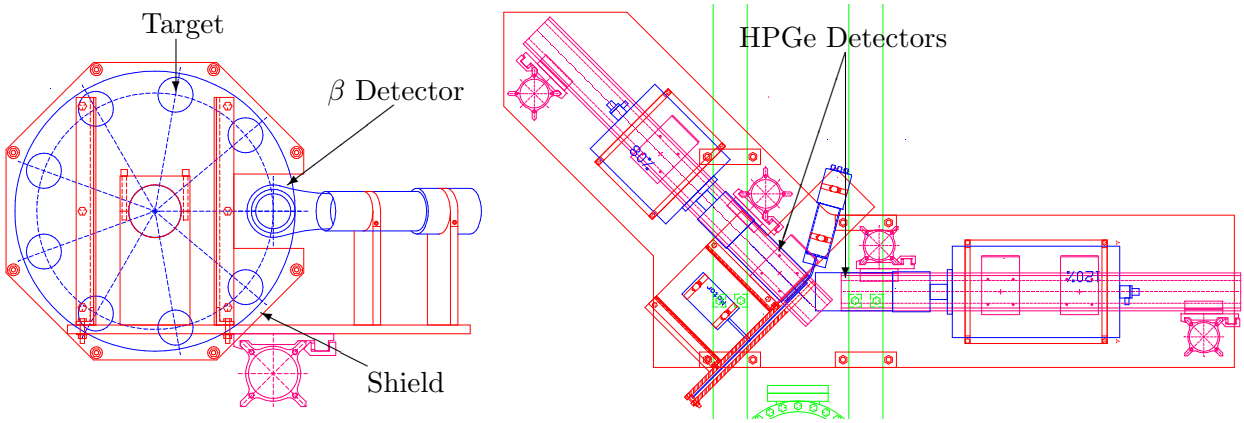

Figure 3.2: Technical drawings showing the layout of the NSCL target wheel setup. On the left shows the target wheel with the β detector centered behind the implantation target. On the right is an overhead view of the system indicating the placement of the two HPGe detectors

to detect γ rays. This setup allowed taking γ-ray singles and β-gated γ-ray singles along with $\gamma\gamma$ and $\beta\gamma\gamma$ coincidence data. The system shown in Fig. 3.2 was designed at MSU and constructed at the NSCL. Details on the results of these measurements will be presented in the following chapter.

3.2 HRIBF Experiments

Experiments at the HRIBF (Fig. 3.3 on the next page) used the ISOL technique to produce radioactive ion beams. Protons accelerated by the Oak Ridge Isochronous Cyclotron (ORIC) impinged upon a uranium carbide pressed powder target resulting in proton-induced fission of ^{238}U. Fission fragments were thermalize and drifted to an ion source where they were given a single positive charge. These radioactive ions were then accelerated from the ion source at 40 keV and sent through a low resolution mass separator to select a single isobar (A). Depending on the experiment, the beam might be passed through a charge exchange cell to produce singly charged negative ions. The charge exchange step was needed for any beams which were to be accelerated by the Oak Ridge Tandem, but was also used for non-accelerated beams where one member of the mass chain could be removed by the charge exchange process. An example of the later is removal of zinc isotopes since zinc does not form a negative ion. The beam was then accelerated to $\approx$ 160 keV before being sent through the high-resolution isobar separator.

The path from this point depended upon the type of experiment which would be done. The initial β decay measurements utilized what we refer to as the Ranging-Out Technique (RO). For RO, the beam of negative ions was accelerated to 2 to 3 MeV/u by the Tandem. These ions were sent to a detector end station composed of a multi-sampling ion chamber which was used to identify, tag, and slow the ions. Since energy loss in the ion chamber gas is proportional to Z^2, the slowing-down process could be used to remove the higher-Z components of the mass separated beam and provide a "pure" beam of the most neutron-rich component of the beam. This was very effectively used to obtain pure copper beams since no zinc ions were accelerated. Examples of RO are shown in Fig. 3.4 on page 15. After the ion chamber, the ions were sent to a detector array which will be describe shortly. A significant portion of the research was carried out using the Low-energy Radioactive Ion Beam Spectroscopy Station (LeRIBSS). LeRIBSS differed from the

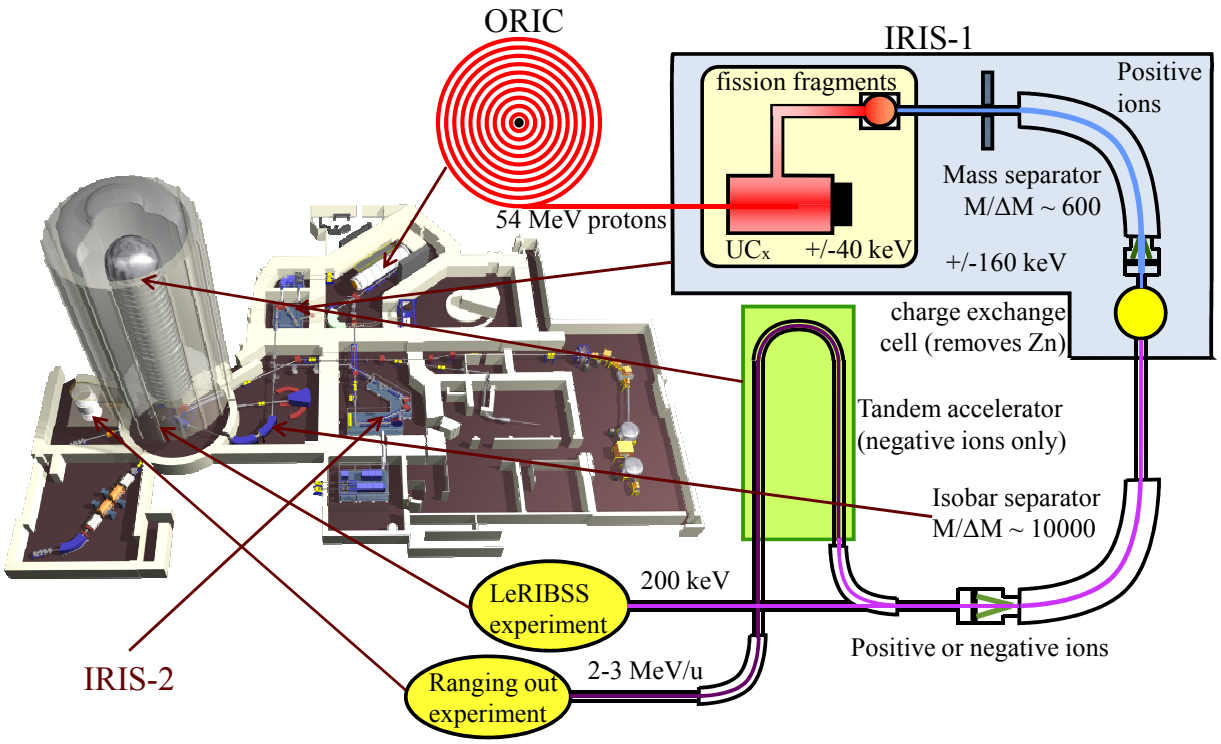

Figure 3.3: Schematic layout of the HRIBF. See text for details.

RO measurements only in that the beam was not accelerated by the Tandem, but was sent directly to the detector array from the high-resolution mass separator. This improved the overall beam rate since the acceleration efficiency did not come into play, but it also removed the ability to detect, count, and tag ions as they were sent to the detector array. Pictures of the two detector setups are shown in Fig. 3.5 on page 16.

Both the RO and LeRIBSS measurement used the same basic detector array which was composed of Moving Tape Collector (MTC), plastic scintillator β detector, and four HPGe detectors mounted in a Clarion Array for Decay Spectroscopy (CARDS) frame. The MTC uses an aluminized 35 mm film to provide an implantation surface for the ions with the ability to quickly move the source to a new location. A long tape was used with the majority of the tape held in the large cassette visible in Fig. 3.5. The tape was fed out of the cassette to a location where the ion beam would be deposited onto the tape. For the RO measurements, two source deposit locations were used. The first was just at the exit of the ion chamber for measurements at high pressure, while the second was at the center of CARDS for the tagging measurements. For LeRIBSS, the source was always deposited at the center of CARDS. The β detector was used to require $\beta\gamma$ coincidences as needed. It was composed of two 3 mm thick half cylinders of plastic scintillator (about 20 cm long) which surrounded the 2 inch beam pipe. Care had to be taken in using the β detector when determining intensities because the efficiency of the detector depends on the total β-decay energy to the daughter state fed by the decay. The four HPGe detectors mounted in CARDS were used to obtain γ-ray singles and $\gamma\gamma$ coincidence data.

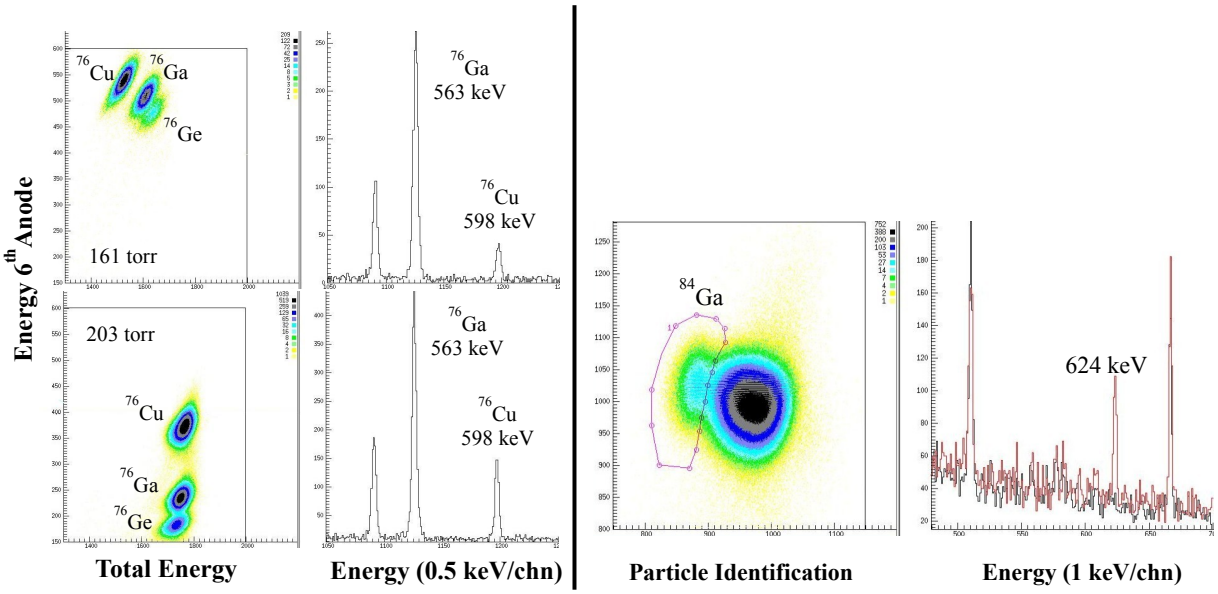

Figure 3.4: Examples from the initial RO experiment. Figure on left shows the effect of increasing gas pressure in the ion chamber to "range out" ^{76}Ga and ^{76}Ge leaving a pure ^{76}Cu beam. Although the γ ray from ^{76}Ga is observed in both cases, at the higher pressure it comes only from the decay chain starting with ^{76}Cu. Figure on the right shows use of the ion chamber as an ion implantation tag. In this case, selection of γ rays in coincidence with the ion chamber events in a defined "gate" enhances the γ rays from this decay relative to all γ rays detected. This is apparent in the γ ray spectrum where red spectrum utilizes the gate while the balck spectrum is from all events but limiting the statistics to match that of the gated spectrum.

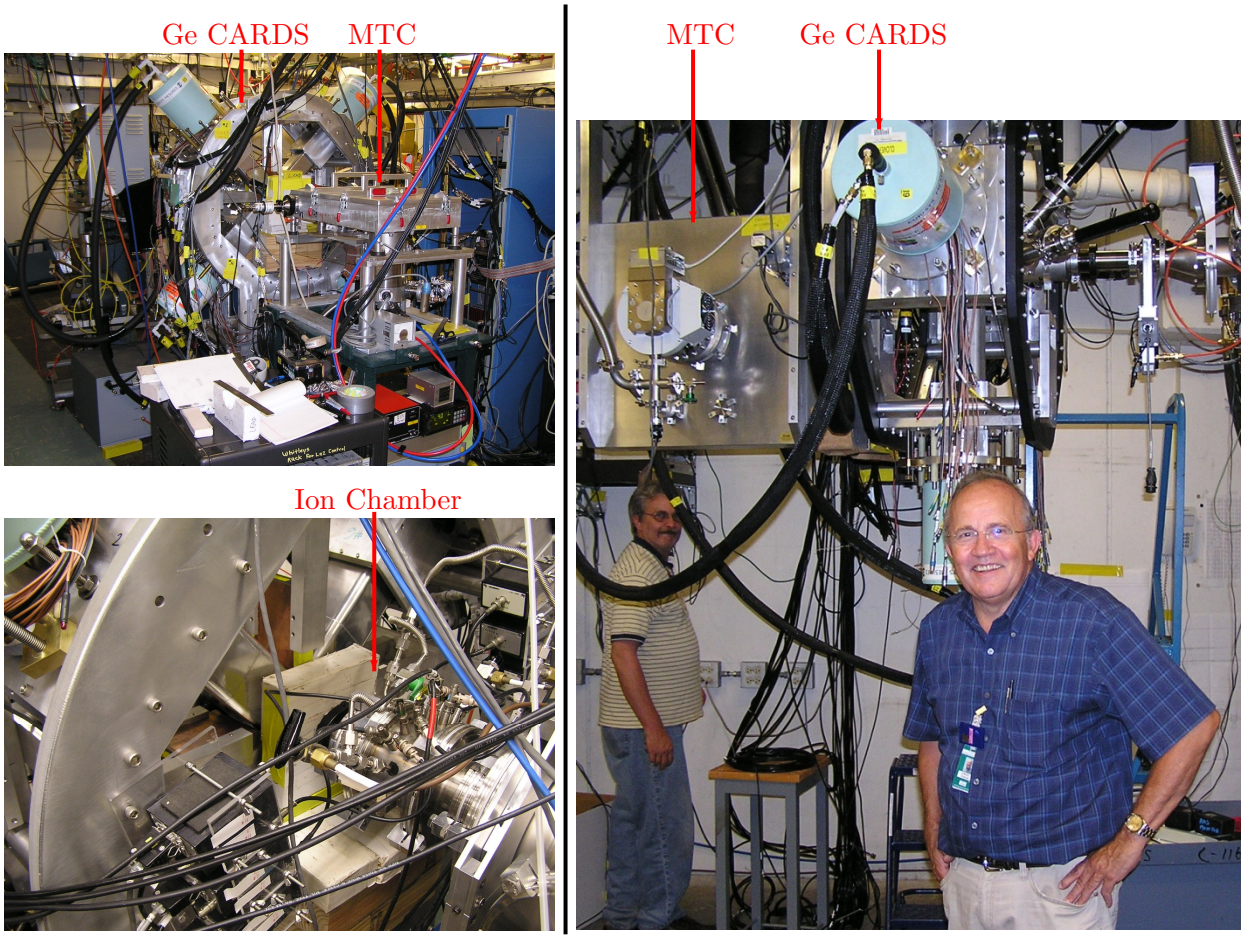

Figure 3.5: Pictures of the RO (left) and LeRIBSS (right) detector setups.

4

Results

4.1 NSCL Experiments

4.1.1 Low-energy structure of ^{40}S through ^{40}P β decay

The first β-decay experiment at the NSCL was meant to look at the systematics of the sulphur isotopes between $N = 20$ and $N = 28$ by observing the decays of the phosphorous parent.[Win01] Specifically, the β decay of ^{40}P was studied. Sources of ^{40}P were produced from a 70 MeV/u ^{48}Ca beam fragmented by a 254 mg/cm^2 Be target with separation of the source as described previously.

The decays of the implanted ions were observed using three detectors, two Ge detectors and one thin plastic scintillator. The β detector consisted of a 1 mm thick by 6.3 cm diameter BC400 plastic scintillator which was attached to a photomultiplier tube by a short lightguide. The 1 mm thick plastic is $\sim$100% efficient in detecting β particles and almost transparent to γ rays. In order to minimize the material through which the β particles must penetrate to reach the detector, the face of the scintillator toward the implantation target was covered with a thin Al foil. An 80% efficient Ge detector, see Fig. 3.2 on page 13, was located just behind the β detector, with both being oriented at 45° relative to the beam direction. A 120% Ge detector was placed at 90° relative to the beam direction. The average distance from the implantation targets to the two Ge detectors were 1.8 cm and 4.1 cm, respectively. The Ge crystals were shielded by a 2.5 cm thick lead box to reduce background radiation from the room, but the orientation of the two detectors resulted in significant backscattering between the detectors. Timing signals from the three detectors were used to set hardware timing gates. Data from the detectors were only collected when two of the detectors were in coincidence based on these timing gates. Further refinement of these gates was performed by use of software gates during off-line analysis. In this way, data on $\beta\gamma$, $\gamma\gamma$, and $\beta\gamma\gamma$ coincidences were obtained. In addition to energy and relative times, the time of each event relative to the beginning of a decay cycle was recorded. The clock for this measurement was reset at the end of each cycle and not restarted until the start of the next decay cycle so that during the growth phase of the timing cycle events did not have a time recorded.

The presence of strong contaminants from ^{43}Cl and ^{42}S, as well as daughter nuclei from these decays, required the use of several timing cycles and A1200 settings in order to positively associate specific γ rays with their radioactive source. With the magnetic rigidity of the A1200 set for maximum transmitted yield of ^{40}P, data were collected using three different timing cycles. Finally, data were collected during two saturation measurements, one at the beginning and the other at the end of the experiment. For these measurements, the beam was implanted into a single target for a period of five minutes before data were collected. This insured that the $A = 40$ decay chain was in saturation and that at least ^{39}S was in saturation in the $A = 39$ decay chain. Additional A1200

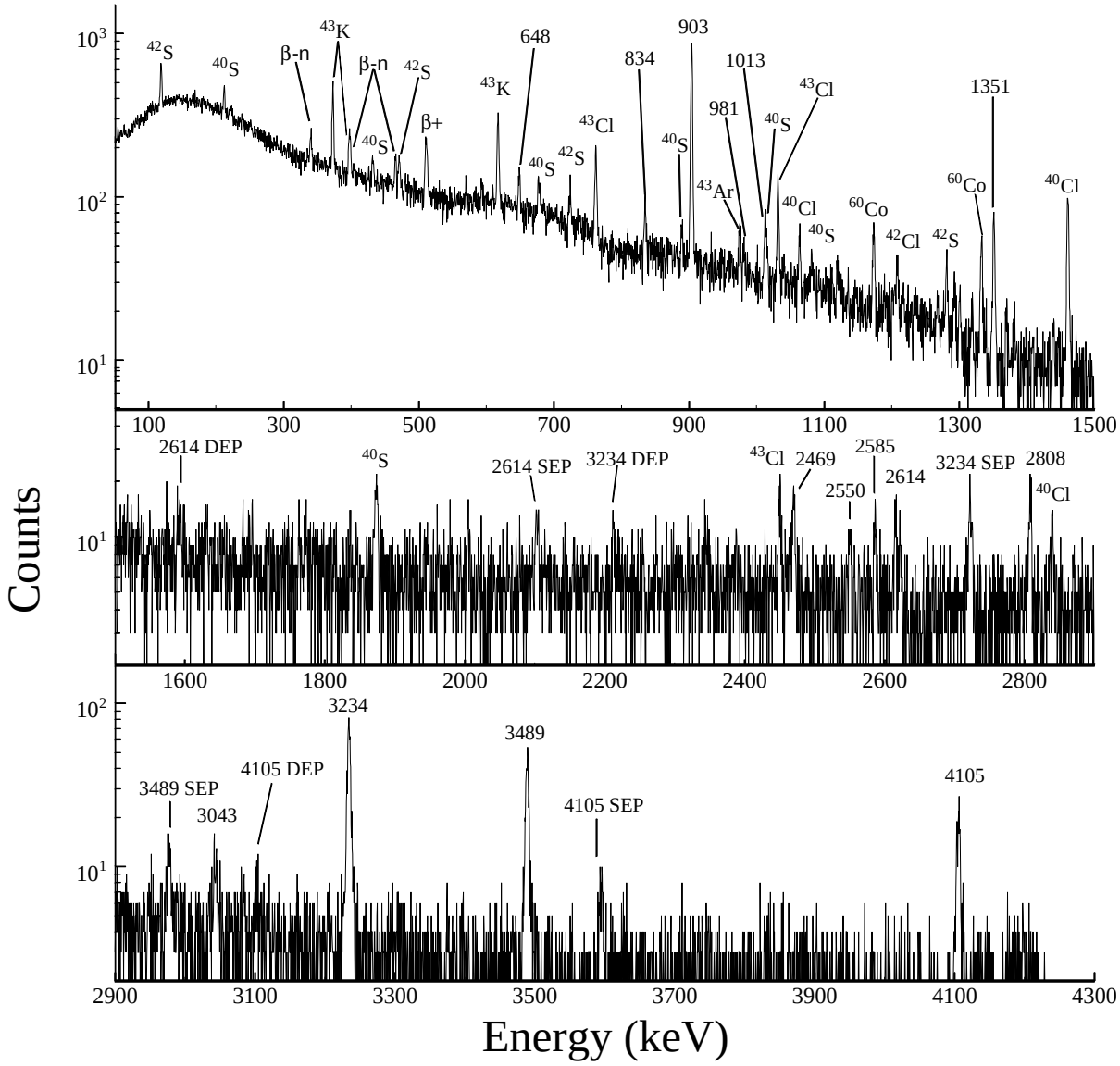

Figure 4.1: β-gated γ-ray singles spectrum with the A1200 set to maximize the transmitted intensity of ^{40}P. γ rays assigned to the decay of ^{40}P are labeled with their energy in keV. Single escape peaks and double escape peaks are labeled with the energy of the original γ ray followed by SEP or DEP, respectively. Three lines associated with the β-delayed neutron branch to states in ^{39}S are indicated by β-n. All other lines are labeled according to their source.

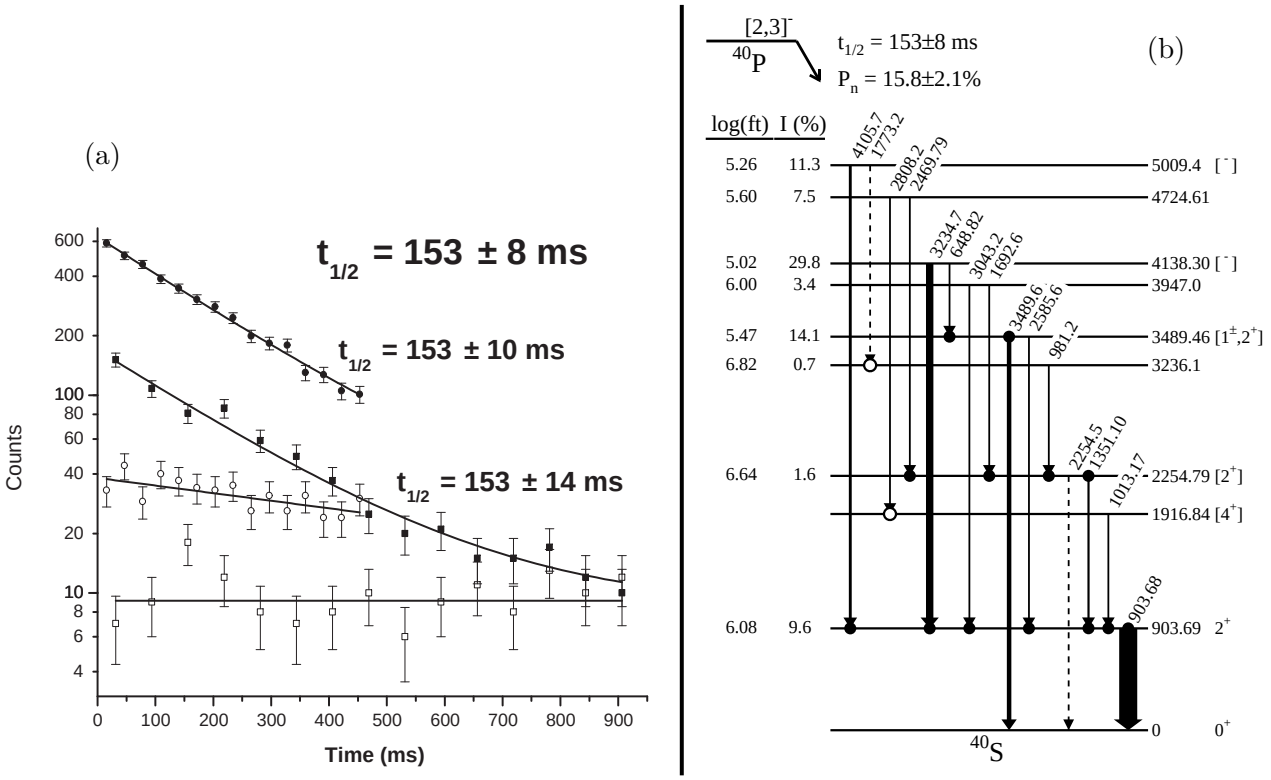

Figure 4.2: a) Half-life curve for the decay of the 903-keV γ ray associated with ^{40}P β decay. In the figure, circles represent data form a short timing cycle and squares a long timing cycle, where closed(open) symbols represent the time spectrum projected by gating on the γ-ray peak(background). A best fit to each data set is shown as solid lines. b) Level scheme for ^{40}S. The width of the lines is proportional to the relative intensity of the γ ray.

settings and timing cycles were used to enhance the separation and observation of both ^{43}Cl and ^{42}S in order to better study these decay chains.

β-gated γ-ray energy spectra for each setting of the system (A1200 setting plus timing cycle) were generated from the event data and fit to provide a complete set of all observed γ rays. A representative β-gated γ-ray singles spectrum is presented in Fig. 4.1. Detailed comparisons between spectra using different conditions allowed the observed γ rays to be associated with particular decays. Additional information was provided by coincidence relationships. Based on this information, a total of 21 γ rays, excluding single and double escape peaks, were associated with the decay of ^{40}P. The strongest γ ray associated with the decay of ^{40}P was observed at 903 keV and corresponds to the energy of the first excited state in ^{40}S in agreement with a previous study.[1] Those γ rays which could not be associated with a particular decay had relative intensities to the 903-keV γ ray of less than 2%. The intensities quoted also include corrections due to coincidence summing which is based on the proposed level scheme.

The half-life of ^{40}P was determined using a time spectrum gated by the 903-keV γ ray with comparison to a background gate of the same width placed at an energy slightly higher than the peak gate. This procedure was performed for both short and long timing cycles. The four spectra obtained in this procedure are displayed in Fig. 4.2. In fitting these time spectra, the background was determined for each timing cycle and then held fixed when fitting the data for the half-life.

Analysis of the time spectra lead to a weighted average for the ^{40}P half-life of 153 ± 8 ms.

Background-subtracted coincidence γ-ray spectra were obtained and used to establish a list of coincident γ rays. Based on the γ-ray singles and coincidence information, 15 γ rays were placed in the decay scheme for ^{40}P which populate nine excited states in ^{40}S. Details of this decay scheme, which is shown in Fig. 4.2b, will be presented in the following paragraphs. Three γ rays (339-, 398-, and 465-keV) were assigned to excited states in ^{39}S populated following β delayed-neutron decay of ^{40}P. This was confirmed in a subsequent experiment which observed the β decay of ^{39}P[Win98]. By considering the relative intensities of γ rays from ^{39}S and ^{40}Cl in the saturation spectrum, we were able to determine a β-delayed emission probability of $15.8 \pm 2.1\%$. This result is significantly lower than that obtained by Lewitowicz *et al.* et al. , but was in close agreement with the predicted value of 14% given by Möller, Nix, and Kratz[Lew89, Mol97].

The observed levels for ^{40}S were compared to a Geometrical Collective Model (GCM) calculation using a restricted nuclear potential of the form

$$V(\beta,\gamma) = C_2 \frac{1}{\sqrt{5}}\beta^2 - C_3\sqrt{\frac{2}{35}}\beta^3 \cos 3\gamma + C_4 \frac{1}{5}\beta^4$$

Since the low-energy structure of ^{40}S is consistent with that of an anharmonic vibrator, it was possible to estimate the anharmonicity of the potential from the data set. The parameters for the calculation were chosen to reproduce the energies of the levels at 903, 1916, and 2254 keV and the $B(E2; 0^+_{gs} \rightarrow 2^+_1)$ value of 334 ± 36 $e^2\text{fm}^4$.[1]

The parameter values obtained are correspond to a β-soft potential with a shallow oblate minimum and a somewhat deeper prolate minimum. However, the depths of these minima are small compared to the zero-point energy of the ground state, and so the nucleus sees essentially an oscillator-like but anharmonic potential. Whereas the Coulomb excitation measurements provide the magnitude of the β_2 value[1], use of β decay to determine the location of the 4^+_1 state at 1916 keV makes it is possible to determine the sign of β_2 as positive.

4.1.2 The β decay of ^{40,42}S and ^{43}Cl

Data from the experiment discussed in the previous section was also used to study the β decays of ^{40,42}S and ^{43}Cl.[Win06] Although the A1200 was tuned for ^{40}P production, there was still sufficient rate to obtain good statistics in a short time for these other nuclides by making small changes in the tune for the second half of the A1200. The design of the setup included a Si PIN diode just before the beam exited the beam line providing active determination of the beam composition as is seen in Fig. 3.1 on page 12. A similar data analyst procedure was then used to obtain the results presented in the following paragraphs.

The β decay of ^{40}S was observed following the β decay of ^{40}P described in the previous section. Due to the timing cycles used in this measurement it was not possible to determine the half-life. A total of 12 γ rays which de-excited 6 levels in ^{40}Cl were associated with this decay. The resultant decay scheme is shown in Fig. 4.3 on the next pagea. Placement of the 431-keV γ ray parallel to the 211-keV γ ray was evidenced by the coincidence spectra. Indeed, all the proposed levels are well established by coincidence and energy sum relationships. The strongest γ ray observed is at 211 keV and corresponds to the de-excitation of the first excited state.[Bal93] The 431, 677, and 889-keV γ rays were also observed by Dufour *et al.*, but were not placed in a level scheme.[Duf86] Balamuth *et al.* also observed the 211, 431, and 677-keV γ rays, but were only able to place the 211-keV γ ray in the level scheme.[Bal93] All three γ rays were found to be consistent with dipole transitions in Ref. [Bal93].

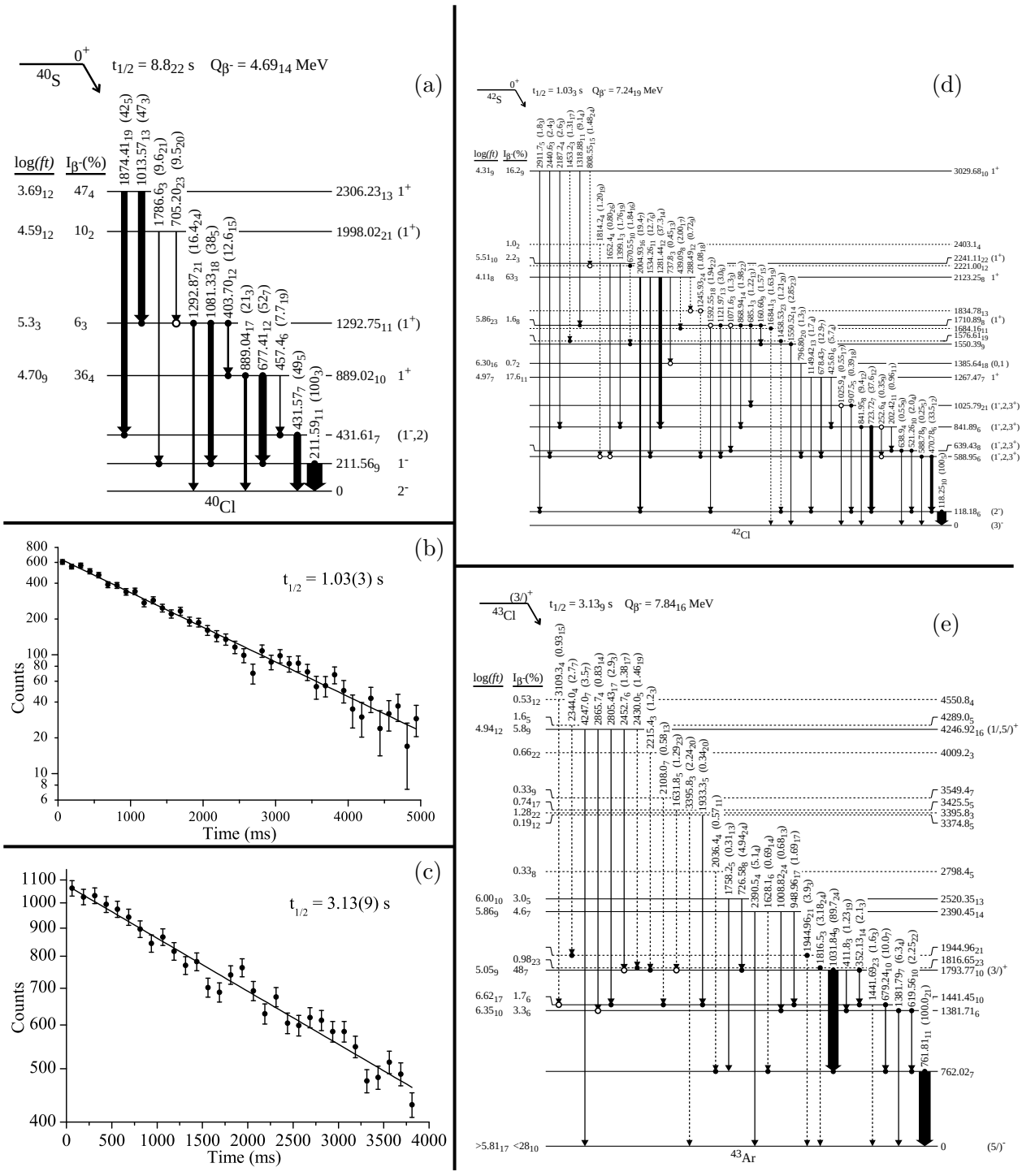

Figure 4.3: a) Decay scheme for ^{40}S. b) Half-life curve for ^{42}S. c) Half-life curve for ^{43}Cl d) Decay scheme for ^{42}S. e) Decay scheme for ^{43}Cl.

The absolute branching ratio for the decay was established by comparison of the γ-ray intensities to the known decay of ^{40}Cl in a saturation measurement. This established the absolute normalization to be 0.52 ± 0.03 for ^{40}S decay. Using this value the level feedings presented in Fig. 4.3a were obtained. This intensity balance analysis indicates that there is no significant feeding to the levels at 211 and 431 keV, while the sum of feeding to the ground state indicates a missing feeding of $3 \pm 9\%$. This latter result is consistent within the measurement uncertainty with the expectation that there is no feeding to the ground state. The assignment of 2^- for the ground state of ^{40}Cl was based on low $\log(ft)$ values for decay to known negative parity states in ^{40}Ar.[Klo72] This assignment is consistent with the results presented here and the expectations from a simple shell model picture. Shell model calculations[War89, Woo86, Ji89] all predict the ground state to be 2^- with a β decay feeding of $< 0.5\%$. This coupled with the observed level feedings allowed estimation of the spin/parity assignments presented in Fig. 4.3a as discussed in Ref. [Win06]. A comparison was also made to shell model calculations as discussed in the paper.[Win06]

The β decay of ^{42}S was studied by tuning the A1200 to provide a nearly pure beam this nuclide as seen in Fig. 3.1 on page 12. The strongest γ rays associated with this decay have energies of 118, 470, 723, and 1281 keV. The half-life was determined using gates set on the first three of these γ rays with adjacent background gates subtracted. The 1281-keV γ ray was not used due to contamination from an adjacent γ ray (1283 keV) from ^{42}Cl decay. The time spectrum obtained is shown in Fig. 4.3b. This spectrum was fitted with a single decaying exponential yielding a half-life of 1.03 ± 0.03 s. This value differs by almost a factor of two with the previously reported value of 0.56 ± 0.06 s by Sorlin *et al.*[Sor95] However, the method used here assures a more accurate determination of the half-life.

A total of 41 γ rays which de-excited 17 levels in ^{42}Cl were associated with this decay. The resultant decay scheme is shown in Fig. 4.3d. The lower level cutoff for relative intensities of γ rays observed in this measurement was $< 0.5\%$ up to an energy of 4 MeV. All γ rays with relative intensities greater than 1% were either assigned as depopulating excited states in ^{42}Cl or associated with another decay based on the available coincidence data and energy-sum relationships. The majority of the levels shown in Fig. 4.3d are firmly established by coincidence and energy sum relationships. The levels at 1576, 1684, 1834, and 2221 keV are intermediate levels in a two γ ray cascade linking established levels. Reversing the order of the cascades would yield levels at 1571, 439, 877, and 2358 keV, respectively. For the 1834-keV level the ordering of the cascade is based on the statistically significant higher intensity of the 1245-keV γ ray. The choice of a level at 1684 keV over 439 keV is based on the assumption that a lower lying level would probably have feeding from other states. None of these levels is expected to receive significant β-decay feeding. The level at 2403 keV is based on a single transition which is suggested by the coincidence relations and would receive direct feeding.

The absolute branching ratio could not be made for this decay based on consideration of the known γ rays from the decays of the daughter and granddaughter for two reasons. First, the absolute normalization for the decay of ^{42}Cl is not known even though some information on the decay is known.[Huc81] Second, the long half-life of ^{42}Ar made it impractical to achieve saturation for its decay. Hence, a different method was used in this case. From the decay of ^{40}S we find that the feeding to the ground state is negligible. There is a strong indication that the ground state of ^{42}Cl is 3^- which would completely preclude a direct decay. Therefore, it is reasonable to assume within the limits of this measurement that there is no direct ground state feeding observed. A small energy window exists for β-delayed neutron emission. A γ ray at 167 keV with a relative intensity of $0.7 \pm 0.2\%$, which may correspond to to a known transition in the decay of ^{41}Cl, was observed in the saturation spectrum for one of the Ge detectors. However, there is no evidence in the data for other γ rays associated with this decay which should have the same or a greater

intensity. The intensity of the 167-keV γ ray sets $P_n < 1\%$. Hence, we have used only the sum of all the γ-ray intensity feeding the ground state to establish the normalization. This results in an absolute normalization factor of 0.87 ± 0.04 for the ^{42}S decay. This normalization leads to a total deduced β feeding of $100 \pm 6\%$, and was used to determine the apparent level feedings and $\log(ft)$ values presented in Fig. 4.3d. A comparison of the experimental results to the shell model calculations of Warburton[War91] was made in the paper.[Win06]

Another small change in the tune for the A1200 allowed for a study of ^{43}Cl β decay. This decay is characterized by two intense γ rays (761 and 1031 keV), with no other γ ray having a relative intensity greater than 10%. The half-life of ^{43}Cl was determined using a background subtracted time spectrum gated by the 761 and 1031 keV γ rays which is shown in Fig. 4.3c. This time spectrum was fitted with a single decaying exponential yielding a half-life of 3.13 ± 0.09 s. This value is in agreement with the two previous measurements,[Vos81, Huc81] but with much better accuracy.

A total of 29 γ rays which de-excited 17 levels in ^{43}Ar were associated with this decay. The resultant decay scheme is shown in Fig. 4.3e. The lower level cutoff for relative intensities for γ rays observed in this measurement was $< 0.5\%$ up to an energy of 4 MeV. All γ rays with relative intensities greater than 0.7% have been either assigned as depopulating excited states in ^{43}Ar or associated with another decay based on the available coincidence data and energy-sum relationships. The γ ray at 4247 keV was not directly observed in the experiment due to an energy cutoff at 4.2 MeV. Its energy and intensity are inferred from the observed single and double escape peaks. For the intensity, the ratio of the intensity of the single escape peak to the full energy peak for a number of high energy γ rays observed in this and another experiment[Win98] were used to determine the energy dependency. In addition, the γ ray at 2344 keV was part of an unresolved doublet with a γ ray from ^{43}Ar decay. The intensity was scaled to remove the contaminant. The decay scheme obtained is in good agreement with that given by Huck *et al.*[Huc81], who were able to place 15 γ rays de-exciting 7 levels.

Of the 17 levels placed in the decay scheme, only 7 are firmly established by coincidence and energy sum relationships. The level at 1816 is established by a two γ ray cascades de-exciting the level at 4246 keV with coincidence relationships supporting this placement. The levels at 1944 and 4289 keV are established by a two γ ray cascade indicated by coincidences and observation that both γ rays have the proper time behavior for ^{43}Cl. In both cases, the order has the more intense γ ray placed lower. Of the remaining levels, 6 are based on single γ rays but with coincidence relationships supporting the placement. The remaining level (3395 keV) is based on a single γ ray which has the proper time behavior for ^{43}Cl but was not in coincidence with any other γ rays. The only difference with the results of Huck *et al.* is in the placement of a level at 2344 keV which is connected by γ rays to the ground state and 1441 keV level (2344 and 903 keV, respectively). This placement is not supported since there is no evidence in the coincidence spectrum gated on the 679 keV γ ray for a peak at 903 keV, placing an upper limit on its relative intensity of $<0.2\%$.

The absolute branching ratio was based comparison of the relative intensities of γ raysto those in ^{43}Ar observed in the saturation spectra. This established the absolute normalization factor to be 0.57 ± 0.08. Using this value the level feedings and $\log(ft)$ values presented in Fig. 4.3e were obtained. An intensity balance analysis indicates that there is no feeding to the first excited state at 761 keV and the total unidentified feeding is $28 \pm 10\%$. There is no evidence in the data for delayed-neutron branching, therefore, all the unassigned β decay intensity is attributed to direct feeding of the ^{43}Ar ground state. Such an assumption leads to a $\log(ft) = 5.81(0.17)$, indicating first forbidden decay. This $\log(ft)$ value represents a lower limit since unseen γ ray strength that may directly feed the ^{43}Ar ground state would reduce the apparent β decay feeding.

The apparent feeding to the ground state by first forbidden β decay from the ground state

of ^{43}Cl contradicts the simple assumption that the ground states connected are $\pi d_{3/2}$ and $\nu f_{7/2}$ single particle states. Although the ground state spin and parity of ^{43}Cl has not been confirmed experimentally, shell model studies suggest that the order of the $3/2^+$ and $1/2^+$ states switches order for ^{43}Cl.[Woo86, Sor04] This results from a decrease in the $\pi d_{3/2} - \pi s_{1/2}$ energy difference as the $\nu f_{7/2}$ subshell is filled so that stronger pairing in the $\pi d_{3/2}$ subshell results in a $\pi s_{1/2}$ hole state. The observed prolate deformation[Sar00] would lead to a similar situation. However, both of these situations would further inhibit direct ground state decay. Evidence from the β decay of ^{43}Ar suggests that the ground state is $5/2^-$.[Cam01] This assignment is supported by theory as the change from a $\nu f_{7/2}^3$ configuration to a $\nu f_{7/2}^{-3}$ configuration results in a change in the order of the $7/2^-$ and $5/2^-$ states observed in ^{41}Ar.[Mar99, War91] A $5/2^-$ ground state for ^{43}Ar allows the possibility for a first forbidden β decay to occur, but only if the ^{43}Cl ground state is $3/2^+$. Hence, the apparent ground state feeding led us to suggest a $3/2^+$ ^{43}Cl ground state. Again, a comparison of the experimental levels to those of Warburton's calculations[War91] was presented in the paper.[Win06]

4.1.3 Other NSCL β decay results

Two additional β-decay experiments were performed at the NSCL. The first experiment was meant to be a continued study of the systematics for the sulphur isotopes by observing the β decay of ^{42}P using an 80 MeV/u ^{48}Ca beam. We encountered a number of difficulties associated with this measurement. First, the production rate for ^{42}P was lower than expected making it very difficult to properly tune the A1200. Second, the target wheel was found to be too massive to make the quick rotations desired for this study. Because of rotational inertia, the wheel would detach from the axle of the stepper motor thus requiring much slower rotational speeds than desired. Third, the higher beam energy made stopping the beam in the targets much more difficult. This also resulted in a significantly higher number of charged particles which would stream into the downstream HPGe detector. Although the initial goal of the experiment was not achieve, we did obtain data on a large number of β decays with results presented at conferences as well as publication in the proceedings of one conference.[Win98] Analysis of ^{44}Cl β decay was also used as the masters thesis for one graduate student (H. H. Yousif, MSU 2003) who left without completing a publishable manuscript. The second experiment sought to perform β-decay studies at the edge of the island of inversion around ^{32}Mg using 80 MeV/u ^{48}Ca and ^{40}Ar primary beams. Of particular interest was observation single particle states in the $N = 20$ nuclide ^{33}Al by ^{33}Mg β decay. There were again beam production issues related to obtaining the primary goal of the experiment although some useful results were obtained. This experiment ran just before shutdown of the NSCL for the coupled cyclotron upgrade. A test experiment with the new A1900 looked to confirm the result obtain in our experiment, but instead obtained contradictory results. This called into question the particle identification which was being used. The following paragraphs will summarize the results from these two experiments.

Although the first experiment was not able to obtain useful data the the β decay of ^{42}P, it did provide useful information for the β decay of ^{39,41}P, ^{41,43}S, and ^{44,45}Cl. For each of these nuclides it was possible to extract a half-life measurement. Various γ-ray gates were used, and often the analysis required a separate fitting of the background near the gate. The results of this analysis are presented in Fig. 4.4 on the next page. Prior to this experiment, the only known half-lives were for ^{44}Cl (434(60) ms)[Sor95] and ^{45}Cl (400(43) ms)[Sor93]. Our result for ^{45}Cl is in agreement with the previous value, but is more precise. For ^{44}Cl our value differs significantly from the previously reported value where β-neutron coincidences were used.[Sor95] It is not obvious why this difference occurs, but suggests the possibility of an isomeric state. After this experiment,

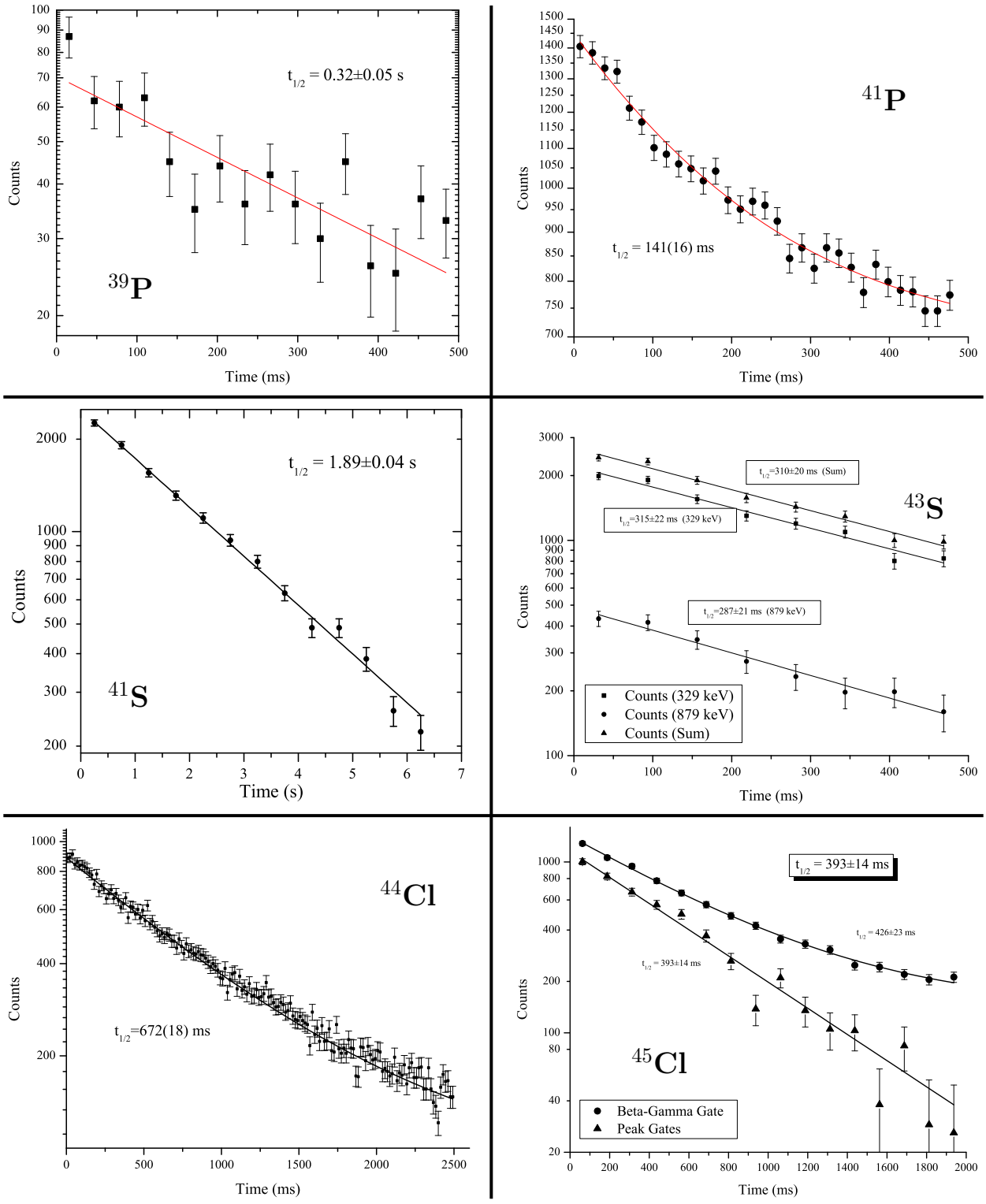

Figure 4.4: Half-life curves for ^{39,41}P, ^{41,43}S, and ^{44,45}Cl.

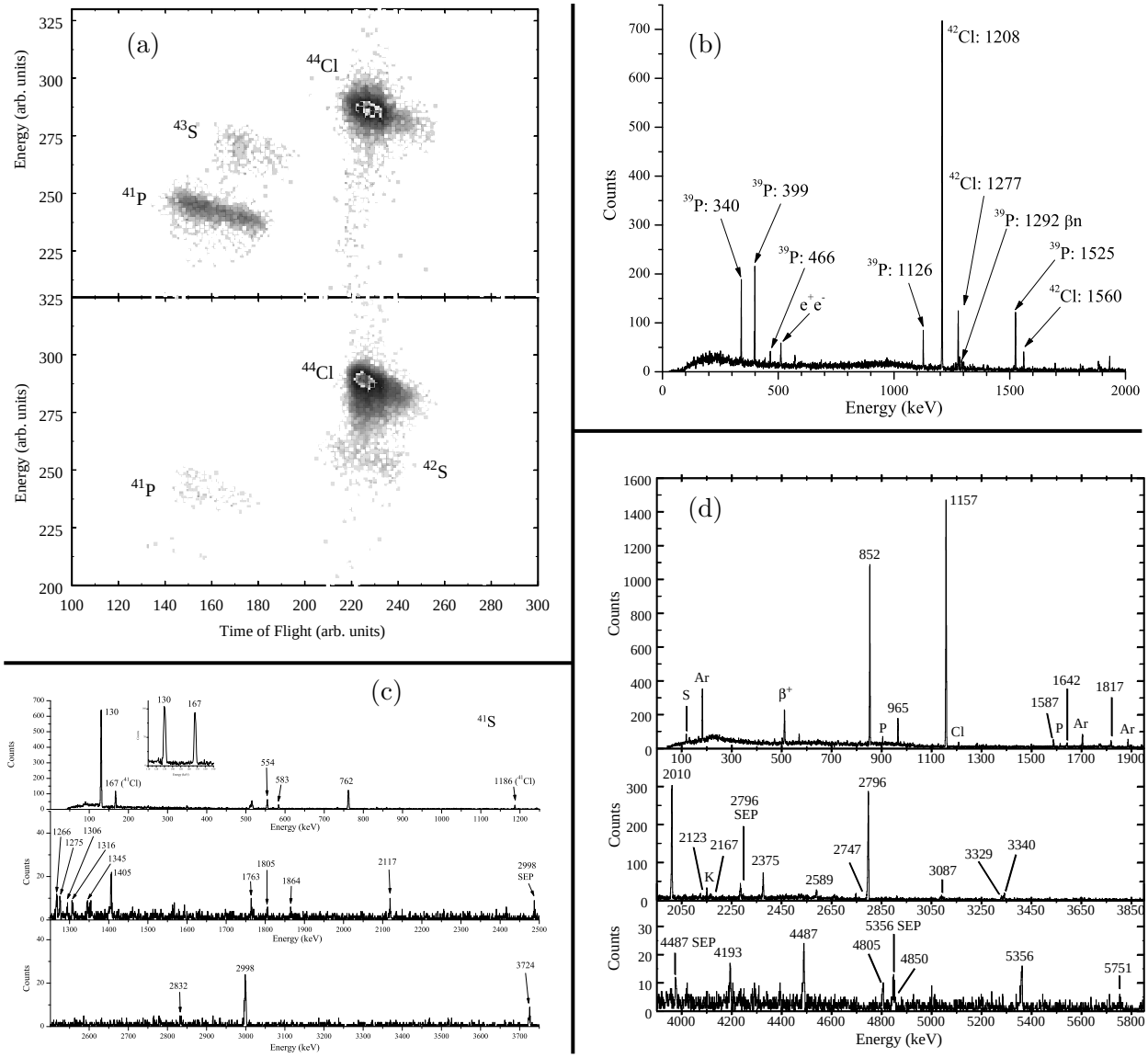

Figure 4.5: a) Particle identification (PID) plot for two A1200 settings. b) γ-ray spectrum for ^{39}P β decay showing the effect of a strong contaminant in the spectrum (^{42}Cl). c) γ-ray spectrum for an A1200 setting which yields nearly pure ^{41}S. The main spectrum was obtained with the wheel cycle optimize ^{41}S relative to its daughter ^{41}Cl. The inset shows a comparison of the two primary γ rays in a saturation spectrum. d) γ-ray spectrum from ^{44}Cl β decayutilizing an A1200 tune and a time cycle where it is enhanced relative to other beam components as well as its daughter.

half-life measurements were made for ^{39}P (0.25(8) s), ^{41}P (100(5) ms), and ^{43}S (282(27) ms).[Gre04] Only the ^{41}P value is an improvement over the vales we obtained, and it is not clear why the two values differ so significantly. For ^{41}S, ours remains the only measured value.

With a goal of observing the β decay of ^{42}P it was also necessary to understand the decays of all the other nuclides in the beam. This was the reason to obtain data on the afore mentioned nuclides. Our system precluded the use of direct tagging to obtain ion-γ correlated events. To understand the problem and the quality of the data obtained, consider the information presented in Fig. 4.5 on the preceding page. Fig. 4.5a shows a PID plot showing two A1200 settings in which ^{44}Cl is the dominant component in both situations. In order to understand the decays of ^{41}P and ^{41,42}S would require also measuring ^{44}Cl. The situation for ^{39}P is similar to that shown in the upper portion of Fig. 4.5a except that all the masses are lowered by 2. Hence, ^{42}Cl will dominate the γ-ray spectrum. This is indeed seen in Fig. 4.5b. Even though the ^{39}P β-decay γ rays are not dominant, it is still possible to extract quality results. This is aided by the slight change in the tune of the A1200 (e.g., Fig. 4.5a lower portion) which allows an almost pure beam for the dominant beam component. This yields spectra like Fig. 4.5c (^{41}S) and Fig. 4.5d (^{44}Cl) which can be used to identify all γ rays associated with these strong beam components making it possible to identify the lower relative intensity γ ray at the other A1200 settings which come from the weaker beam components. The usefulness of the a single beam component within a mass chain is shown in inset of Fig. 4.5c where the strongest γ ray from the daughter ^{42}Cl does not become dominant even in a saturation spectrum. Instead, a comparison of the intensities of these γ rays allows determination of the absolute branching ratios including β-delayed neutron emission probabilities. At the optimal A1200 setting for ^{42}P production, the dominant beam component was ^{45}Cl, however we also needed to know details in the $A=41$ β-decay chain to check from γ rays form β-delayed neutron emission.

Both ^{39}P and ^{41}P were weak components in the beam compared to the sulphur and chlorine isotopes which came with them. This severely limited the data obtained for these two decays. Nevertheless, we were able to obtain preliminary decay schemes for both nuclei (see Fig. 4.6 on the next page). For ^{39}P β decay we associated 9 γ ray with the decay thus establishing 6 excited states in ^{39}S. This was complicated by a strong ^{42}Cl contaminant where the γ-ray intensity of the 1525-keV transition was only 4% the intensity of the 1207-keV γ ray from ^{42}Cl decay. The γ rays at 340-, 399-, and 466-keV were previously observed in ^{40}P β decay,[Win01] but a level scheme was not published. Both the 139-1386 and 1077-465 cascades could be reversed since there is no evidence to favor one sequence over the other. In addition to the γ rays shown, we also observe a 1292.1-keV γ ray from the β-delayed neutron branch. An attempt was made to establish the absolute branching ratio for the decay based on comparison to known members of the $A=39$ β-decay chain. However, this result was inconsistent resulting in greater than 100% feeding to states in ^{39}S. This calls into question the published branching ratios for the ^{39}S and ^{39}Cl The level feedings given in Fig. 4.6a are based on the assumption that there is no feeding to the lowest two states in ^{39}S and using a β-delayed neutron emission probability ($P_{\beta n}$ value) based on comparison to the $A=38$ branch. There is apparent feeding to three states which are fed by allowed or first forbidden β transitions. There is strong evidence for a 59-keV isomeric state which has not been observed in other studies. The situation for ^{41}P was even worse where it was an even smaller component of the beam. We only able to positively identify 4 γ ray associated with this decay provisionally establishing 3 excited states in ^{41}S as seen in Fig. 4.6. Since the γ rays in both cascades have equal intensity, the ordering of the cascades could be switched. Hence, only the state at 2116 keV is firmly established. This is also the only state with direct β feeding since a direct decay to the ground state is highly forbidden. We also observed the 903.6-keV γ ray from the β-delayed neutron branch. We were unable to establish an absolute branching ratio for the decay, nor obtain an estimate for the $P_{\beta n}$ value. However, the intensity of the 904-keV γ ray is larger than any of the other 4 transitions

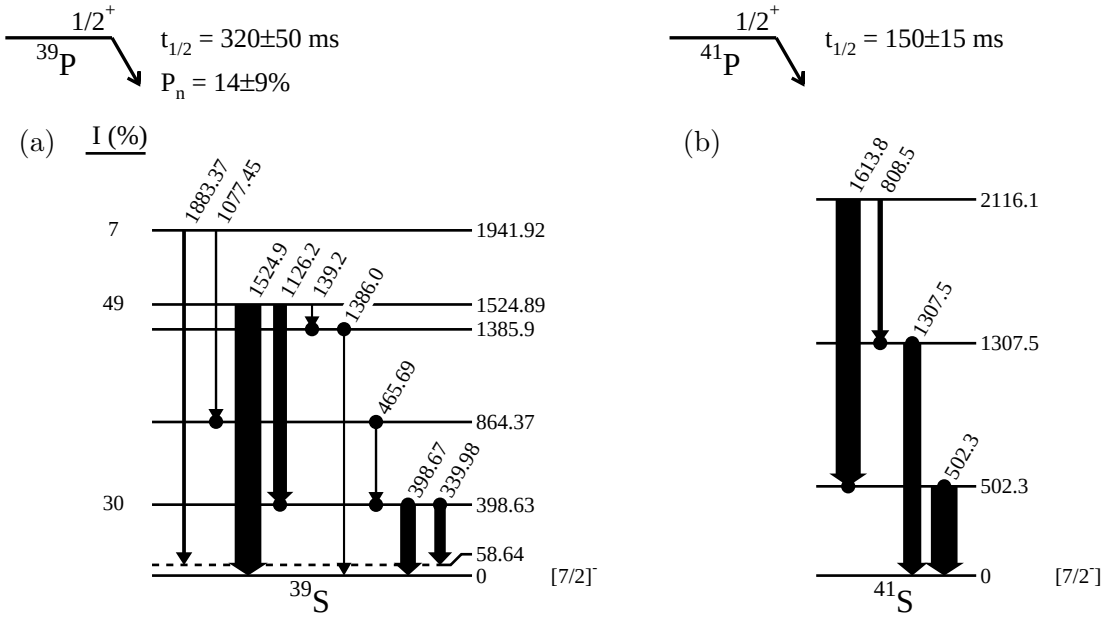

Figure 4.6: Preliminary decay schemes for a) ^{39}P and b) ^{41}P. The half-lives were measured in this experiment (Fig. 4.4), as well as the $P_{\beta n}$value.

indicating that the $P_{\beta n}$ value is very large. Assuming all the β feeding is observed in the γ ray, which is highly unlikely, yields $P_{\beta n}$= 48(6)%. This is consistent with the value of 30(10)% reported in Ref. [Lew89], but slightly larger suggesting some missing feeding in the β branch. This later situation is probable since $S_n = 4242(6)$ keV for ^{41}S.

The β decay of ^{41}S was studied using an A1200 setting which yielded a pure beam. This fact is evident in the γ-ray spectrum shown in Fig. 4.5c which has γ rays only from the $A = 41$ mass chain. It was studied primarily to establish the γ rays associated with the β-decay daughters and granddaughters of ^{41}P to aid in the analysis of that nuclide. The cleanliness of the beam and good statistics allowed for detailed study of this decay as seen in Fig. 4.7 on the following page. A total of 48 γ rays are placed in the decay scheme establishing 25 excited states in ^{41}Cl. The five states indicated with spins and parities correspond to the yrast band as determined by Ollier *et al.*[Oll03] The absolute branching ratio for the 761-keV γ ray was determined to be 0.37(8) by comparison to the 1293-keV γ ray from $^{41Ar}\beta$ decay. A primary source of uncertainty in the branching ratio determination was due to the mass chain not being in equilibrium. This resulted from the very long half-life (109.61 minutes) for ^{41}Ar decay. The data also allowed construction of a decay scheme for ^{41}Cl shown in Fig. 4.8 on page 30 involving 26 γ rays and 13 excited states in ^{41}Ar. There is good agreement with Ref. [Huc81], but with many more details presented. For this decay the absolute branching ratio for the 1186-keV γ ray was determined to be 0.38(8). As expected, the decay proceeds primarily by allowed and first forbidden β decays to $1/2^{\pm}$ and $3/2^{\pm}$ state in ^{41}Ar.

The β decay of ^{43}S was studied because of its significant production at the desired A1200 setting to observe ^{42}P β decay. The beam was primarily composed of both ^{43}S and ^{45}Cl, which will be discussed later. This represents the first detailed β-decay spectroscopy measurement for this nuclide. We were able to identify 14 γ rays which were placed into a decay scheme with 11 excited states as shown in Fig. 4.9 on page 31. Three additional γ rays were associated with the decay, but were not placed into the level scheme. A further 11 γ rays were observed in the spectrum but

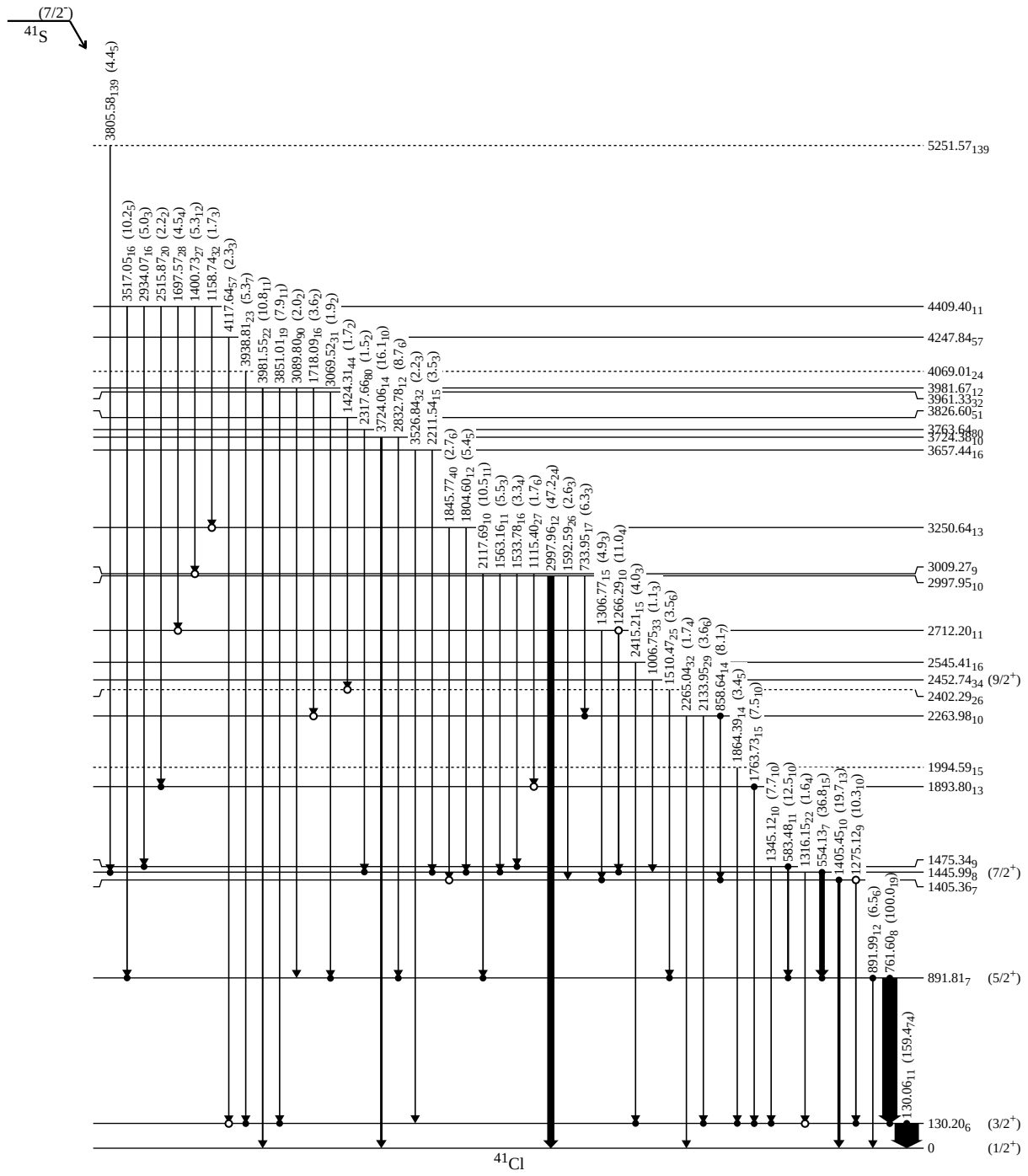

Figure 4.7: Preliminary decay scheme for ^{41}S. The designated spins and parities are based on a deep-inelastic collision measurement which populated the yrast states.[Oll03] Closed circles indicae definite coincidences while open circles indicate possible coincidences.

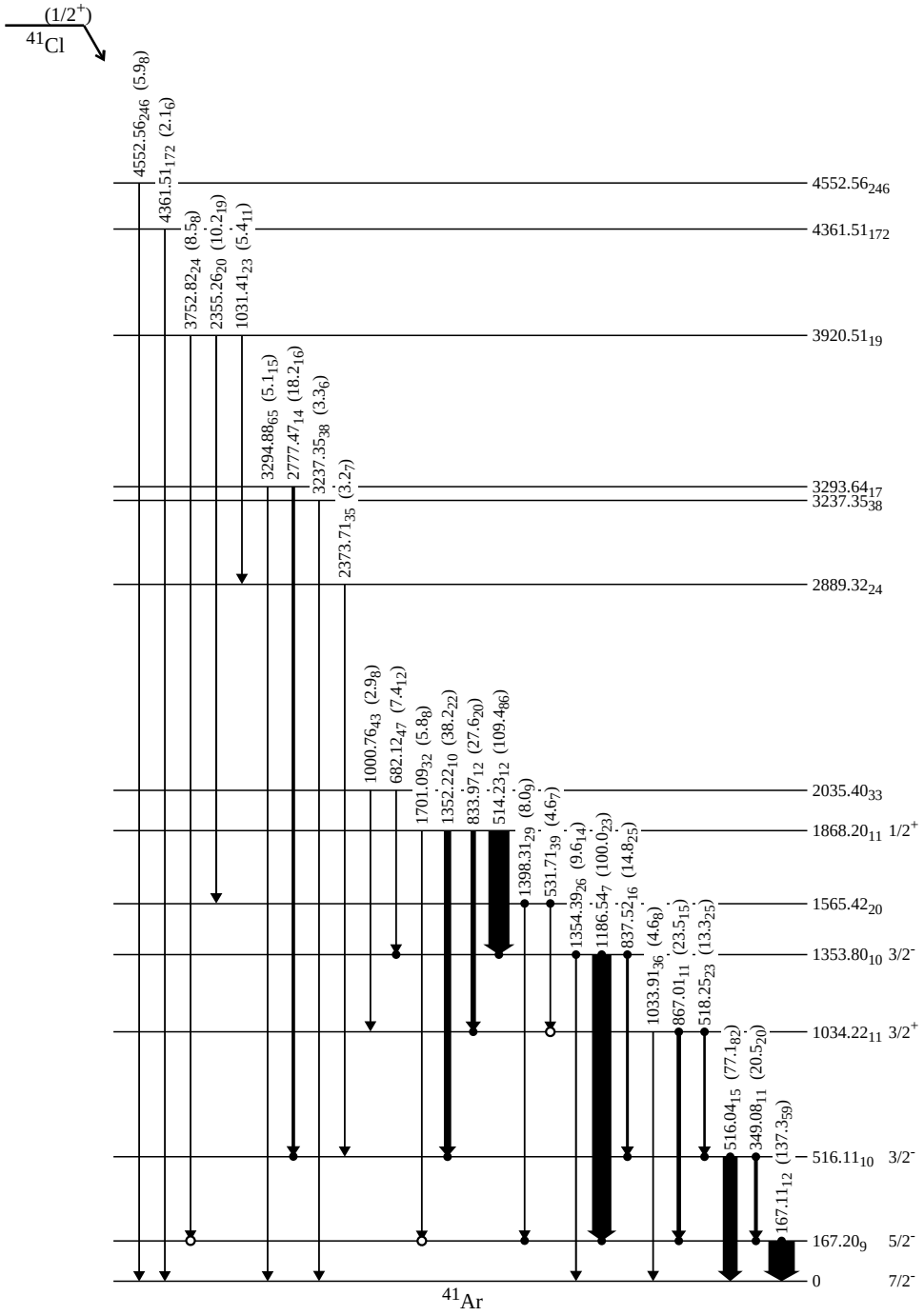

Figure 4.8: Preliminary decay scheme for ^{41}Cl. Spin and parity assignments come from the NNDC.[NNDC] Closed circles indicae definite coincidences while open circles indicate possible coincidences.

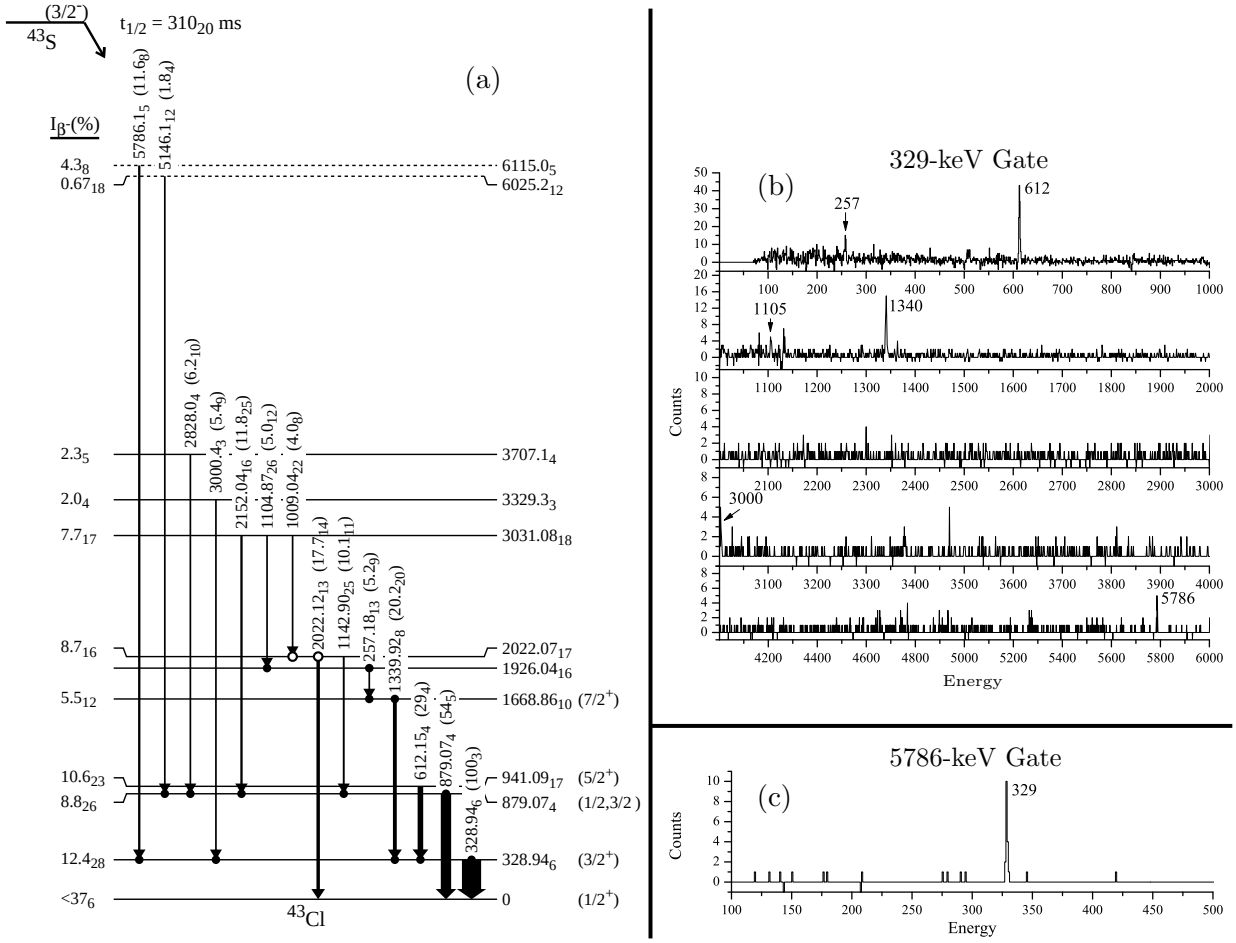

Figure 4.9: a) Preliminary decay schemes for ^{43}S. Spin and parity assignments come from the NNDC.[NNDC] Closed circles indicae definite coincidences while open circles indicate possible coincidences. The half-life was measured in this experiment (Fig. 4.4. b) $\gamma\gamma$-coincidence spectrum gated on the 329-keV γ ray. c) $\gamma\gamma$-coincidence spectrum gated on the 5786-keV γ ray.

not assigned to any specific decay. The levels in Fig. 4.9a are well established by $\gamma\gamma$ coincidence data. The ordering of the 1105-257 cascade cannot be determined from this data, but Stroberg *et al.* did not observe the 1105-keV γ ray suggesting that the 257-keV line does lie lower in the decay scheme.[Str12] We also provide strong evidence for the 1340-keV γ ray to de-excite a level at 1669 keV as suggested by Stroberg *et al.*[Str12]

The absolute branching ratio for the 329-keV γ ray was determined be 0.37(6) by comparison in a saturation spectrum to known γ rays form ^{43}Cl and ^{43}Ar β decay. This value was used to estimate the level feedings shown in Fig. 4.9a. Based on a proposed $3/2^-$ ground state for ^{43}S, we expect to observe allowed decays to $1/2^-$, $3/2^-$, and $5/2^-$ states and first forbidden decays to $1/2^+$, $3/2^+$, and $5/2^+$ states. Feeding by a first forbidden unique decay would be significantly hindered relative to the other decays. For the states with known spin and parity values this appears to be correct. The only exception is the apparent feeding to the 1669-keV $7/2^+$ state. It is certainly possible that there is missing feeding into this state which would reduce the total observed direct feeding. However, there is no reasonable evidence in the 1340-keV $\gamma\gamma$ coincidence gate to suggest any other

strong transitions feeding this state, and the strongest of the unplaced and unassigned γ rays would be evident. This seems to indicate that the 1669-keV state is actually an expected $5/2^+$ state from the two theoretical calculations given in Ref. [Str12], while the 1926-keV level which has no apparent feeding is actually the $7/2^+$ state. The 257-1340-329 cascade would then be similar to the 554-761-130 cascade observed in ^{41}Cl. By comparison to the theoretical calculations, the 879-keV state would correspond to the expected $3/2^+$ member of the doublet of states near 1 MeV. The 2022-keV state is also not likely to be the second $7/2^+$ state expected from the SDPF-U calculation, but instead must be related to one of the lower-spin states predicted by the EPQQM calculation.[Str12] Since M1 transitions appear to dominate between the states below 2 MeV in ^{43}Cl, the observation connections to the $1/2^+$ ground state and the 879-keV $3/2^+$ state by transitions of similar intensity suggest this might be a $1/2^+$ state.

However, there is a problem with the decay scheme as it is presented. Specifically, the two γ rays coming from the states above 6 MeV should not exist because Q_{β^-} is less than 5 MeV for ^{43}S according to Ref. [AME12]. The value in the mass evaluation is based on systematics, but such a large deviation is not likely. Nevertheless, the placement is based on strong coincidence data. For example, the 5786-keV γ ray is clearly seen in the 329-keV $\gamma\gamma$ coincidence gate (Fig. 4.9b), while the 329-keV γ ray is seen in the 5787-keV gate (Fig. 4.9c). The fact that the 5786-keV γ ray is not seen in the 879-keV coincidence gate, but instead a 5146-keV γ ray is observed indicates that the coincidence is not due to a "glitch" in the data. In fact, the γ-ray singles spectrum clearly show peaks at these energies and no similar peaks are observed at other A1200 settings. This mystery needs to be resolved before publication of the results.

^{44}Cl was another case where an essentially pure beam was obtained as is seen in the lower half of the PID plot shown in Fig. 4.5a. This resulted in the γ ray spectrum seen in Fig. 4.5d. Data were taken with a short cycle and an approximate "saturation" spectrum. The data was then analyzed in two sets: the "saturation" data, and a sum of all data. This was done independently for each detector and average values for energies and intensities were obtained. A total of 39 γ rays were associated with ^{44}Cl β decay while we have placed 23 γ rays in a decay scheme containing 11 excited states as seen in Fig. 4.10a. Additional γ rays will be placed based on $\gamma\gamma$ coincidences, we are just trying to confirm placement before adding them to the decay scheme. The most intense γ ray observed in the decay is at 1157.72(8) keV. This was a problem since the strongest transition from ^{44}K occurs at 1157.018(3) keV. Although the two unresolved γ rays were fit as separate peaks in the spectrum, we did some additional checks to determine whether the intensity was properly split between the two γ rays. The first check involved comparison of the 1157-keV γ ray from ^{44}K to the 2150-keV γ ray from the same decay to determine the expected number of counts in the fitted peak for ^{44}K. As a second check, a comparison of the area of the 1157-keV γ ray from ^{44}Cl was compared to the area of the 852-keV γ ray from the same decay in the full data set and the ratio was used to estimate the peak area in the saturation spectrum. For both checks, the estimated peak areas were in agreement with the fitted values. Having consistently established the peak areas for the 1157-keV γ rays, we were then able to establish viable relative intensities.

The ground state of ^{44}Cl is proposed to be highly mixed state composed of the $(\pi d_{3/2})^3 \otimes (\nu f_{7/2})^7$ configuration and the $(\pi s_{1/2})^1 \otimes (\nu p_{3/2})^1$ configuration leading to a 2^- state.[Ryd10] This suggests that any direct β-decay feeding to the ground state will be small. We can test this hypothesis by determining the absolute branching ratio for the 1157-keV γ ray. This was done by a comparison of the intensity for this line to six γ rays from the decay of ^{44}K in a long ("saturation") data run. Due to the long half-lives of the daughter nuclei, a true saturation spectrum was not obtained. However, it was easy enough to determine the saturation fraction for the decays from the run parameters. It was also necessary to take into account a possible β-delayed neutron branch ($P_{\beta n} < 8\%$[Sor95]). We observed a weak 975-keV γ ray which we associated with ^{43}Ar β decay. Determination of the

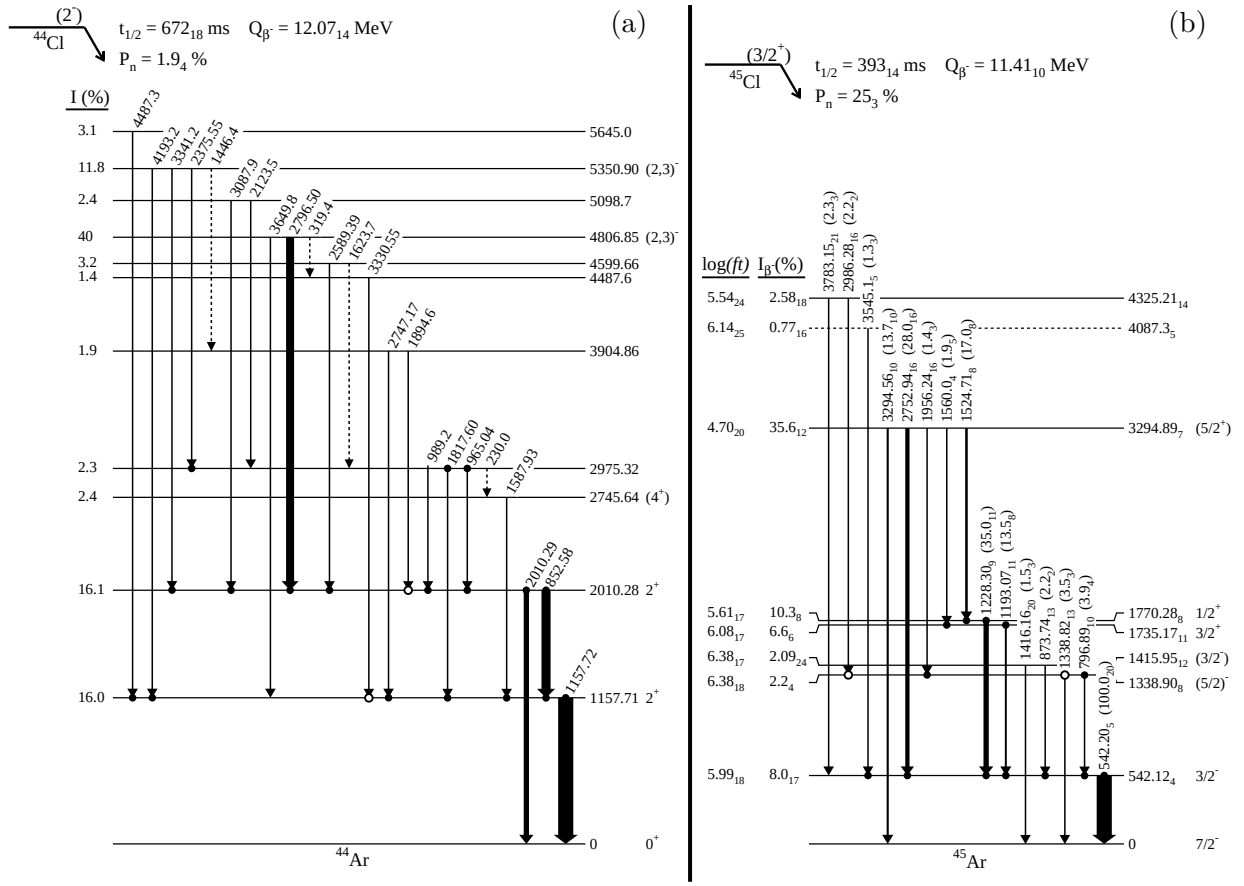

Figure 4.10: Preliminary decay schemes for a) ^{44}Cl and b) ^{45}Cl. Closed circles indicae definite coincidences while open circles indicate possible coincidences. Spin and parity assignments are based on the current measurement along with comparison to other experiments[NNDC] as discussed in the text. The half-life and $P_{\beta n}$ values were measured in this experiment (Fig. 4.4). The Q_β value comes from the NNDC.[NNDC]

β and βn branching percentages involved comparison of the relative intensities of γ rays from the daughter and granddaughter decays to the 1157-keV γ ray from ^{44}Cl decay. It was very evident from this analysis that the absolute branching ratio for ^{44}Ar β decay as given in the NNDC database (66(9)%)[NNDC] is incorrect since this value would require greater than 100% feeding through the 1157-keV γ ray. Therefore, determination of the feeding through the β branch was based on comparison to the six strongest transitions from ^{44}K β decay. This results in an absolute branching ratio for the 1157-keV γ ray of 75(13)% where the primary source of uncertainty is from the absolute branching ratio for the ^{44}K β decay. We also estimate $P_{\beta n}$= 1.9(4)% for ^{44}Cl. Finally, our analysis indicates the correct branching ratio for ^{44}Ar should be 34(7)%. (This value includes the results from ^{45}Cl β decay as well.) Applying our absolute branching ratio to the decay scheme yields the apparent level feedings presented in Fig. 4.10a. Although it is likely that there are γ rays are missing from the scheme and we do have 21% relative intensity of γ rays that are not currently placed, these γ rays will not affect the overall feeding to excited state unless they connect directly to the ground state. E.g., any γ ray that feeds into the 1157-keV level will reduce the feeding to that level but shift an equal amount of intensity to a higher-energy excited state, thus not changing the total observed feeding. The sum of the observed feeding was found to be 101(9)% strongly indicating that no direct feeding to the grand state has been missed. This also places the lowest spin states not having a ground-state transition to be 2^+ or 2^-. Furthermore, any unplaced feeding probably goes through the first two excited states thus reducing the feeding to these states. Since there does not appear to be any direct feeding to the ground state, we can also estimate the absolute branching ratio by using the total observed relative intensity feeding the excited states. The resulting value is 74.1(25)%. Although the later value is more precise and in agreement with the previous value, we have retained 75(13)% for further analysis.

The first two excited states in ^{44}Ar are well established by strong coincidence relationships. They have also been observed in multiple experiments.[NNDC] The 2^+ assignment for the 2010-keV state is based on the strong ground state transition,and is confirmed by a Coulomb Excitation measurement.[Zie09] The apparent level feedings for these states does seem high, but, as explained previously, they are over estimates since many unplaced γ rays will feed through these levels. The apparent level feedings for the other states shown in Fig. 4.10 suggest first forbidden decays to all states except the levels at 4807 and 5351 keV. The 2746-keV level has been more contentious. We do observe a 2746-keV γ ray with a relative intensity of 1.72(16)%. However, this transition has a definite coincidence with the 1158-keV γ ray, and is place as feeding the first excited state. Therefore, we do not see any evidence for a strong ground-state transition as originally suggested and listed at the NNDC.[NNDC] The lack of a ground-state transition then suggests either a 0^+ or 4^+ assignment, while a first forbidden β decay is consistent with a 1^+, 2^+, or 3^+ state. However there is again a strong probably that we are missing some γ rays which feed into this level. The state has been observed in subsequent experiments[For00, Men10] and seems to be solidly a 4^+ state. The states above 2900 keV have only been identified in this β-decay study. The state at 2975-keV has a β feeding and decay pattern which is consistent with being either a 3^+ or 4^+ state. The former would be consistent with shell-model calculations which predict a 3^+ state just above the first 4^+ state.[Ret97] The strong β-decay feeding to the 4807 and 5351-keV states suggests that these are negative parity states with a spin between 1 and 3. The lack of a ground state E1 transition from either of these levels eliminates a possible 1^- assignment. These negative parity states would require breaking of a neutron pair or some type of deformation.

The beam purity for the study of ^{45}Cl β decay was even better than for ^{44}Cl since all contaminants could be removed. The reason for studying this decay was because it was the strongest beam component at the optimal setting for observing ^{42}P, the primary focus of the measurement. Due to the beam purity, we were able to associate positively associate nearly all the observed γ ray in

the β-gated γ-ray spectrum with a member of the decay chain. Hence, of the 59 γ rays observed, only 2 have not been assigned to a decay. For ^{45}Cl we have associated 17 γ rays with the decay and 15 placed in the level scheme for ^{45}Ar while the other two (852- and 1157-keV) come from feeding states in ^{44}Ar in the βn branch. Since the γ rays for other members of the decay chain are fairly well known, it is likely the two unplaced γ rays are also associated with ^{45}Cl β-decay . The ^{45}Cl decay scheme is seen in Fig. 4.10 on page 33. As with ^{44}Cl, we had to check the splitting of intensity between unresolved doublets. In all cases, the estimated counts matched well with the values obtained by fitting the spectra.

The absolute branching ratio for the 542-keV γ ray was determined in two ways. First, comparison was made to known transitions in the daughters and granddaughters in a "saturation" spectrum as was outlined previously. The comparison involved γ rays the the decays of ^{44,45}K and ^{45}Ar, with the ^{44}Ar result being rejected as discussed previously. There was no discrepancy between the values obtained for the $A=45$ decay chain, so both of these values were treated equally. This analysis results in an absolute branching ratio for the 542-keV γ ray of 59(6)%. The analysis also gives $P_{\beta n}$= 25(3)% in agreement with the previously measured value of 24(4)%.[Sor04] Second, the absolute branching ratio was measured directly by comparison of the number of counts observed in the 542-keV peak to the total number of ^{45}Cl measured in the PID spectrum. This analysis results in a value of 57(5)%. The weighted average of these values, and our accepted value for the absolute branching ratio, is 57(4)%. This value was then used to establish the level feedings and $\log(ft)$ values shown in Fig. 4.10b.

The total observed feeding for ^{45}Cl β decay is 93(4)%, leaving only 7(4)% missing. The two unplaced γ rays have a total absolute intensity of only 0.9(3)%, so placing these transitions as feeding the ground state cannot account for all the missing intensity. It is possible that there are numerous additional unobserved γ rays which feed directly to the ground state which would reduce the fraction of the missing feeding which is due to direct β decay to the ground state. However, we cannot discount the possibility of direct feeding to the ground state of about 5%. This level of feeding would be consistent with a first forbidden decay. The ground state of ^{45}Cl has been proposed to be $1/2^+$.[Gad06] (A $3/2^+$ ground state is also possible as discussed later.) A first forbidden decay from a $1/2^+$ state would go to a $1/2^-$ or $3/2^-$ state. The ground state of ^{45}Ar has been determined in particle transfer reactions to be an $L=3$, $7/2^-$ state corresponding to a single hole in the $\nu f_{7/2}$ orbital.[Gau08, Lu13] Therefore direct β decay to the ground state is forbidden. Consequently, we would not expect to see any measurable feeding to the ground state thus indicating that the missing feeding must come from either unobserved γ rays which feed directly to the ground state or through other unplaced transitions for levels not connected to the current decay scheme, or the absolute branching ratio is wrong. To test the latter situation, we can estimate the absolute branching ratio by assuming no feeding to the ground state. This requires changing the absolute branching ratio to 63(4)%. Although this value would give better consistency with a propose $1/2^+$ ^{45}Cl ground state, we choose to retain the previously presented value which is based on known situations.

The observed level feedings and $\log(ft)$ values in Fig. 4.10b can help in understanding the possible spin/parity assignments for the observed levels. The $3/2^-$ first excited state has been established in numerous experiments,[NNDC] and is associated with hole in the $\nu p_{3/2}$ orbital.[Gau08, Lu13] This is consistent with the observed feeding which suggest a first-forbidden β decay from either a $1/2^+$ or $3/2^+$ ground state. The 1339- and 1416-keV levels have β-decay feeding consistent with a first forbidden decay suggesting these are negative parity states ($1/2^-$, $3/2^-$, or $5/2^-$). The observed transitions to the ground and first excited states restricts these two $3/2^-$ and $5/2^-$. Dombrádi *et al.* observed a state at 1352 keV for which they suggest a minimum spin of 5/2, while Gaudefroy *et al.* observe an $L=1$ state at 1420 keV. These states could correspond to those observed in this study. Both papers present shell model calculations which predict closely spaced

$3/2^-$ and $5/2^-$ states near these energies. It is certainly reasonable to assume that the observed states correspond to those predicted by the shell model, but there is no clear way to determine an assignment. However, based on both experimental observations and the shell model calculations, we propose $5/2^-$ and $3/2^-$ for the 1339- and 1416-keV levels, respectively. States at 1735- and 1770-keV have been identified as a $L = 2$, $3/2^+$ ($\nu {d_{3/2}}^{-1}$) state and a $L = 0$, $1/2^+$ ($\nu {s_{1/2}}^{-1}$) state, respectively, in a p(^{46}Ar,d)^{45}Ar pickup reaction.[Lu13] The two states at the same energy observed in this measurement are likely to correspond to these two states, although the shell model calculations predict an additional $1/2^-$ state near 1750 keV.[Dom03, Gau08] The level feeding to these states does show an increase over the states at lower energies, and the $\log(ft)$ values, although not strongly indicative of an allowed β transition, are consistent with this assignment. Both states de-excite only by transitions to the $3/2^-$ first excited state which would be consistent with a E1 multipolarity for the γ rays. However, a $1/2^-$ state would also not show a ground-state transition. Nevertheless, we believe these two states to correspond to the two positive parity states while expecting that the $1/2^-$ state must not be fed in the decay for reasons to be argued shortly. The state at 3295 keV provides the key to solidify some spin/parity assignments. The state is strongly fed in β decay indicating an allowed transition to a $1/2^+$, $3/2^+$, or $5/2^+$ state. However, the strong transitions (E1) to the ground and first excites states limits the spin/parity assignment to $5/2^+$. This assignment is also consistent with the observed transitions to the $3/2^+$ and $1/2^+$ states. Based on the observed γ-ray transitions, we assume this is most likely the $\nu d_{5/2}$ single hole state. This means that the ground state of ^{45}Cl cannot be $1/2^+$ as proposed by Gade *et al.*,[Gad06] but is the $\pi d_{3/2}$ state proposed by Stroberg *et al.*[Str12] This explains why the expected $1/2^-$ states are not observed since they would require a much weaker first-forbidden unique β decay. It also allows for the possibility of direct feeding to the ground state by a first forbidden transition at the 5% level as mentioned earlier. The two states above 4 MeV cannot be given firm spin/parity assignments, and it is not clear that either corresponds to a state observed in previous measurements. However, some limits can be placed on the possible spin/parity assignments. We will assume that E1 transitions will dominate over M1/E2 transitions since there are multiple paths available for either type of transition. Both states then exhibit E1 transitions to negative parity states suggesting that they are of positive parity. Although the feeding is weaker than expected to the 4087-keV level, the $\log(ft)$ values are consistent with allowed transitions. The lack of a ground-state transition rules out a $5/2^+$ assignment, so these are most likely $1/2^+$ or $3/2^+$ states.

The last NSCL experiment (June 1999) was a search for single particle states in the ^{32}Mg region. The primary goal of the experiment was to study the β decay of ^{33}Mg into single proton excited states in ^{33}Al. In addition, we would obtain information on the β decays of ^{33,34,35}Al. This was the last experiment run with the A1200 separator prior to the shutdown of the NSCL for the Coupled Cyclotron Facility (CCF) upgrade. Several issues cropped up during the experiment which resulted in marginal results. First, the HPGe detector behind the catcher foil exhibited poor resolution which may have been due to light ions punching through the catcher foil and β detector into the HPGe detector. This left only one detector providing viable results. Second, the catcher wheel frequently became detached from the stepper motor axle due to the rapid timing cycles needed for the very short half-lives being studied. This was compensated for by pulsing the beam on and off on the same target for several cycles before having the wheel rotate. However, it took time to work out this solution to the problem. Finally, the production rates were not as high as predicted. Nevertheless, we were able to obtain reasonable data for each of the aluminum decays. Some of the results are presented in Fig. 4.11 on the following page.

During the analysis we became aware of a measurement from ISOLDE on the β decay of ^{34,35}Al.[Num01] Our results are very comparable to those of the ISOLDE experiment. For example, our measured half-lives ^{34}Al (54.5(24)ms, see Fig. 4.11b) and ^{35}Al (41(4)ms) were consistent with

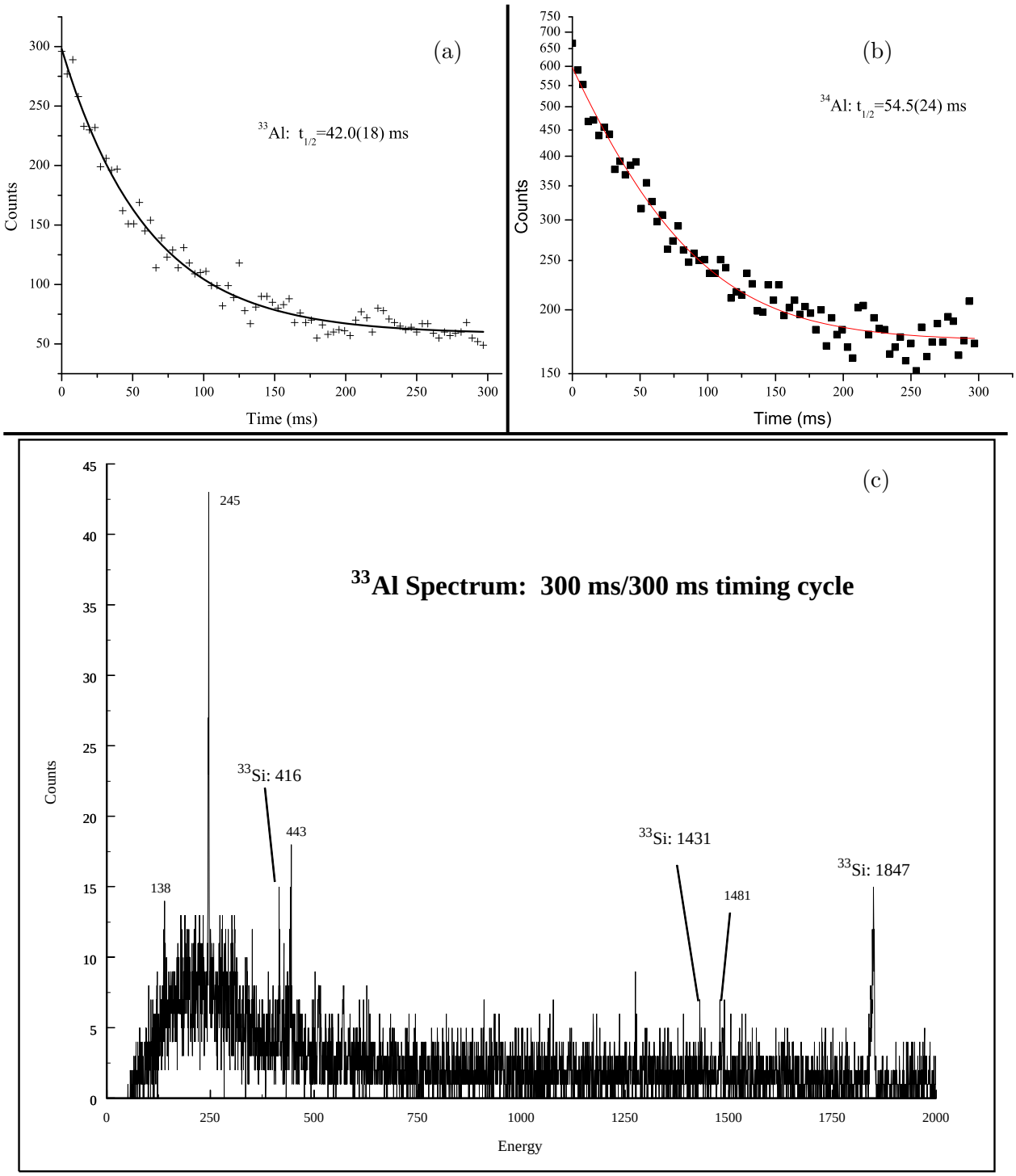

Figure 4.11: a) Half-life curve for ^{33}Al taken from the β detector. b) Half-life curve for ^{34}Al taken from the β detector. c) γ-ray spectrum for ^{33}Al β decay.

their measured values of 56.3(5)ms and 38.6(4)ms, respectively. We identified almost all the same γ rays as in the ISOLDE experiment with consistent intensities. Since our results were not an improvement on their results, no further analysis was performed.

The analysis for the ^{33}Mg and ^{33}Al β decays continued with identification of several new γ rays (Fig. 4.11) and a half-life measurement for ^{33}Al. The ^{33}Al data was obtained in order to distinguish between ^{33}Mg and ^{33}Al β-decay γ rays. At the optimal A1200 setting for ^{33}Mg the beam components included ^{34,35}Al and ^{36}Si, hence the decision to look into ^{34,35}Al. (^{36}Si had been studied previously.[NNDC]) However we obtained no conclusive evidence in the data for γ rays from ^{33}Mg, nor did we observe any γ rays from the $A = 33$ β-decay chain. This left ^{33}Al as the best shot for obtaining a publishable result. As seen in Fig. 4.11c, we observed several γ rays in a spectrum obtained with a nearly pure beam. The main contaminants in the beam were ^{30}Na and ^{31,32}Mg. The peak at 1481-keV is likely to be from ^{31}Na β decay. No observed γ rays are assigned to either ^{31,32}Mg β decay. Although ^{31}Mg was the strongest contaminant in the beam, its half-life of 236(20)ms resulted in it being significantly reduced in the short timing cycle used in the measurement. We end up with two γ rays which seem to be from ^{33}Al β decay, 245 and 443 keV. The strength of the 245-keV line suggests a significant feeding through this transition. By this point the CCF and A1900 had been completed. Since the ^{33}Mg β-decay experiment had been inconclusive, a group at the NSCL decided to redo the experiment using a tagging technique.[Mor02] They were able to measure a half-life (90.5(16)ms) for ^{33}Mg, but observed no γ rays. They also measured the half-life (41.7(2)ms compared to our value of 42.0(18)ms) for ^{33}Al and associate three γ rays with this decay: 1010, 1941, and 4341 keV. All three γ rays are only weakly fed in the β decay, and we did not observe any of these transitions. This severely called into question the veracity of our results. The first question to ask is if the two γ rays could come from a different source in the beam? The lack of other beam components in the PID spectrum seems to rule this out. With the low Z and high beam energy, all the ions should be fully stripped, and there is no evidence for different charge states. Second, could the γ rays come from a process other than de-excitation of an excited state fed by β decay? The two γ rays do have nearly identical intensities, so it is possible they could come as a cascade from an isomeric state. This seems unlikely since a $\beta\gamma$ coincidence was required, and any delay would have negated the coincidence. There has also been no evidence in either ^{33}Al or ^{33}Si for such a state in subsequent experiments. Therefore, the source for these two γ rays remains a mystery.

4.2 HRIBF Experiments

4.2.1 Large β-delayed neutron emission probabilities in the ^{78}Ni region

Absolute βn emission probabilities ($P_{\beta n}$) are notoriously difficult to measure because of the experimental problems associated with neutron counting and the contamination of the samples. Using experimental data taken HRIBF, we demonstrated that existing data might be unreliable.[Win09]

To address the difficult task of making reliable $P_{\beta n}$ measurements, a new technique using γ spectroscopy of isotopically purified beams of neutron-rich nuclei was developed at the HRIBF. Beams of Cu and Ga ions were were mass separated, passed through a charge exchange cell to produce negative ions and sent through a high resolution mass separator prior to acceleration in the HRIBF Tandem accelerator. The ions were tagged in time using a microchannel plate (MCP) detector [Sha00], passed through a six-segment ionization chamber (IC) [Gro05] filled with CF_4, and implanted onto the tape of a Moving Tape Collector (MTC). The atomic number Z of the ions passing through the IC could be clearly identified by energy loss. This permitted easy tuning of the high-resolution isobar separator to optimize the beam for rate and purity. For example, when tuning the mass 76 isobars the rate for ^{76}Ga was reduced by a factor of 60 compared to ^{76}Cu while reducing the maximum achieved ^{76}Cu rate by only $\sim$30%. The collected sources were observed by four Ge clover detectors and two plastic β detectors which surrounded the beam pipe. All detector signals were processed using digital pulse processing [Grz03]. For ^{76,77}Cu and ^{83}Ga the γ ray singles spectra were analyzed to obtain βn probabilities, while for ^{78}Cu the β-gated γ-ray spectra were used and the appropriate β detection efficiency determined. Representative spectra for the decays of $^{76-78}$Cu are shown in Fig. 4.12a-c.

Two modes of operation were used in the experiment: the "ranging-out" (RO) mode [Gro05] with $\sim$ 200 torr gas pressure in the IC, and the "pass-through" (PT) mode with $\sim$ 100 torr gas pressure in the IC. The RO mode takes advantage of the different stopping powers for the components of the beam. This was further enhanced in the case of Cu ions since negative Zn ions do not form in the charge exchange cell and are removed from the beam before post-acceleration while the remaining $Z > 30$ contaminant isobars could be completely removed. The particle identification plot for the mass 76 isobars in this mode is shown in Fig. 4.12d.

For the RO mode, the MTC collection point was placed within 1 cm of the exit window of the IC and periodically moved to a position at the center of the detector array. With Cu isotopes as the only component of the beam, the timing cycle was designed to maximize the detection rates for γ rays from the Zn daughters, thus precluding its use to study the short-lived Cu isotopes. In PT mode, the ions are implanted on the MTC in the center of the detector array with identification of individual ions in the IC allowing for absolute measurements. Our results are shown in Table 4.1 together with calculations of Ref. [Bor05].

The $P_{\beta n}$ value for ^{76}Cu has been previously reported as 3(2)%[Rud93] and 2.4(5)%[Pfe02]. A recent work on ^{76}Cu decay [Van05] could not find any evidence for βn emission. However, the decay of ^{76}Cu can be considered as a good test case for βn studies since the decays of the daughter nuclei (^{75,76}Zn) are well characterized with known absolute branching ratios [NNDC]. Here, the determination of $P_{\beta n}$ was made by comparing the relative intensities of the 228-keV (^{75}Zn), 199-keV (^{76}Zn) transitions (Fig. 4.12a), and 563-keV (^{76}Ga) γ ray, as well as comparing the absolute intensities of these γ rays to the measured number of ^{76}Cu ions in the IC in order to directly measure $P_{\beta n}$ and P_{β}. Since there is disagreement over the possibility of a β-decaying isomer for ^{76}Cu [Win90, Van05], we present here the result obtained from a saturation measurement using the PT mode with 68% beam purity and no ^{76}Zn present in the beam. For the relative intensity measurement, a $P_{\beta n}$ value of 7.3(6)% was obtained. For the absolute measurement, we obtained

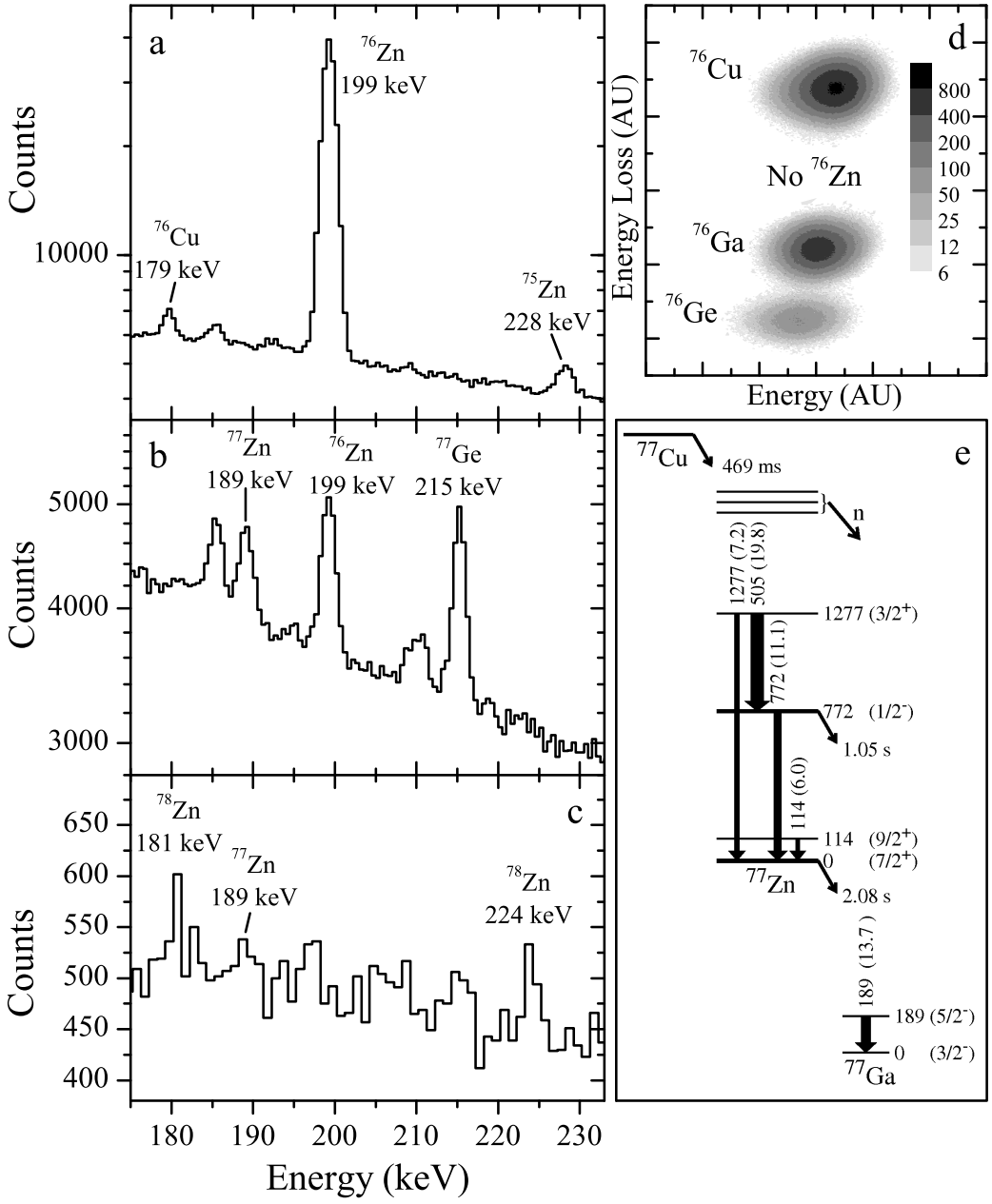

Figure 4.12: The γ-ray spectra recorded for the βn precursors ^{76}Cu (a), ^{77}Cu (b) and ^{78}Cu (c) and showing the decays of respective Zn isotopes used to determine the $P_{\beta n}$ values. For ^{76,77}Cu the γ-ray singles spectra taken in saturation mode are shown. For ^{78}Cu a β-gated spectrum taken using a 5.2 s MTC cycle is shown. For ^{76}Cu, the corresponding particle identification plot for the mass 76 isobars in the RO mode is shown in (d). Zinc ions are removed by the charge exchange cell while the higher-Z components of the beam (^{76}Ga and ^{76}Ge) are stopped by the ion chamber resulting in a pure ^{76}Cu beam. The partial decay scheme for ^{77}Cu indicating the significance of the 772-keV isomer in ^{77}Zn to the $P_{\beta n}$ value analysis is shown in (e). The number in parenthesis following the γ-ray energy is the measured absolute γ-ray intensity from comparison of the γ-ray peak areas to the number of implanted ^{77}Cu ions.

Table 4.1: Measured β-delayed neutron emission probabilities. Mode indicates whether the ranging-out (RO) or pass-through (PT) mode of operation was used. MTC indicates the MTC cycle beam time on or if a saturation (Sat) spectrum was being taken. Rel indicates values obtained by comparison of the relative intensities of the most intense γ rays from nuclides in β and βn branches. Abs indicates values obtained by comparison of absolute intensities of the most intense γ rays from nuclei in the βn branch to the number of ions deposited.

			$P_{\beta n}(\%)$				
						Ref.	
Nuclide	Mode	MTC	Rel	Abs	Adopt	[Bor05]	Theory
^{76}Cu	PT	Sat	7.3_6	7.0_6	7.2_5	4.2	5.6
^{77}Cu	RO	10.2 s	29_3	29_3	30.0_{27}	20	40
		20.2 s	28_4	28.7_{25}			
	PT	7.2 s	31.5_{24}	34.0_{23}			
		Sat	32.1_{21}	28.5_{19}			
^{78}Cu	PT	5.2 s		65_8	65_8	43	53
^{83}Ga	PT	20.2 s		64_3	62.8_{25}	16	51
		Sat		61_4			

values of 7.0(6)% and 88(3)% for $P_{\beta n}$ and P_β, respectively. Although we slightly under estimate the total feeding (95(3)%), the overall agreement is quite good. We use a weighted average of the two results for our adopted value of 7.2(5)%.

The $P_{\beta n}$ value for ^{77}Cu was previously reported as 15^{+10}_{-5}% [Pfe02]. The only information on states in ^{77}Zn prior to this experiment was a 1.05 s $(1/2^-)$ $\nu p_{1/2}$ isomer decaying to the $(7/2^+)$ $\nu g_{9/2}$ ground-state via a 772.4-keV E3 transition [Eks86] and states at 114.9 and 803.6 keV observed in the βn branch of ^{78}Cu decay [Van05]. We have observed over 40 γ rays associated with the β decay of ^{77}Cu. A relevant subset of the decay scheme (to be published in a subsequent paper) is shown in Fig. 4.12e. The assignment of spins and parities is based on systematics and the measured relative γ-ray intensities of the 505 and 1277-keV γ rays which are presumed to be E1 and E2, respectively. A significant amount of difficulty in the analysis is brought about by the presence of the $1/2^-$ ^{77}Zn isomer. The observed intensity of the 772-keV γ ray indicates a 66(5)% β-decay branch from the isomer for which nearly 100% will directly feed the ground state of ^{77}Ga bypassing the 189-keV level. Including this in our analysis, we could determine the appropriate branching through the 189-keV level as well as the effects of the different half-lives for each MTC cycle. A summary of these consistent results is presented in Table 4.1. For the absolute measurement we also obtain a P_β value of 70(7)% indicating that we have correctly accounted for all the β decay intensity. We adopt a $P_{\beta n}$value of 30.0(27)% which is taken from a weighted average of the values from the absolute measurement.

The β decay of ^{78}Cu was measured using the PT mode (see Table 4.1). Determination of the $P_{\beta n}$ value for ^{78}Cu was again hampered by the presence of the isomeric state in ^{77}Zn. Although the 114-keV γ ray is clearly seen in the data, the 189-keV γ ray (^{77gs}Zn$\rightarrow^{77}$Ga*) is surprisingly weak (see Fig. 4.12c). However, it is consistent with the primary βn branch going by way of the $1/2^-$ isomeric state. The β branching probability is based on the 181 and 224-keV γ rays from ^{78}Zn decay which give a P_β of 35(8)%, yielding a value of 65(8)% for the βn probability which is consistent with the *lower limit* of $P_{\beta n} \leq 65(20)$% reported by Van Roosbroeck *et al.*[Van05] but significantly higher than the value of 15^{+10}_{-5} % listed in Ref. [Pfe02]. Van Roosbroeck *et al.* based

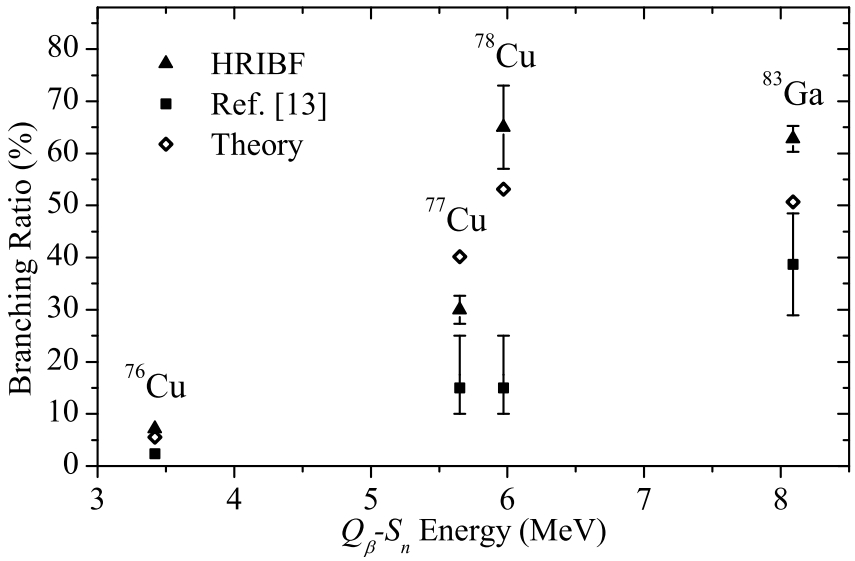

Figure 4.13: The probability of β-delayed neutron emission as a function of the energy window for this decay mode. Results of this experiment (▲) are compared to those listed in Refs. [Pfe02] (■) and to our new theoretical estimates (◇), see text.

their limit estimate on the relative intensities of the 730 and 114-keV γ rays fed in the β and βn branches of ^{78}Cu decay.[Van05] We observe that the full intensity within the βn decay branch does not go through the 114-keV transition, so any agreement is coincidental.

The βn branching ratio for ^{83}Ga has been measured several times yielding discrepant data from 62.8(63)% to 14.9(18)%, see Ref. [Rud93]. In our study, the determination of the βn branching ratio required a measured absolute branching ratio in the $A=82$ decay chain since ^{83}Ge was not completely removed from the beam. The strongest transition observed in a saturation measurement is the 1092-keV γ ray from ^{82}Ge β decay indicating that the βn branch must dominate in the decay. The most logical explanation for this observation requires the assumption that the decay of ^{82}Ge is primarily to a single 1^+ excited state at 1092 keV with no feeding to the 2^- ground state in ^{82}As as was originally proposed by Hoff and Fogelberg [Hof81]. This sets the absolute branching ratios within the $A=82$ decay chain. Using this value, we obtained 62.8(25)% for the βn branching ratio for ^{83}Ga, a value which is a factor of five larger than the presumably previous best measurement [Rud93] and almost twice the recommended value of 37(17)% listed at the NNDC [NNDC].

The measured $P_{\beta n}$ values are given in Table 4.1 and are shown in Fig. 4.13 plotted as a function of the βn energy window $Q_\beta - S_n$. The comparison of previous experimental results, shown in Fig. 4.13, to our $P_{\beta n}$ values obtained with purified radioactive beams of known intensity clearly calls for a verification of earlier experiments. These experimental results also prompted new theoretical analysis of the βn emission process, with the results given in Fig. 4.13. The earlier calculations of $P_{\beta n}$ [Bor05] within the continuum quasiparticle random-phase approximation underestimated the previously reported as well as our new, much larger, experimental $P_{\beta n}$ values. The new modeling of β-decay and β-delayed neutron emission followed the approach of Ref. [Bor05], however, updated Q_β and S_n values were taken from new mass measurements [Hak08] together with data from Ref. [Aud03]. Additionally, an inversion of the $2p_{3/2}$ and $1f_{5/2}$ proton orbitals for $N>44$ isotones was assumed. The latter assumption follows indications from recent studies, e.g., [Ots05, Fla08] and our decay data, that this inversion occurs. By applying the blocking approximation within

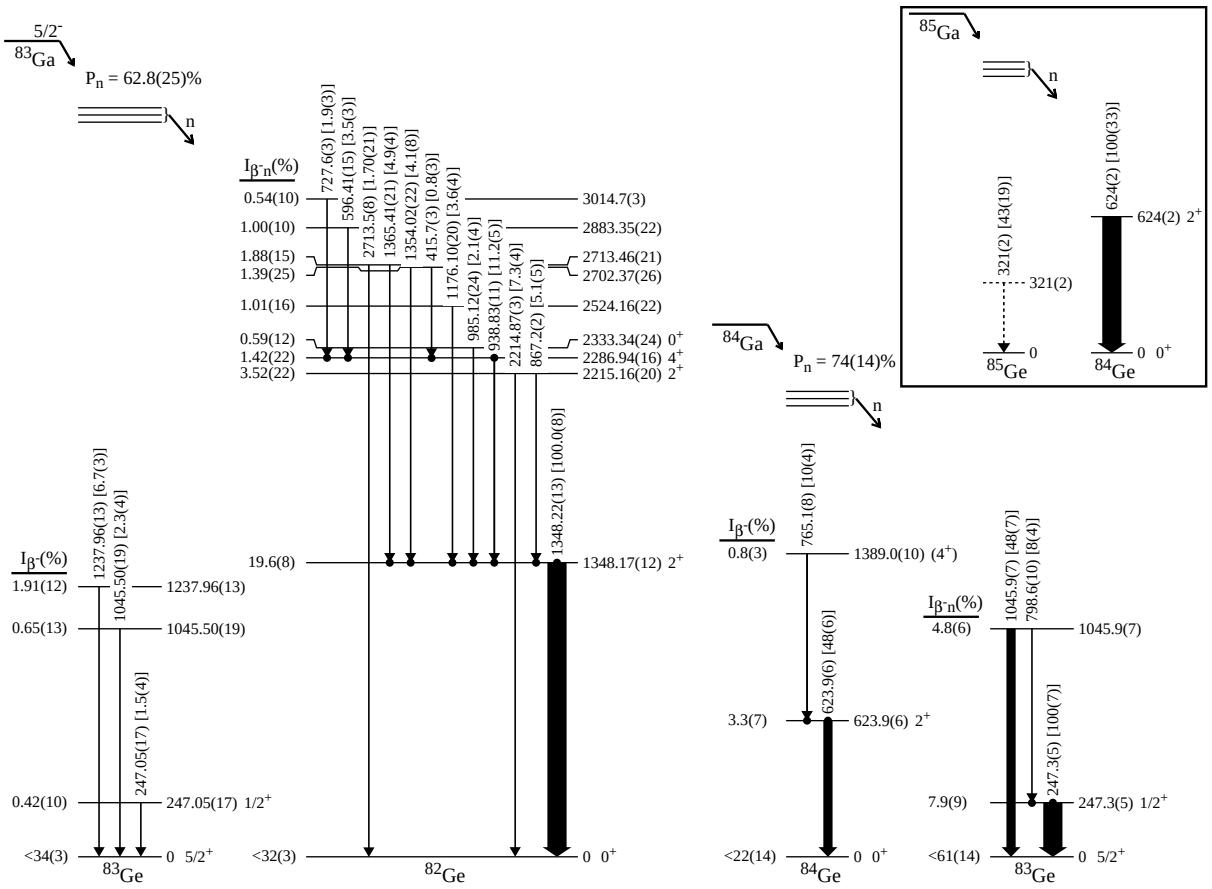

Figure 4.14: Proposed decay schemes for ^{83}Ga, ^{84}Ga and ^{85}Ga (inset). The intensity for each γ ray relative to the strongest γ ray from that decay is given in square brackets. The absolute β feedings for the ^{83,84}Ga decays are based on the measured absolute branching ratio for the 1348-keV γ ray (^{83}Ga) of 28.4(10)% and the 247-keV γ ray (^{84}Ga) of 8.6(8)%, respectively. The upper limits for the ground-state β-decay feedings reflect potentially unobserved γ-ray transitions.

the standard density functional DF3 framework [Bor96], the ground state proton orbital was set to be $1f_{5/2}$ state for the ^{76,77,78}Cu and ^{83}Ga βn precursors. Compared to previous calculations [Bor05], we observe a steeper increase of the βn probabilities towards the $N=50$ shell closure. The new calculations agree much better with our data, see Table 4.1 and Fig. 4.13, and illustrate the importance of using the correct SPE sequence and masses for the modeling of β-decay properties.

4.2.2 Evidence for a sub-shell closure at $N=58$ beyond ^{78}Ni

Neutron-rich radioactive beams of ^{83,84,85}Ga were produce at the HRIBF and studied using the RO system described previously. The system allowed identification and counting of individual ions,[Gro05] as well as to establish correlations between the implantation of the identified ion and any subsequent decays. Although the Ga beams obtained were not pure, the measured yields of the Ge ions were comparable to or less than those for the respective Ga isobars. The measured Ga content in the beams was 22% ^{83}Ga ($\sim$ 29 ions per second), 3% ^{84}Ga ($\sim$ 2 ions per second), and 0.5% ^{85}Ga ($\sim$0.1 ions per second). For the cases of ^{84}Ga ($t_{1/2}=85(10)$ ms [Kra91]) and ^{85}Ga ($t_{1/2}<100$ ms) ion tagging was used to unambiguously assign γ rays to the specific parent. The

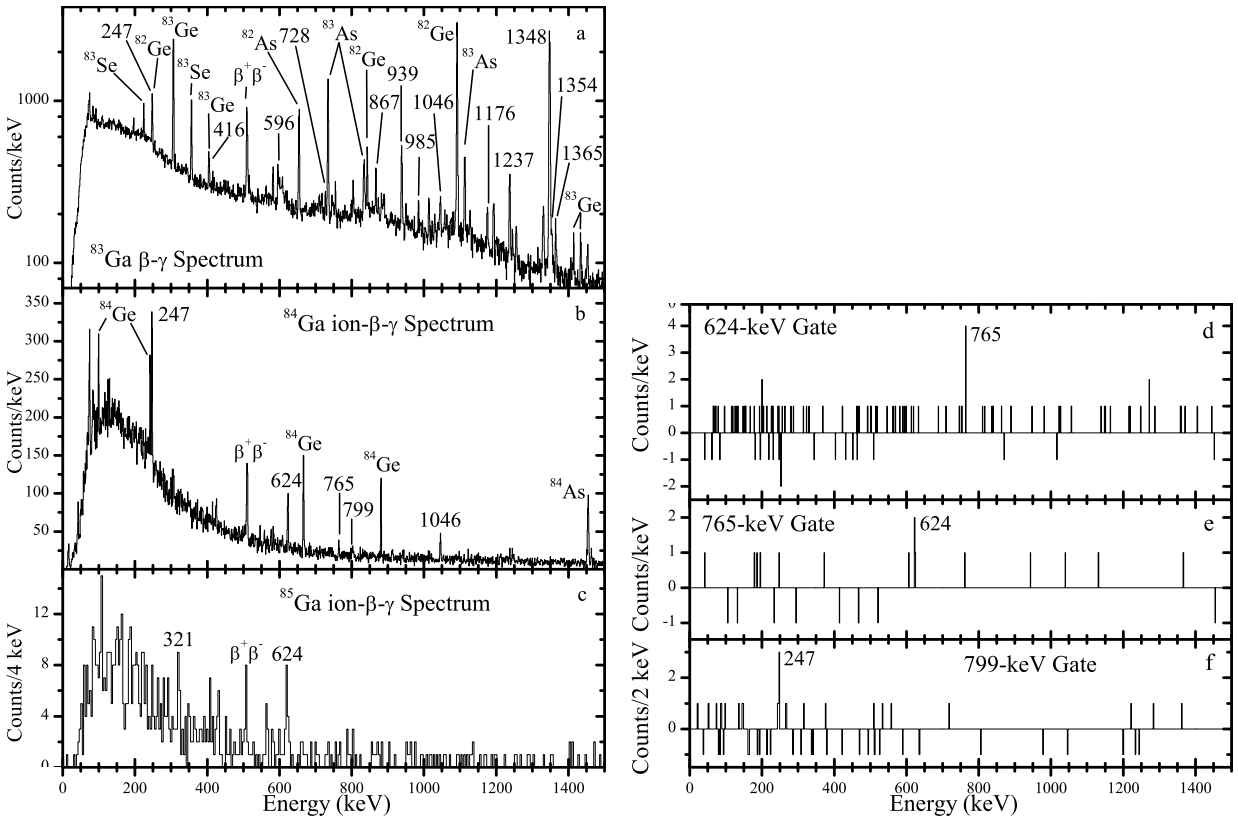

Figure 4.15: β-gated γ ray spectrum obtained with a 2.5 second MTC cycle for the $A=83$ data set (a), within 300 ms of a ^{84}Ga ion implantation (b), and within 190 ms of a ^{85}Ga ion implantation (c). ^{84}Ga ion-$\beta\gamma\gamma$ spectra gated on the 624 (d), 765 (e), and 798-keV (f) γ rays. γ rays are identified by their energy in keV or source of origin.

observed decay schemes for ^{83,84,85}Ga are presented in Fig. 4.14 on the previous page and discussed below as well as in Ref. [Win10].

The method used for assignment of γ rays to a particular decay varied depending on the rate for the Ga parent. In the case of ^{83}Ga where some γ rays were already known [Win88, Per06], the rate and purity were sufficient to directly use the $\beta-\gamma$ spectrum (see Fig. 4.15a). To establish the assignment for the most intense γ rays, a comparison was made between spectra cut from different time segments of the MTC cycle as well as comparison between the MTC cycle and saturation measurements. For the cases of ^{84,85}Ga where the rates and purities were lower, ion-tagged $\beta-\gamma$ spectra (see Fig. 4.15b and c) from time windows just following the observed implantation of a Ga ion (early spectrum) and an equal length time window just following the first time window (late spectrum) were generated. A comparison between the early and late spectra allowed definite assignment of γ rays to a specific parent activity. Additional γ-rays were identified by their observation in $\gamma\gamma$ coincidence spectra gated on the previously identified γ rays. Information from the $\gamma\gamma$ coincidence spectra were then used to establish the decay schemes shown in Fig. 4.14. The calibration of γ-ray energies is based on background activity in the spectra, while the absolute γ-ray efficiency was determined using standard sources as in Ref. [Win09].

The most intense γ ray from ^{83}Ga decay has been known to be the 1348-keV $2_1^+ \rightarrow 0_1^+$ transition in ^{82}Ge fed by the β-delayed neutron (βn) branch [Win88]. A ^{83}Ga β decay experiment using the PARRNe separator at Orsay observed two γ rays (938 and 1348 keV) from the βn branch as well

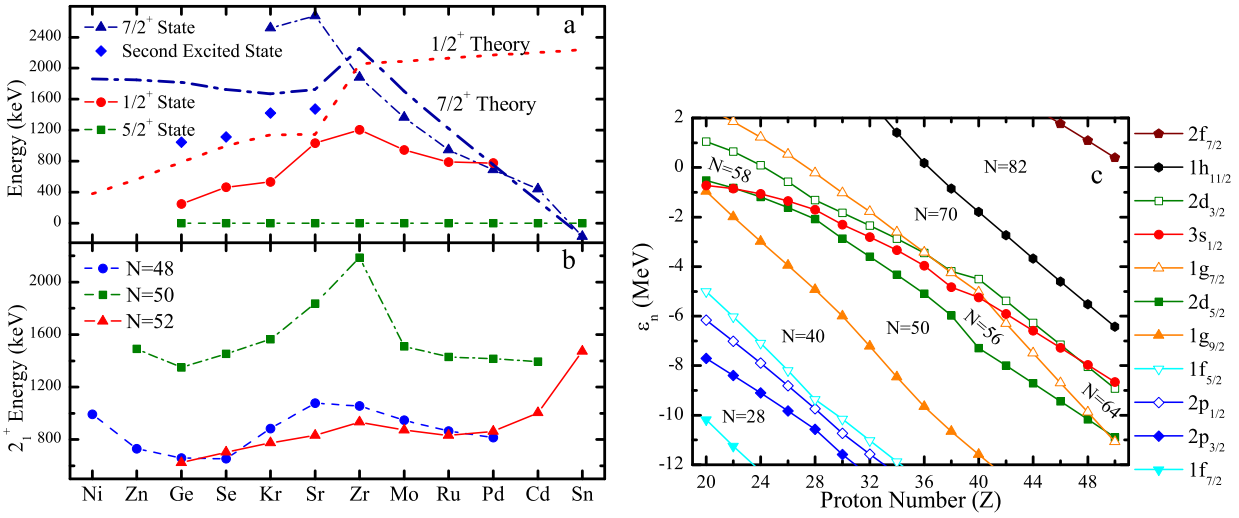

Figure 4.16: a) Systematics of the proposed $\nu 3s_{1/2}$ first excited state, the second excited state, and the $\nu 1g_{7/2}$ state relative to the $\nu 2d_{5/2}$ state for the $N = 51$ isotones. The dotted and dot-dashed lines shows the theoretical predictions for the energy difference between the $\nu 2d_{5/2}$ and $\nu 3s_{1/2}$ and $\nu g_{7/2}$ single-particle states, respectively. b) Systematics of the 2_1^+ energy in the $N = 48$, 50, and 52 isotones between $Z = 28$ and 50. c) Theoretical predictions for the dependence of neutron single particle energies on proton number for the $N = 50$ isotones. Also indicated are the predicted shell and sub-shell closures.

as two γ rays (867 and 1238 keV) which were associated with states in ^{83}Ge [Per06]. However, they were unable to observe a γ ray from the first excited $\nu 3s_{1/2}$ state reported at 280 ± 20 keV [Tho05]. We have assigned 12 γ rays to the βn branch depopulating 9 excited states in ^{82}Ge, see the β-gated γ-ray spectrum in Fig. 4.15a and the decay scheme shown in Fig. 4.14. The βn branch of the decay scheme matches closely with that for ^{82}Ga β decay [Hil88]. This includes observation of all three states near 2.3 MeV in ^{82}Ge, with the strongest feeding to the 2^+ state at 2215 keV [Per06, Urb07]. In addition, new levels at 2524, 2713, 2883, and 3014 keV have been firmly established. We confirmed observation of a 1238-keV γ ray which is not in coincidence with any γ rays in the βn branch. The 867-keV γ ray previously assigned to a state in ^{83}Ge [Per06] has been placed as feeding the 1348-keV level in ^{82}Ge based on firm $\gamma\gamma$ coincidence information. The intensity of the 867-keV γ ray in a gate on the 1348-keV γ ray is consistent with all the intensity feeding into the 1348-keV level. A previously unobserved γ ray at 1046 keV has been assigned to the decay of ^{83}Ga based on its growth behavior in the MTC cycle. No $\gamma\gamma$ coincidences were observed for this γ ray thus precluding its placement within the βn branch. It has therefore been placed as de-exciting a level at 1046 keV in ^{83}Ge. This placement was confirmed by its observation in our study of ^{84}Ga where the presence of this level is given additional support by observation of a 247-799 keV $\gamma\gamma$ coincidence, see Fig. 4.15f. Finally, during our ^{83}Ga study, we observed a 247-keV γ ray (Fig. 4.14) which is assigned as depopulating the $\nu 3s_{1/2}$ state [Tho05] with an absolute branching ratio of 0.42(0.10)%, which was determined using the procedure described in Ref. [Win09]. Placement of this transition was confirmed by its observation in the β decay of ^{84}Ga, see Fig. 4.14 and Fig. 4.15b. This confirmation was important since the 247-keV γ ray is part of a doublet with the 248-keV γ ray from ^{82}Ge β decay fed by the ^{83}Ga βn branch. The weak

absolute feeding and corresponding high $\log(ft)$ value (7.57(11)) to this $1/2^+$ state suggests the ground state of ^{83}Ga to be originating from the $\pi 1f_{5/2}$ orbital, not from the $\pi 1p_{3/2}$ orbital (see Ref. [Ots05, Ily09]), thus establishing the spin and parity for the ^{83}Ga ground state to be $5/2^-$.

The ^{84,85}Ga activities were studied using an ion-tagged spectrum, see Fig. 4.15b and c, allowing us to precisely assign γ rays to these decays. Previous measurements for ^{84}Ga decay observing the β-delayed neutrons provided $t_{1/2} = 85(10)$ ms and $P_{\beta n}$= 70(15)%, respectively [Kra91]. An 820-keV γ-ray was reported as observed by Perru *et al.* in the β-decay of ^{84}Ga at the PARRNe facility and assigned as the 2^+ to 0^+ transition in ^{84}Ge [Per03]. Later, the authors questioned this interpretation [Per04] citing unpublished ISOLDE-CERN data that pointed to a 624-keV transition following ^{84}Ga decay, see, e.g., [Koe03]. Perru *et al.* also reported observation of an 867-keV γ ray, assumed to be in the βn branch of ^{84}Ga decay, which they offered as confirmation of associating the same transition with the β branch of ^{83}Ga decay [Per06]. We found no evidence in our data, of much better statistics and studied sample purity, for an 867-keV γ ray. Recently, Lebois *et al.* published a paper on the β decay of ^{84}Ga decay [Leb09], assigning γ rays at 248, 624, and 1046 keV to this decay, as we had reported previously [Win08, Gro09]. They assigned the 248 and 624-keV γ rays as de-exciting the first excited states in ^{83}Ge and ^{84}Ge, respectively, and the 1046-keV γ ray as the 4^+ to 2^+ transition in ^{84}Ge. Based on ion-correlated β-γ and γ-γ coincidence information, see Fig. 4.15, we were able to clearly assign two γ rays to depopulate excited states in ^{84}Ge and three γ rays, including the 1046-keV transition, to depopulate excited states in ^{83}Ge as shown in Fig. 4.14. The state at 1389 keV in ^{84}Ge is firmly established by the observed coincidence between the 624 and 765-keV γ rays in the ^{84}Ga ion-correlated $\gamma\gamma$ coincidence spectra shown in Figs. 4.15d and 4.15e. The spin/parity for this state is tentatively assigned as 4^+ based on the fact that there is no observed direct transition to the ground state as is observed for the 2_2^+ state in ^{80,82}Ge. One should note that there is no evidence for two β-decaying states of ^{84}Ga [Leb09] in our data. The concept of two β-decaying states was used in Ref. [Leb09] to justify an incorrect placement of the 1046-keV γ ray and the respective intensity balance, triggering a theoretical discussion leading to an incorrect understanding of the properties of ^{84}Ga and ^{84}Ge. Our data clearly indicates that the 1046-keV γ ray is in ^{83}Ge. Using a ^{85}Ga-ion tagged γ-ray spectrum, see Fig. 4.15c, we were able to confirm placement of the 624-keV transition as the first excited state in ^{84}Ge, as well as a 321-keV γ ray which is assumed to be in the β branch, see Fig. 4.14. We were also able to estimate the ^{85}Ga half-life as less than 100 ms since all events associated with the 624-keV γ ray occur in the first 190 ms after implantation.

The β-delayed neutron branching ratios ($P_{\beta n}$values) were determined as described in Ref. [Win09] in which the value for ^{83}Ga of 62.8(25)% was presented. Determining this value for the decay of ^{84}Ga suffers from the lack of measured absolute branching ratios in the $A = 83$ decay chain. To establish an absolute branching ratio for this decay chain, we used our data for the decay of ^{83}Ga to ^{83}Ge which required estimating the fraction of ^{83}Ge in the beam. A careful analysis of the IC energy-loss spectra indicates a ratio of 15.5(9)% for ^{83}Ge relative to ^{83}Ga. This was then used to estimate the absolute branching ratio for the 306-keV γ ray from ^{83}Ge decay to be 15.3(11)%. The observed intensity of the 306-keV γ ray fed in the βn decay of ^{84}Ga then gives a $P_{\beta n}$ value of 74(14)% in good agreement with the earlier estimated value of 70(15)% [Kra91]. Our value is dependent on the absolute branching ratio for the 306-keV γ ray which should be independently verified in an absolute measurement optimized for ^{83}Ge decay. A similar analysis could not be done reliably for ^{85}Ga due to low statistics.

Our experimental results can now be used to extend the level systematics for the $N = 51$ and 52 isotones as shown in Fig. 4.16a and b. The observed systematic trends lead us to some interesting conjectures about the structure of neighboring nuclei. First, the possibility for isomers in the $N = 51$ and 53 isotones near $Z = 28$, with $1/2^+$ halo states for weakly bound systems. Second, the

emergence of an $N=58$ sub-shell closure for neutron-rich nuclei. Third, a weakening of the $Z=28$ shell closure for $N>50$. The experimental evidence pointing to these behaviors will be presented in the following paragraphs.

The energy-level systematics of the $N=51$ isotones are presented in Fig. 4.16a. For all these nuclei except ^{101}Sn, a $5/2^+$ ground state is observed. For the $Z \leq 44$ nuclei where it has been measured in a (d,p) or similar reaction, a spectroscopic factor ≥ 0.33 suggests this state has a large single-particle component. For the $Z \leq 42$, $N=51$ isotones, a $1/2^+$ state with a significant single-particle contribution, a spectroscopic factor ≥ 0.46 in a (d,p) reaction, is observed as the first excited state. The systematics show that the energy separation between the $1/2^+$ first excited state originating from the $\nu 3s_{1/2}$ orbital and the $5/2^+$ ground state assigned to the $\nu 2d_{5/2}$ orbital is continuously decreasing as $Z=28$ is approached. Thomas *et al.* observed in $Z=32$ ^{83}Ge that these states contain about 50% of the single-particle strength [Tho05]. We would therefore expect that this energy separation will mimic the separation between the single-particle states. If the observed decrease in the energy separation continues towards the magic number $Z=28$, nearly degenerate $\nu 3s_{1/2}$ and $\nu 2d_{5/2}$ orbitals may result for the $N=51$ isotones ^{81}Zn [Ver07] and ^{79}Ni. The energy degeneracy of the $\nu 3s_{1/2}$ and $\nu 2d_{5/2}$ states may create a low-energy isomeric state of $J^\pi = 1/2^+$ in odd-N isotones beyond ^{78}Ni given that the lifetime of a 100-keV E2 transition in the Ni isotopes is in the μs to ms range. In addition, since the $\nu 3s_{1/2}$ state can hold only two neutrons, the $N=53$ isotones may have a $1/2^+$ isomeric level with either a $1/2^+\{(2d_{5/2})^2 \otimes (3s_{1/2})^1\}$ configuration for a $2d_{5/2} - 3s_{1/2}$ level sequence or a $1/2^+\{(2d_{5/2})^2 \otimes (3s_{1/2})^{-1}\}$ configuration if the $3s_{1/2}$ orbital is below the $2d_{5/2}$ orbital. Interestingly, $N=53$ ^{81}Ni is predicted to be weakly bound, with a neutron separation energy calculated to be only 170 keV [Mol97]. Reduction of the binding energy in the $1/2^+$ isomeric state may lead to a system with an $l=0$ wave function bound much less than the neutron-halo nucleus ^{11}Li [Smi08].

While the energy separation between the $3s_{1/2}$ and $2d_{5/2}$ single-particle states is seen to decrease, the opposite trend is observed for the energy of the $\nu 1g_{7/2}$ single-particle state. As shown in Fig. 4.16a, the energy of the lowest lying $7/2^+$ state which contains a significant single-particle contribution, a spectroscopic factor ≥ 0.26 in a (d,p) reaction for $Z \leq 42$, has been plotted. This state is observed to increase in energy down to $Z=38$ before showing a slight decrease. Unfortunately, this state is not known in the lighter isotones, so whether or not the downward trend continues is unknown. However, for the $Z \leq 40$, $N=51$ isotones the second excited state can be used to provide some insight. This state in ^{87}Kr, ^{89}Sr, and ^{91}Zr is not the $\nu 1g_{7/2}$ single-particle state but likely results from a three-particle configuration since they either have a very small spectroscopic factor or were not fed in a (d,p) reaction while other $l=4$ states were observed. The spin and parity of this state is tentatively identified as either $5/2^+$ or $7/2^+$. Being a state composed from the coupling a multiple orbitals, its energy will be affected by the single-particle energies of the orbitals from which it is composed which would include the $\nu 1g_{7/2}$ orbital. It is observed that the energy gap between the first excited $1/2^+$ state and known second excited state in ^{83}Ge (0.80 MeV, this work) and ^{85}Se (0.65 MeV [Omt91]) is clearly increasing when approaching neutron-rich nuclei (Fig. 4.16a) suggesting that the $7/2^+$ single-particle state does not drop in energy. Therefore, a relatively large energy gap may occur after filling the close-lying $\nu 3s_{1/2}$ and $\nu 2d_{5/2}$ orbits leading to a significant spherical energy gap (a possible new sub-shell closure) at neutron number $N=58$ similar to that at $Z=38$ and 40. In the Sr and Zr isotopes, the spherical ground state energy gap is eventually overwhelmed by the deformation driving $1g_{9/2}$ orbital as $N=Z$ is approached. However, if the deformation driving orbits lie above the spherical single particle orbitals as in $^{90-96}$Zr, a sub-shell closure may occur at $N=58$.

A comparison of the systematics of the 2_1^+ states in the $N=48$, 50, and 52 isotones is shown in Fig. 4.16b. The observed continued dropping of the energy of the 2_1^+ state in the $N=52$ isotones

may be an indication of a weakening in the ^{78}Ni core as has been suggested elsewhere [Urb07]. It is expected that the 2_1^+ energy would reach a minimum at the mid-shell nucleus ^{86}Se ($Z=34$) and begin to rise to the shell closure at ^{80}Ni. This suggests that there is a weakened shell closure at $Z=28$. However, the continued lowering of the 2_1^+ state is not conclusive evidence for a weakening of the shell since a similar behavior is observed in the $N=50$ isotones where the 2_1^+ energy reaches a minimum at ^{82}Ge and shows a distinct rise at ^{80}Zn [Van07]. For the $N=48$ isotones, a sub-shell closure at $Z=38$ is apparent with the minimum energy being observed at ^{82}Se as would be expected. For $N=50$ and 52, a smooth trend is observed down to the Germanium isotopes. To search for any difference in this trend we considered the relative change in the energy of the 2_1^+ state and found that it continues to increase its downward slope for the $N=52$ isotones in comparison with the $N=50$ isotones [Win08]. The energy of the proposed 4_1^+ state does not indicate a trend toward deformation since its ratio to the 2_1^+ energy is similar to the value for the $N=52$ isotones ^{86}Se and ^{88}Kr and less than the value for the corresponding $N=48$ isotones. These observations provide additional support for the conjecture that the doubly-magic character of the ^{78}Ni core is weakening for more neutron-rich nuclei. Additional experimental data, especially identification of the 2_1^+ state in ^{82}Zn, along with detailed shell model calculations are needed to corroborate the observed effect.

To analyze the theoretical origin for merging of the $\nu 2d_{5/2}$ and $\nu 3s_{1/2}$ levels, we have calculated the global dependence on the proton number of neutron single particle orbitals around $N=50$ (see Fig. 4.16c). These spherical HFB calculations with an SkO$_T$ functional [Rei99] include the tensor term [Zal08], and were described and used recently in Ref. [Kar08]. For all isotones, the plotted energies of the $\nu 1g_{7/2}$ orbital were lowered by 1.55 MeV as compared to the calculated values, so as to match the experimental value (172 keV) of the relative $\nu 2d_{5/2}-\nu 1g_{7/2}$ energy difference, recently established for the $N=51$ isotone ^{101}Sn [Dar09] with just one neutron above the doubly magic ^{100}Sn core. A very similar pattern for the neutron states near neutron number $N=50$ was recently obtained in the independent calculations by Otsuka *et al.* [Ots09] for atomic elements between $Z=40$ and 50. The modeling using the SkO$_T$ functional predicts the observed trends in the separation of the $\nu 2d_{5/2}$ to the $\nu 3s_{1/2}$ and $\nu 1g_{7/2}$ states as shown in Fig. 4.16a. The $\nu 1g_{7/2}$ orbital, below the $\nu 2d_{5/2}$ orbital in proton-rich ^{101}Sn, increases in energy towards neutron-rich isotones, and peaks near $Z=40$ before leveling off. Note that our adjustment using the ^{101}Sn data [Dar09] actually makes the $\nu 2d_{5/2}-\nu 1g_{7/2}$ energy difference smaller, but not small enough to diminish the effect of an emerging energy gap at $N=58$. For very exotic nuclei near ^{70}Ca, the theoretical modeling of the neutron orbitals predicts a vanishing of the $N=50$ shell closure, while the proposed $N=58$ shell closure will persist. It is very hard to judge the validity of the presented calculations for the "open quantum system" near ^{70}Ca, but the predicted trend for the energy difference between the $\nu 2d_{5/2}$ and $\nu 3s_{1/2}$ orbitals follows the observed trend in the energy difference between the $1/2^+$ and $5/2^+$ states (Fig. 4.16a). In fact, the predicted $\nu 2d_{5/2}-\nu 1g_{7/2}$ energy difference lies ~ 500 keV higher in energy suggesting that the crossing of the $\nu 2d_{5/2}$ and $\nu 1g_{7/2}$ orbitals could occur closer to $Z=28$.

4.2.3 β decay of the $\pi f_{5/2}$ ground state of ^{77}Cu

Beams of purified ^{77}Cu ions were produced at the HRIBF and used in two experiments. In the first experiment, the Cu ions were accelerated to 225 MeV by the ORNL Tandem before being sent to a detector station using the RO mode [Gro05]. In the second experiment, the low-energy ions (200 keV) were sent directly to the LeRIBSS detector station with a resultant factor of 10 increase in the beam intensity. In both cases, the ions passed through a charge exchange cell which removed all zinc ions from the beam. This, along with careful tuning of the high-resolution

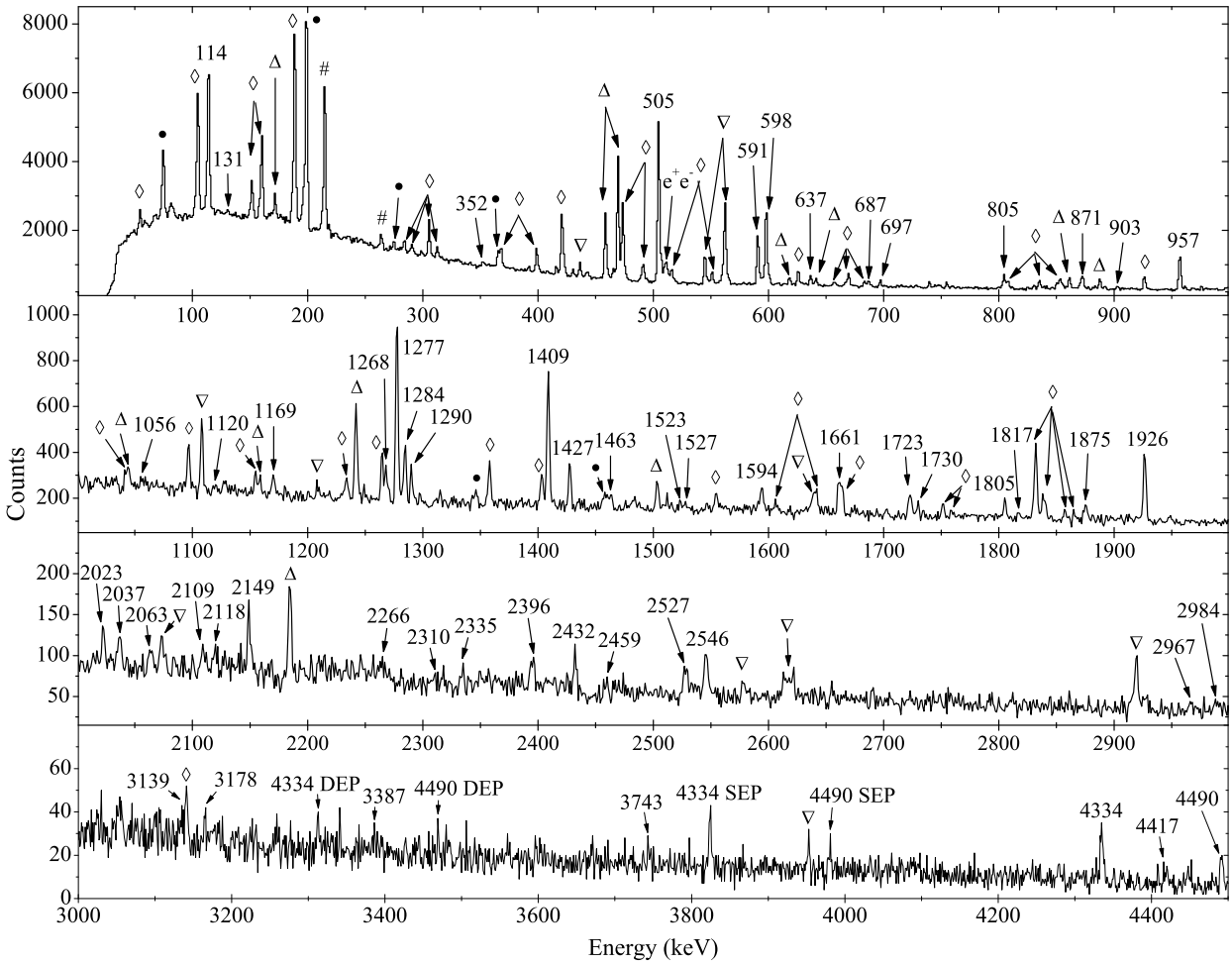

Figure 4.17: Saturation spectrum in coincidence with the β detectors obtained in the LeRIBSS data run with a purified ^{77}Cu beam. The γ-ray peaks assigned to ^{77}Cu are indicated by their energy with single and double escape peaks marked as SEP and DEP, respectively. Other members of the two decay chains are indicated by symbols: ^{77}Zn($\diamond$), ^{76}Zn($\bullet$), ^{77}Ga($\triangle$), ^{76}Ga(∇), and ^{77}Ge(#).

isobar separator and/or selective ranging out, provided highly purified beams of ^{77}Cu ions for these studies. In the RO experiment the beam purity was measured to be $\sim 68\%$ with ^{77}Ga being the only significant contaminant. In the LeRIBSS experiment, a comparison of γ rays from ^{77}Cu and ^{77}Ga decays indicated a similar purity was obtained. For both measurements, the collected activity was observed by four clover Ge detectors and two plastic β detectors.

In the first experiment, the accelerated ions with an average rate of about 15 ions per second were time tagged using a MCP detector, passed throug the IC, and implanted onto the MTC with a tape transport time of 525 ms. By passing through the IC, the ions could be clearly identified by energy loss in the six segments and counted on an event-by-event basis. This allowed us to measure the absolute number of ^{77}Cu ions in the studied samples. Presented in this paper are results based on data obtained in the pass through mode in which the ion chamber was run at a low pressure which insured that $> 99\%$ of the identified and counted ^{77}Cu ions would exit the IC and be implanted on the MTC at a point in the center of the detector array. While running in this

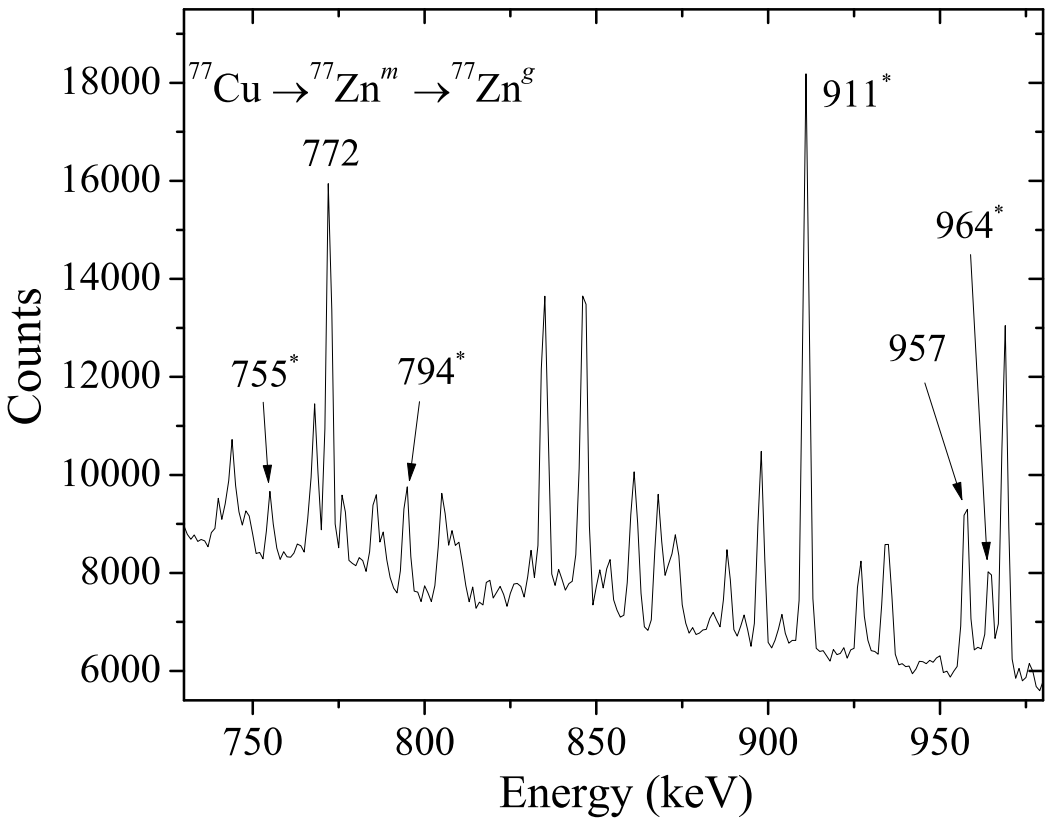

Figure 4.18: Portion of the γ-ray singles saturation spectrum from the LeRIBSS data run showing the presence of the 772-keV γ ray from de-excitation of ^{77}Zn^{m}. Also labeled in the figure are lines from the β decay of ^{228}Ac(*) in the background and the 957-keV line from ^{77}Cu β decay.

mode, an exact count of the number of ions implanted on the MTC could be made allowing for the direct determination of absolute branching ratios. The MTC cycle used involved a period of beam deposition while the decays were observed followed by movement of the tape to a shielded location in order to remove long lived daughters before starting the next cycle. Since the Zn ions were removed from the beam, the MTC cycle time was set to limit the build-up of ^{77}Ga ($t_{1/2}$ = 13.2(2) s) in the sample. Data were taken with a 7 s MTC cycle. Additional data were obtained while running with the beam in saturation. All γ ray intensities for this experiment were determined using the γ-ray singles spectra which were used only to determine absolute branching ratios.

The LeRIBSS was used to perform a second study for ^{77}Cu β decay with an average rate of about 130 ions per second deposited on the MTC. Improvements in the tuning of the high-resolution isobar separator allowed us to achieve a high purity beam of ^{77}Cu ions without using the ranging-out technique. Additional improvements over the first experiment included implementation of a system to rapidly deflect the beam before the high-resolution isobar separator which allowed for the study of the growth and decay of the deposited sources. In addition, LeRIBSS utilized a new MTC with a transport time of 210 ms, making it a better choice for the study of short-lived nuclei. A typical MTC cycle would include a growth period with beam deposition, deflection of the beam for a decay period, followed by movement of the tape, with data obtained during both the growth and decay periods. A 3 second growth/3 second decay MTC cycle was used in the study of ^{77}Cu. Finally, a saturation measurement was made. Since ^{77}Cu was the primary component of the beam, none

of the daughter activities became dominant in the spectrum. A representative β-gated spectrum from the saturation measurement is shown in Fig. 4.17 on page 49. A portion of this spectrum taken in γ-ray singles mode is shown in Fig. 4.18 on the previous page indicating the presence of the 772-keV γ ray depopulating the $J^\pi = 1/2^-$ ^{77}Zn^m as will be discussed in more detail later. Analysis of these spectra as well as $\gamma - \gamma$ coincidence data allowed construction of the decay scheme shown in Fig. 4.19.

The relative γ-ray intensities were taken from the LeRIBSS measurement. For the stronger γ rays it was possible to extract these intensities from the γ-ray singles spectrum. However, identifying weaker γ rays and determining their relative intensities required the use of a β-gated spectrum (Fig. 4.17). In order to extract correct relative intensities for these γ rays, it was necessary to determine the β detection efficiency (β_{eff}) for γ rays depopulating any given level. This efficiency was found to range from 15 to 65%, depending on the β energies of the levels fed which in turn determine the fraction of the β particles which could reach the β detectors. For some levels there was a strong transition (e.g., 957 and 1926 keV) which would allow the direct determination of β_{eff}, while for a number of levels it was necessary to obtain a reasonable estimate for this value. Obtaining these estimates was based on some simple assumptions. First, β_{eff} should be a smoothly varying function of the maximum β energy directly feeding a level since different fractions of the β-energy spectrum are being sampled. Second, over a range of a few MeV, β_{eff} will vary linearly. These assumptions allow us to define an effective Q value (Q_{eff}) based on both direct and indirect feeding of the level as determined from the decay scheme. There is a problem with doing this since missing γ rays in the decay scheme will result in too high a value for Q_{eff}. The choice of γ rays used to establish the efficiency curve was therefore limited to those γ rays for which it was reasonable to assume that the feeding had been correctly determined. This uncertainty in the feeding results in cases where β_{eff} is very precisely known while Q_{eff} has a large uncertainty. Conversely, γ rays from high-lying states where mainly direct feeding will occur have a very precise Q_{eff} but imprecise β_{eff} due to low statistics. For $Q_{eff} \leq 5$ MeV, averages for several states fed in the decays of ^{76,77}Zn and ^{76}Ga with similar values for Q_{eff} were used. Above this energy, γ rays from the decay of ^{77}Cu were used. For each level, it was assumed that some percentage of the unobserved feeding could come from feeding to states in a 0.5 MeV window just below the neutron separation energy. For states where no missed feeding is assumed, a nominal uncertainty of 50 keV was used. For states with missed feeding assumed, the value of Q_{eff} is reduced and the uncertainty becomes much larger. Data points used in estimating β_{eff} are plotted in Fig. 4.20. The data were fit to a linear function where the weighting factor included the uncertainties in both β_{eff} and Q_{eff}. The relative intensities for all γ rays associated with ^{77}Cu decay were scaled using β_{eff} values from direct measurement of strong transitions or estimates based on the observed decay scheme with the assumption that 50% of any unobserved feeding to a level comes from the states near the neutron separation energy. For the later group of γ rays, the adjustment for β_{eff} usually was within the statistical uncertainty so that the compensation for β_{eff} primarily results in an increased uncertainty in the relative intensity. It is evident in this analysis that except for the levels at 1363 and 2235 keV, which have the highest values for β_{eff}, the observed feedings are overestimates.

The only published information on states in ^{77}Zn prior to these experiments was a 1.05 s E3 isomer at 772 keV and states at 114 and 803 keV observed in the βn branch of ^{78}Cu decay [Eks86, Van05]. We were able to identify 72 γ rays associated with the β decay of ^{77}Cu and produce the decay scheme shown in Fig. 4.19 on the following page, where the intensities shown are normalized relative to the 505-keV γ ray. The intensities were taken from the γ-ray singles spectrum for stronger transitions which could be fit cleanly, while the intensities for the other transitions were taken from a β-gated spectrum and were corrected for the observed variation in β

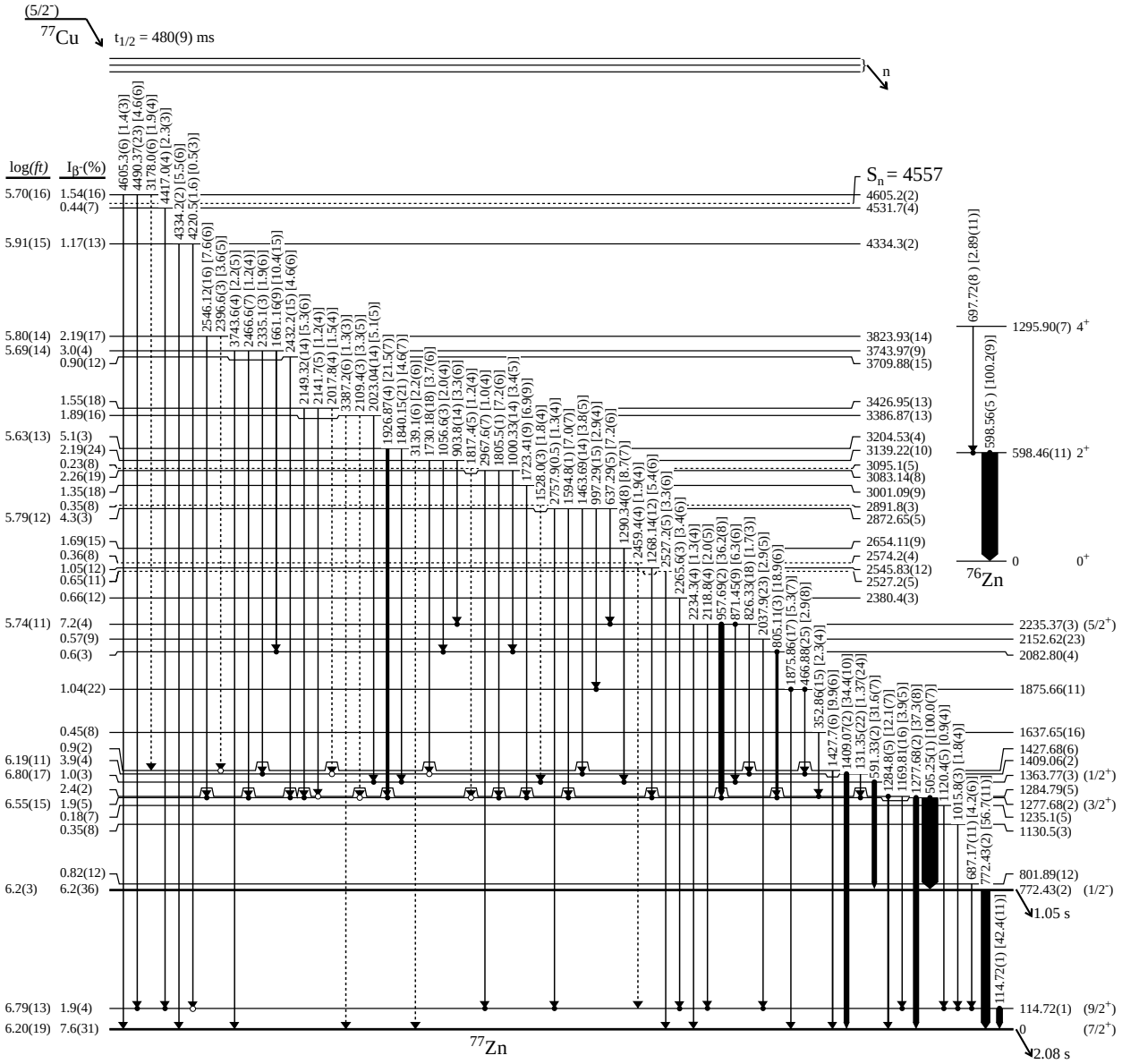

Figure 4.19: Proposed decay scheme for ^{77}Cu to excited states in ^{76,77}Zn. The relative intensities of the γ rays to the 505-keV transition are indicated in square brackets. Closed circles indicate $\gamma - \gamma$ coincidences seen both ways, while open circles indicate a coincidence observed only from the upper transition. Transitions and levels without strong coincidence relationships and/or other linking transitions are indicated by dashed lines. The level feedings are based on the measured absolute branching ratio for the 505-keV transition (19.1(6)%) as described in the text. All energies are in keV unless otherwise noted.

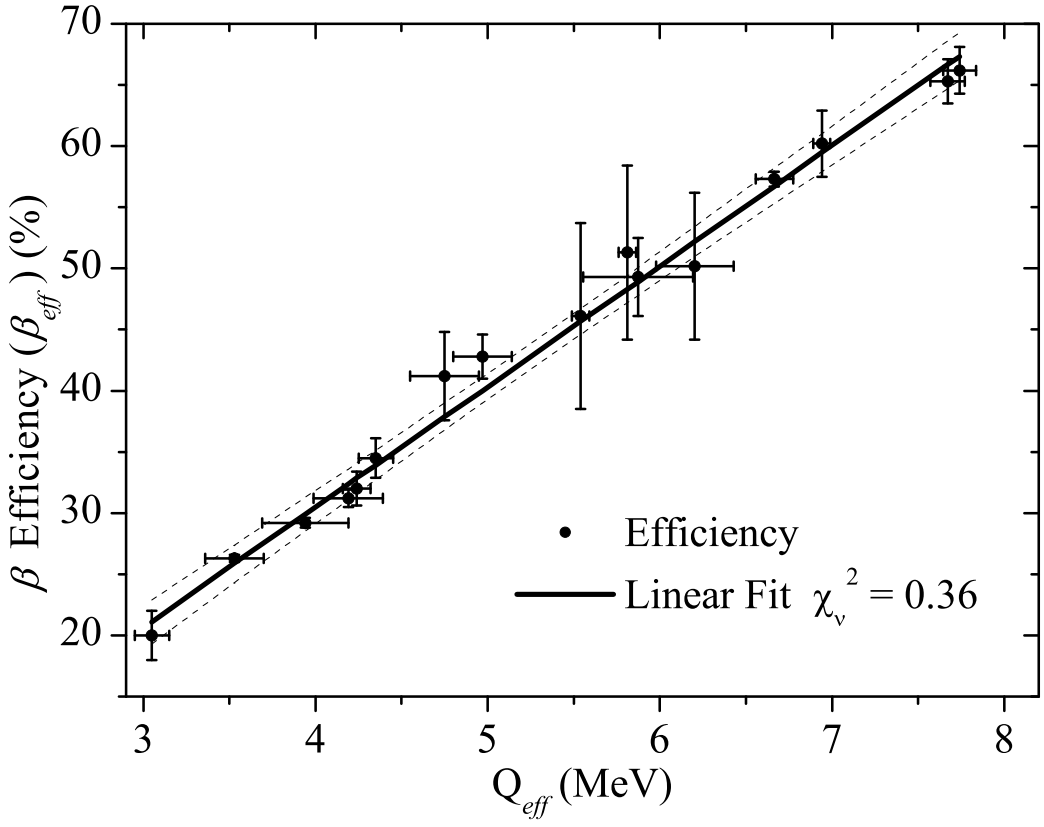

Figure 4.20: The β detection efficiency (β_{eff}) as a function of the effective Q value (Q_{eff}) for the LeRIBSS measurement. The solid line is from a fit to the data while the dashed lines show the $\pm 2\sigma$ limits.

detection efficiency. Summing corrections based on the proposed decay scheme are also included. All γ rays associated with this decay were observed to have the correct time behavior in the MTC cycle as well as $\gamma - \gamma$ coincidence relationships with the stronger transitions. All γ rays observed in the spectrum with a relative intensity of 2% or greater have been placed in the level scheme or firmly assigned to the decay of a daughter activity. Some weaker γ rays, with relative intensities between 1 and 2%, have the proper time behavior to be associated with ^{77}Cu decay but could not be placed in the decay scheme due to a lack of solid $\gamma - \gamma$ coincidence information. It is possible that some of these transitions could directly feed the ground or isomeric states. All transitions and excited states in the decay scheme are supported by $\gamma - \gamma$ coincidences, although there is some uncertainty in the placement leading to the "dashed" levels and transitions. Bound excited states are observed up to the neutron separation energy at $S_n = 4.557(5)$ MeV [Hak08]. One state, at 4.605 MeV, was found to lie about 50 keV above the S_n value.

One unique feature of the decay scheme presented in Fig. 4.19 on the previous page is that except for the 1277-keV level, no states have strong transitions to both the isomeric state and the ground/first-excited state. In fact, only six states have transitions to either of the two lowest energy states and the 1277-keV level. None of the strongest γ rays are in coincidence with 114-keV ground-state transition (Fig. 4.21 on the following page) and the 114-keV γ ray sees primarily higher energy lines. In the RO experiment where the weaker transitions were not observed, this

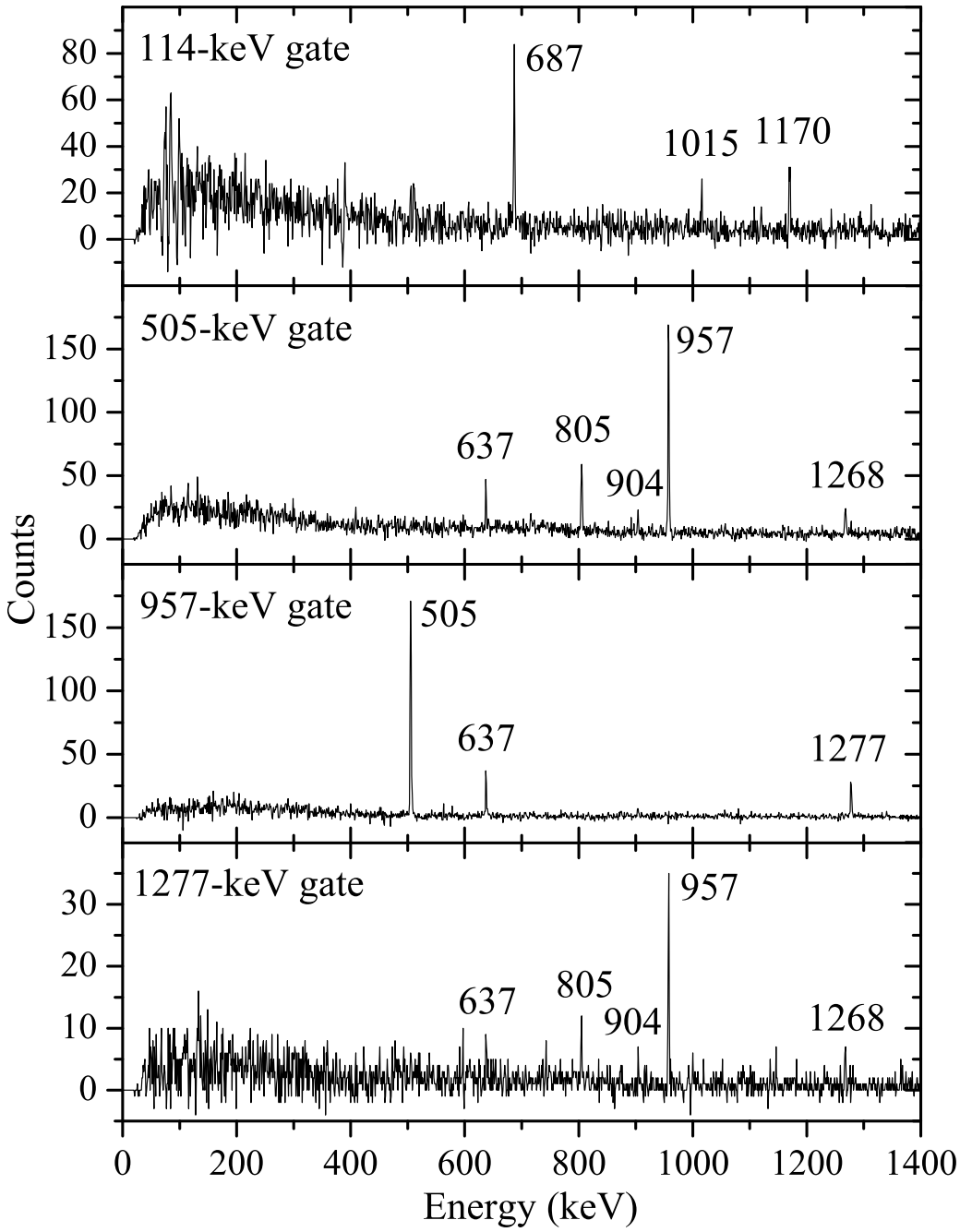

Figure 4.21: β-gated γ-ray coincidence spectra for gates on the 114-, 505-, 957-, and 1277-keV transitions.

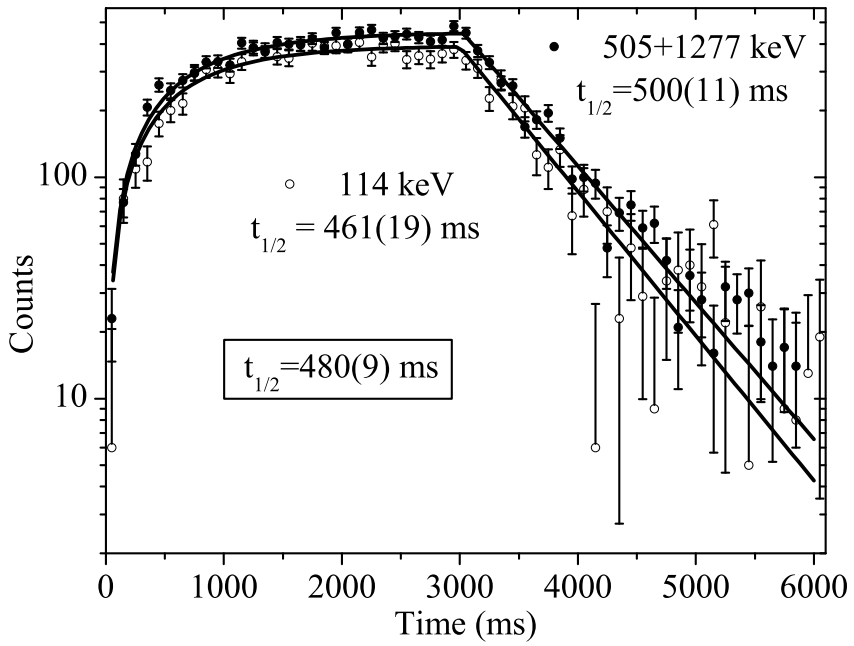

Figure 4.22: Half-life curves for the γ rays depopulating the 114- and 1277-keV levels. The data were fit in both the growth and decay portions of the curve, to optimize statistics, using a non-linear least squares fit routine. Data between 1 and 3 seconds has little effect on the fitted values, therefore the initial grow-in and decay portions determine the half-life.

arrangement suggested the possibility of a β-decaying isomer in ^{77}Cu. In the LeRIBSS experiment we concentrated on looking into this possibility. A comparison of the half-lives for the 114-keV and 505-+1277-keV γ rays (Fig. 4.22) shows excellent agreement suggesting a single β-decaying state for ^{77}Cu with a half-life of 480(9) ms. However, in principle, these results cannot exclude a ^{77}Cu isomer with a half-life close to that of the ground state and nearly the same βn emission probability.

The strongest transition observed in the decay of ^{77}Cu to states in ^{77}Zn is at 505 keV. The absolute intensity of this γ ray was determined in the RO experiment by comparing the peak area in a γ-ray singles spectrum to the number of ^{77}Cu ions identified and counted in the IC with corrections made for absolute efficiency and coincidence summing. Values were obtained from measurements with an MTC cycle and in saturation yielding an average value of 19.1$\pm$0.6%, see Fig. 4.23 on the following page. A similar technique was used to establish the absolute branching ratios for the 772-keV γ ray from the IT decay of ^{77}Zn^m and the 189-, 199- and 563-keV γ rays from the β decays of ^{77}Zn^g, ^{76}Zn and ^{76}Ga, respectively, as described in the following paragraphs, see Fig. 4.23. For these later cases, the LeRIBSS data were also used where the absolute normalization was made relative to the 505-keV γ ray. This absolute normalization was also used to determine the apparent absolute feedings to the levels shown in Fig. 4.19 on page 52. It is obvious that the decay of ^{77}Cu is highly fragmented, weakly feeding a large number of states. Since some γ rays from this decay could have intensities below our detection limit, these feedings should only be considered as the apparent feedings to the levels (upper limits). Corresponding lower limits for the log(ft) values for selected levels were determined using our half-life of 480(9) ms and a Q_β of 10.21(40) MeV for ^{77}Cu [Hak08, Aud03], and are shown in Fig. 4.19. Additional information on the decay scheme will

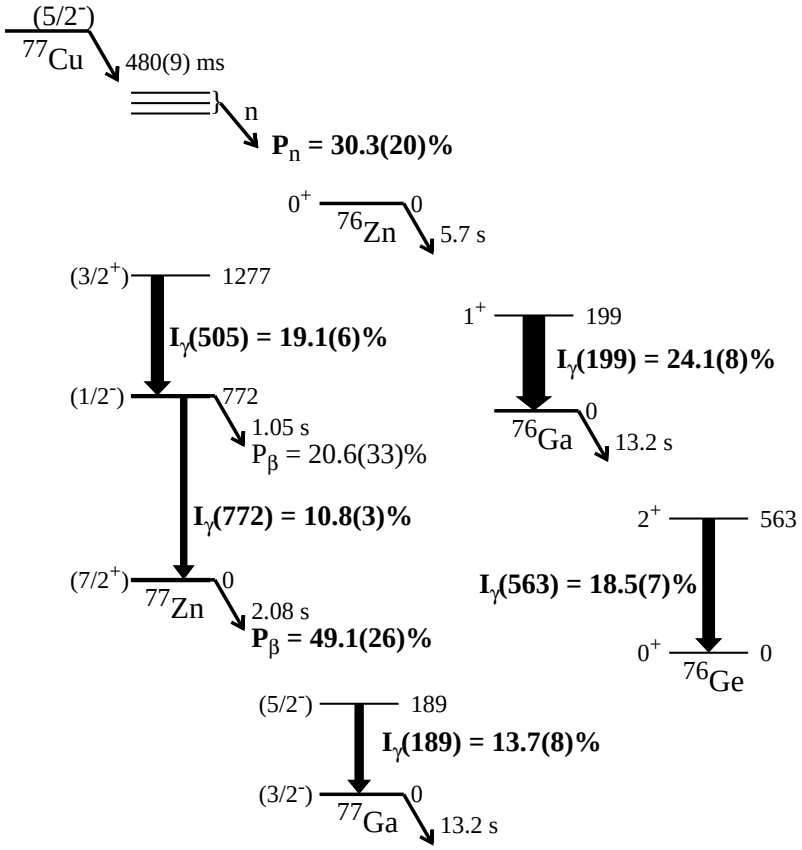

Figure 4.23: Subset of the decay schemes of ^{77}Cu and it's daughter activities showing, in bold, the directly measured absolute branching ratios per ^{77}Cu decay. The intensities of the five γ rays were determined solely in the current experiments while $P_{\beta n}$and $P_{\beta}$for ^{77}Zn^{g} incorporate additional information as discussed in the text. Also shown is the β decay probability for ^{77}Zn^{m} as derived from the other values. Energies shown, in keV, are not to scale while the widths of the γ-ray transitions are to scale.

be presented following a discussion of the measured absolute branching ratios.

Determination of the intensity for the 772-keV γ ray first required determination of the contamination to the peak area due to an unresolved background component from ^{228}Ac belonging to the ^{232}Th decay chain, see Fig. 4.18 on page 50. The 772-keV line from the background has a relative intensity of only 5.8% of the 911-keV γ ray and should be comparable to the intensity of the 755-keV γ ray. It is evident in the spectrum that there is a significant component due to the ^{77}Zn^m IT decay. Since the detection efficiency for the background γ rays is different from that of the activity, a number of stronger γ rays from the decay of ^{228}Ac were used to map out this variation and to extract the background component of the 772-keV peak area. The average value obtained for all measurements from the two experiments for the absolute branching ratio of the 772-keV γ ray per ^{77}Cu decay is 10.8(3)%, see Fig. 4.23.

As suggested in Ref. [Win09], β decay from the ^{77}Zn^m $1/2^-$ state will go preferentially by an allowed transition to the $3/2^-$ ground state, or the $1/2^-$ 105-keV and $3/2^-$ 160-keV levels, of ^{77}Ga bypassing the $5/2^-$ 189-keV level which would require a second forbidden decay. Therefore, the absolute branching ratio for the 189-keV γ ray should reflect the absolute branch from the decay of ^{77}Cu which eventually feeds through the ground state, i.e. the total intensity from the decay which ends up in the ground state by either direct population or γ-ray cascades. By comparison of the peak area to the number of ^{77}Cu ions measured in the IC (RO experiment) or the relative intensity to the 505-keV γ ray (LeRIBSS experiment) yields an absolute intensity of 13.7(8)% per ^{77}Cu decay for the 189-keV γ ray. Combining these result with the published absolute branching ratio and internal conversion coefficient for the 189-keV γ ray from ^{77}Zn^g β decay (28.1(13)% and 0.013(2), respectively [NNDC]) yields an average absolute branch of P_β= 49.1(26)% per ^{77}Cu decay, see Fig. 4.23.

In Ref. [Win09], we presented a β-delayed neutron emission probability of 30.0(27)% based on the measured absolute branching ratios of the 199- and 563-keV γ rays from the decays of ^{76}Zn and ^{76}Ga, respectively. This measurement used the peak areas of these γ rays, the number of ^{77}Cu ions measured in the IC, and the published absolute branching ratios of the parent decays ($I_\gamma(199\,\mathrm{keV}) = 77.5(18)\%$ and $I_\gamma(563\,\mathrm{keV}) = 66(3)\%$ [NNDC]) as well as the internal conversion coefficient for the 199-keV γ ray (0.010(2) [NNDC]). A determination of this branch was also made for the LeRIBSS data using the intensities of these γ rays relative to the 505-keV γ ray. In both experiments, we observed that the value obtained from ^{76}Ga decay was slightly smaller than the value obtained from ^{76}Zn decay. This is probably due to slight inaccuracies in the published absolute branching ratios and/or incomplete decay schemes. The average values from the two experiments for these decays are 31.6(12)% and 28.0(16)% for ^{76}Zn and ^{76}Ga, respectively, which are averaged to give our proposed value of 30.3(20)%, see Fig. 4.23.

Using the measured absolute branching ratios, it is now possible to estimate the direct feeding to the ground and isomeric states. Since we have measured the feeding from ^{77}Cu decay through the β-delayed neutron branch and ^{77}Zn^g β decay, we can determine the absolute branch through β decay of ^{77}Zn^m to be 20.6(33)%. Since the feeding by the IT decay from ^{77}Zn^m is 10.8(3)%, see Fig. 4.23, the total feeding from ^{77}Cu decay going through the isomeric state is 31.4(33)% with 34(7)% of the decay out of this state going by IT decay. The isomeric state is only observed to be fed by the 505 and 591 keV γ rays which have a combined absolute intensity of 25.2(8)%. Therefore, a total of 6.3(34)% of the feeding to this state has not been observed in γ-ray intensity. To determine the observed feeding to the ground state from prompt γ rays, it was first necessary to estimate the internal conversion coefficient for the 114-keV γ ray. In ^{73,75}Ge the de-excitation γ ray between the lowest $7/2^+$ and $9/2^+$ states, with energies of about 65 keV, had measured internal conversion coefficients consistent with an almost pure M1 transition ($\delta \approx 0.1$) [NNDC]. Since the levels connected by the 114-keV γ ray are of the same spin and parity, and the energies are

similar, we assume the same level of mixing for ^{77}Zn which yields an internal conversion coefficient of 0.046(2) which was used to obtain a total relative intensity for the 114-keV γ ray of 42.4(11)%. We then observe a total absolute feeding from prompt γ rays and the IT transition of 41.1(11)% while the intensity leaving this state is 49.1(26)%. The difference of 8.0(28)% corresponds to the unobserved intensity feeding this level. If the 114-keV γ ray is assumed to be a pure E2 transition ($\alpha = 0.394(11)$), then the unobserved feeding is only reduced to 5.3(29)%. For both the ground and isomeric states, the missing intensity could come from unobserved prompt γ rays or from direct feeding in the β decay of ^{77}Cu. The former case is a strong possibility since the lower limit for assigning γ rays was a relative intensity of about 1% (0.2% absolute), but seems to be a more likely possibility for the isomeric state than for the ground state. Finally, it is noted that the total observed intensity from prompt γ rays feeding either the ground or isomeric state and the measured β-delayed neutron branch corresponds to a total of 96.5(24)% of the total decay intensity. Hence, there is only a small amount of unobserved feeding not accounted for in the current analysis.

The β decay of ^{77}Cu is observed to feed the 2_1^+ and 4_1^+ states in even-even ^{76}Zn [Van05, Win90] through the β-delayed neutron branch. The 598-keV γ ray has an intensity (100.2(9)%) equivalent to the 505-keV γ ray in the β branch. This equivalent intensity is not obvious in the β-gated spectrum shown in Fig. 4.17 since the β detection efficiency is much lower for the high-lying unbound states in ^{77}Zn which are fed by this branch. Indeed, the measured β detection efficiency for the 598-keV γ ray is consistent with an average feeding in the β decay of ^{77}Cu (Q_β=10.21 MeV) to states with an excitation energy of about 6.5 MeV in ^{77}Zn. The 698-keV $4_1^+ \rightarrow 2_1^+$ transition in ^{76}Zn, with a relative intensity of 2.89(11)%, has a β detection efficiency consistent with average feeding to levels above 8 MeV in excitation. For both γ rays the intensity is taken from the γ-ray singles spectrum. Although the β-delayed neutron feeding to excited states is strong, 35(8)% of this decay branch appears to go to ^{76}Zn^g.

The ground state of ^{77}Zn has been proposed to be composed primarily of a $(\nu g_{9/2})^3$ three quasiparticle configuration [Eks86]. The first excited state at 114 keV was first observed in the β-delayed neutron branch of ^{78}Cu decay [Van05]. We observe a strong 114-keV γ ray which is in coincidence with numerous high energy γ rays and is assigned as de-exciting the 114-keV level. This level has been assigned as having a large component of the $J^\pi = 9/2^+$, $\nu g_{9/2}$ single particle configuration, similar to other Zn and Ge isotopes in this region [Ehr67, Yoh76]. The presence of the $1/2^-$ isomeric state leaves out any other option for this assignment since a spin less than 7/2 or negative parity would provide an alternative path for the decay of the isomeric state. In addition, this assignment is supported by the lack of a coincidence between the 957-keV γ ray, the third strongest transition observed in the decay, and the 114-keV γ ray indicating there are no transitions linking the 1277- and the 114-keV states. Although there is an apparent absolute feeding to the 114-keV state of 1.9(4)%, the β detection efficiency can only be explained if this missing feeding comes through states above 4 MeV in excitation. Therefore, it is very likely there is no direct feeding to this state. This level is observed to be fed by 13 γ rays, all with relative intensities less than 5%. The feeding states are most likely to have positive parity and spins greater than 5/2. It is interesting to note that of these 13 states, only 5 also have transitions to the ground state. This may be an indication of an inhibition for these decays due to the change to the three quasiparticle structure of the ground state. The opposite seems to be true for the 1409, 1427, and 1875 keV levels which decay to the ground state but not the first excited state. This may be an indication that these states, which probably also have $J \geq 5/2$, are of three quasiparticle nature with a significant $(\nu g_{9/2})^3$ component. The β detection efficiency for the 1409-keV γ ray suggests that all the feeding to this state comes from higher lying levels.

The 1277-keV level is established based on the observation that both 505- and 1277-keV transitions are in coincidence with the 957-keV γ ray and not with each other (Fig. 4.21). In addition,

the difference in the energy of these two γ rays matches the known energy of the 772-keV isomeric level. This level forms the backbone for the remainder of the level scheme since only two currently observed transitions feed the isomeric level while a large number of γ rays feed through the 1277-keV level. Since the 1277-keV level links to both the ground state ($7/2^+$) and the isomeric state ($1/2^-$), the spin-parity for this level is limited to $3/2^\pm$ or $5/2^\pm$. A $5/2^+$ assignment is precluded by the lack of even a weak E2 transition to the first excited $9/2^+$ state and an E2 transition to the ground state will dominate a M2 transition to the isomer. The $5/2^-$ assignment can also be rejected since an E1 ground-state transition should be stronger. Finally, a $3/2^-$ assignment is rejected since an M1 transition to the isomeric state should dominate. Hence the only logical assignment requires assuming the 505- and 1277-keV γ rays as E1 and E2 transitions, respectively, yielding a spin-parity of $3/2^+$ for the 1277-keV level.

The level at 1363 keV is the only state other than the 1277-keV level which is observed to feed, by the 591-keV γ ray, the isomeric state. The position of this level is established by transitions from the levels at 2235 and 3204 keV which also connect to the 1277-keV level. Since this state does not decay to the ground state, the spin parity must be $1/2^\pm$ or $3/2^-$ and connect to the isomeric level by an E1 or M1 transition. There is no evidence in the data to suggest even a weak 86-keV transition from this state to the 1277-keV level. This suggests a strong E1 transition to the isomeric state and $J^\pi = 1/2^+$.

The 2235-keV level is established by numerous transitions to lower lying states which feed both the $J^\pi = 7/2^+$ ground state and the $J^\pi = 1/2^-$ isomeric state. This state is somewhat unique in that it has a transition to almost all the states below it except for those which decay only to the first excited state. It is observed to decay by its strongest transition to the ($3/2^+$) 1277-keV level, with weaker transitions to the ($7/2^+$) ground state, ($9/2^+$) 114-keV level, ($1/2^+$) 1363-keV level, and ($J \geq 5/2$) 1409-keV level. However, no transition is observed going to the $1/2^-$ isomeric state. The observation of transitions to states ranging from $1/2^+$ to $9/2^+$ implies a $J^\pi = 5/2^+$ assignment if the spin-parity assignments for the other states are correct.

Based on the observed β-decay feedings for ^{77}Cu into states of ^{77}Zn, it is possible to estimate the ground state spin-parity assignment for ^{77}Cu. The arguments here are based on the assumption that the ground state will be dominated by either a $\pi p_{3/2}$ or a $\pi f_{5/2}$ orbital. The $\log(ft)$ values shown in Fig. 4.19 on page 52 do not strongly indicate any state fed by an allowed Gamow-Teller (GT) transition. An exception might be the state at 4605 keV, above the S_n energy of 4.557 MeV, which is undoubtedly directly fed in the β decay. As argued previously, the decay pattern of states which decay to the first excited state suggests a minimum spin of 5/2. The 4605-keV level has transitions to both the ground state and the first excited state which suggests that the spin is probably higher. An allowed β transition from a $5/2^-$ ^{77}Cu^g to a $7/2^-$ state would be consistent with this observation, whereas a second forbidden decay from a $3/2^-$ state would be precluded. It is not obvious that either the $7/2^+$ ground state or $1/2^-$ isomeric state are directly fed in the decay since some γ ray intensity is missing. The apparent $\log(ft)$ values for both states are consistent with strong first forbidden decays. This makes sense for the ground state if $J^\pi = 5/2^-$ for the ^{77}Cu^g. Conversely, if $J^\pi = 3/2^-$ were assigned to the ^{77}Cu^g then we would expect a transition with an allowed GT component to the $1/2^-$ isomeric state with much stronger direct β feeding. For comparison, the β decay of a $\pi p_{3/2}$ ground state of ^{73}Cu to the $\nu p_{1/2}$ ground state of ^{73}Zn has a measured $\log(ft)$ value of 5.4 [Huh98]. Such a low $\log(ft)$ value for the decay of ^{77}Cu would require feeding of about 35% to the isomeric state which we do not find. This evidence combines to strongly suggest that the ground state of ^{77}Cu is the $\pi f_{5/2}$ single particle state in agreement with the laser spectroscopy results obtained by Flanagan *et al* [Fla09].

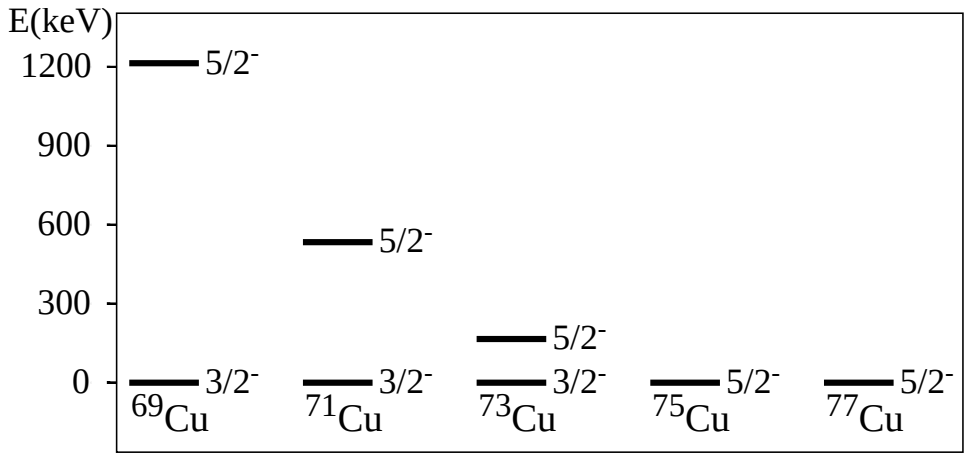

Figure 4.24: Low-energy level systematics of odd-A copper isotopes. (See text for references.)

4.2.4 β-decay study of the transitional nucleus ^{75}Cu and the structure of ^{75}Zn

Acquiring empirical information on nuclei with large neutron-to-proton asymmetry, with respect to the stable isotopes, leads us to better understanding of the nucleon-nucleon interactions in nuclear matter. In particular, the evolution of single particle properties can now be studied for very neutron-rich systems, where the sequence of orbitals known near the β-stability path has been proven inadequate in describing properties of exotic isotopes [Sch04, Gau06, Mic06].

Having just one particle outside the closed $Z=28$ core makes copper a logical choice to study the strength of the shell effects and particularly the details of the residual interactions. In a traditional shell model view, a single-particle coupling suggests $J^\pi=3/2^-$ for the ground-state spin and parity in odd-A copper owing to the 29^{th} proton being in the $\pi 2p_{3/2}$ single particle orbital. Earlier works [Run83, Huh98] confirmed this prediction by observing β-feeding to the $J^\pi=1/2^-$ and $5/2^-$ states in the zinc daughter nuclei for the odd-A copper isotopes up to ^{73}Cu.

However, energy level systematics for $^{69-73}$Cu (Fig. 4.24) indicate a lowering of the $5/2^-$ state relative to the $3/2^-$ ground state. Recently, a combination of in-source and collinear laser spectroscopy measurements of the hyperfine structure of ^{75}Cu revealed $\mu(^{75}\mathrm{Cu}) = +1.0062(13)\mu_N$ corresponding to spin $J=5/2$ for ^{75}Cu [Fla09]. Additionally, both recently completed studies on β decay of ^{77}Cu [Ily09, Pat09] suggest $5/2^-$ for its ground state. This behavior is consistent with theoretical calculations in this region [Ots05] predicting changes in the $\pi 2p_{3/2} - \pi 1f_{5/2}$ orbital ordering due to the monopole component of the residual nucleon-nucleon interaction. The β decay properties of ^{75}Cu are of current concern as this nuclide lies near the $\pi 2p_{3/2} - \pi 1f_{5/2}$ orbital crossing point, while β decay information is very limited. Prior to this study, the only data available on the β decay of ^{75}Cu included its half-life (1.224(3)s [Kra91]) and delayed-neutron emission probability (3.5$\pm$0.6% [Ree85]).

Information concerning the low-lying levels of the odd-A zinc ($Z=30$) isotopes with $A=67$, 69, 71 is known from β-decay and (d,p) neutron transfer reaction studies [Lin63, Ehr67]. The structure of ^{73}Zn was investigated with a multi-nucleon transfer reaction [Run85] as well as the β decay of ^{73}Cu produced in the fragmentation of a ^{76}Ge beam in a beryllium target [Huh98]. Finally, states in ^{77}Zn are known from β-decay studies [Pat09, Ily09]. However, no information on excited states in ^{75}Zn has been available.

Of special interest for the odd-A zinc isotopes is the evolution of the $1/2^-$ state relative to

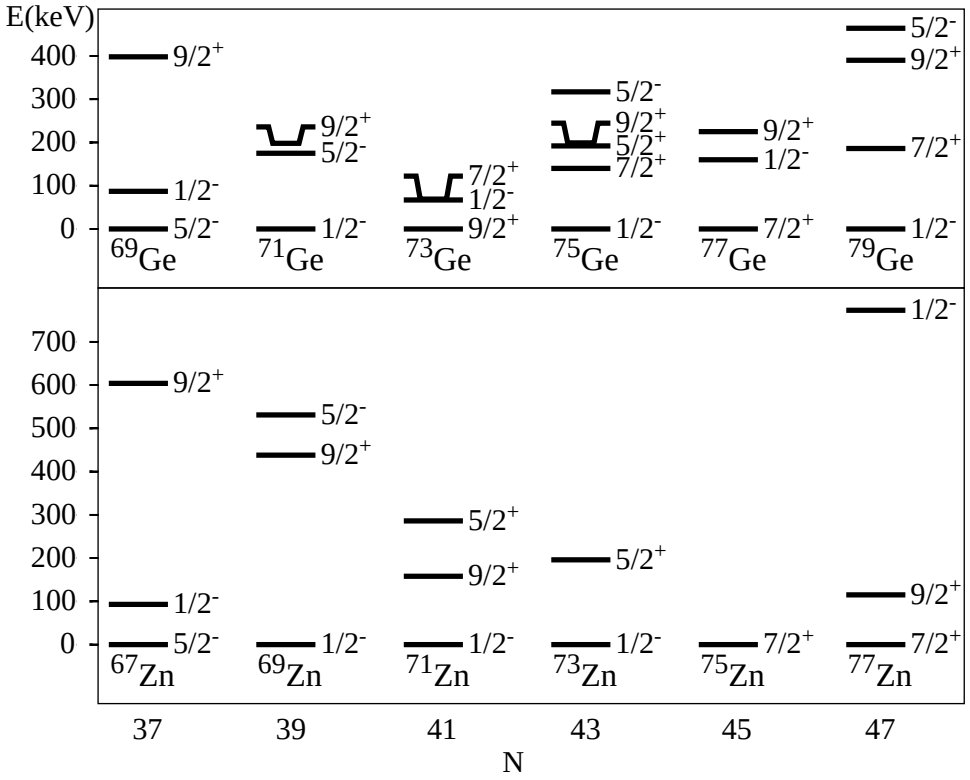

Figure 4.25: Low-energy level systematics of odd-A Z=30 zinc (lower panel) and Z=32 germanium (upper panel) isotopes. Levels in germanium are taken from [NNDC], those in zinc from [Huh98], [Lin63], and [Ehr67]. For discussion, see text.

the $9/2^+$ and $7/2^+$ states. The $9/2^+$ state is observed (Fig. 4.25, lower panel) to progressively decrease in energy relative to the $1/2^-$ state with each additional neutron pair to the $1g_{9/2}$ orbital up to $N = 41$, where this state could be expected to become the ground state with one $\nu 1g_{9/2}$ particle above the N=40 core. The observation that the ground state of ^{71}Zn is $1/2^-$ may be due to the stronger pair binding in the $\nu 1g_{9/2}$ orbital. The $9/2^+$ state has not been identified in ^{73}Zn, however a possible $7/2^+$ state which would be associated with the $\nu 1g_{9/2}$ orbital has been reported. However, there exists some controversy about this state as discussed in the following paragraph. Both the $7/2^+$ ground state and $9/2^+$ first excited state have been tentatively assigned in ^{77}Zn where the $9/2^+$ state lies ~ 600 keV below the $1/2^-$ state [Ily09]. Identifying the $1/2^-$ and $9/2^+$ states in ^{75}Zn shall complete the information on the evolution of shell structure near Fermi level in this region.

A comparison of the systematics of the zinc and germanium energy levels illustrates the similarities in the overall low-energy structure between these two isotopic chains up to $N = 43$ as seen in Fig. 4.25. One exception is ^{73}Zn where a comparison with its isotonic counterpart (^{75}Ge) suggests the existence of three low-lying positive parity states, though only one state has been clearly observed in β decay studies [Huh98, Run85]. A 5.8 s half-life for a state depopulated by 42.1- and 195.5-keV γ rays was reported in the β-decay studies of the $A = 73$ group for even-Z nuclei [Run85]. The 195.5-keV transition was deduced to have $E3$ multipolarity and assigned to the isomeric decay of ^{73}Zn, while the 42-keV transition was assumed to be from a state in ^{73}Ga. However, in a subsequent β-decay study [Huh98], a 195.5-keV γ ray was observed whose transition

probability was found to be greater with a half-life measured as 13.0 ms which implies a larger $M2$ admixture. These two apparently contradictory observations could be accounted for by the presence of two closely spaced levels in ^{73}Zn with the 5.8 s 195.5-keV isomer observed earlier [Run85] likely to be the $7/2^+$ level expected at low energy according to the level systematics. In addition, the $E3$ character of the isomeric transitions in most neighboring nuclei has been established by internal conversion measurements (see, for example, Ref. [Bur54] and references therein). Further, the occurrence of a triplet of positive parity states having $J^\pi = 5/2^+, 7/2^+$, and $9/2^+$ has also been predicted by particle-triaxial rotor model calculations assuming a ground state quadrupole deformation of $\beta_2 = 0.20$ [Huh98]. Although, the predicted $9/2^+$ state seems a particularly tempting candidate for placement of the 42-keV γ ray, its location was substantiated by the half-life analysis of copper and gallium K X-rays and the fact that the 42-keV transition was seen in $\beta\gamma$ coincidence spectra [Run85] to be a transition in ^{73}Ga. The NSCL experiment [Huh98] was not conclusive on this point since 42 keV was below their energy threshold thus leaving existence of a $7/2^+$ state in ^{73}Zn uncertain. It therefore appears that ^{73}Zn and ^{75}Ge do have very similar structures. The question then becomes why the level structure in ^{77}Zn differs so radically from that of its neighboring $N=47$ isotone ^{79}Ge and will a similar change be observed for ^{75}Zn.

Another peculiarity related to the structure of ^{75}Zn is isomerism. Although, isomerism is certainly expected in ^{75}Zn due to the proximity of $\nu 2p_{1/2}$ and $\nu 1g_{9/2}$ orbitals, it has not been observed. Again, analysis of neighboring nuclei (Fig. 4.26) shows that all even-Z, N=45 isotones are observed to have a three-quasi-particle type $7/2^+$ ground state, a consequence of Coriolis mixing of three neutrons in the $1g_{9/2}$ orbital [Gol51] and a $1/2^-$ isomeric state due to the nearby $\nu 2p_{1/2}$ orbital. It has been suggested [Eks86] that the $1/2^-$ state in ^{75}Zn might have a very short half-life caused by the presence of a $5/2^+$ intruder state located below it or a half-life comparable to that of the ground state such that the γ-rays are thus not easily assigned to a specific isomer. The latter hypothesis was rejected on the basis of available data on the β decay of ^{75}Zn, although this is insufficient evidence to assert the non-existence of isomerism.

It is apparent that ^{75}Zn lies at a transition point in nuclear structure. Therefore, determination of the energies of the $1/2^-$ and $9/2^+$ states could provide a better understanding of the evolution of structure in this region. This work extends our knowledge on the β decay properties of ^{75}Cu presenting the first detailed level structure of ^{75}Zn. Evidence will also be presented for a low-lying β-decaying isomeric state.

Radioactive nuclei were produced at the HRIBF using the LeRIBSS setup. Just as with ^{77}Cu, use of the charge exchange cell removed zinc ions from the beam. Since available rates for ^{75}Cu were higher than we could effectively use, we narrowed the high resolution isobar separator image and object slits to obtain a nearly pure beam with an average ion rate of > 2000 ions/s. Due to the beam purification steps taken, the only significant contaminant was relatively long lived ^{75}Ga. Given the half-lives of ^{75}Cu (1.22 s), ^{75}Zn (10.2 s), and ^{75}Ga (126 s), an MTC cycle with a grow-in time of 5 s and a decay time of 7 s was used to minimize the effects of ^{75}Ga accumulation. At this MTC cycle we could accumulate ^{75}Cu ions to nearly the saturation point (5 s $\approx 4t_{1/2}$) and observe over a long decay time (7 s $\approx 5t_{1/2}$). All decays associated with ^{75}Zn came through the decay chain meaning that no γ rays from ^{75}Zn or ^{75}Ga dominated in the spectrum. Use of tape cycles helped us correctly identify γ rays associated with particular decays. Additional data were taken with the MTC stopped to obtain a saturation spectrum. The overall run time was less than 3 hours including building saturation spectra. A representative β-gated spectrum from the saturation measurement is shown in Fig. 4.27. Analysis of the data resulted in 126 γ transitions being assigned to the decay of ^{75}Cu and allowed construction of the decay scheme shown in Figs. 4.28 on page 65 and 4.29 on page 66.

The half-life of ^{75}Cu was measured by observing the decay of the 109-, 193-, 268-, 345-, 421-,

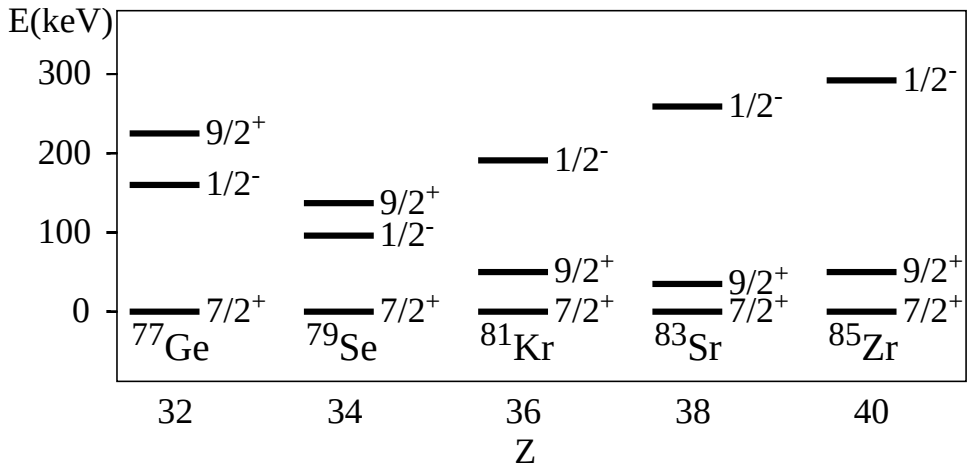

Figure 4.26: Low-energy level systematics of odd-A $N = 45$ isotones. Levels are taken from [NNDC]. For discussion, see text.

476-, 724-, and 799-keV γ rays assigned to its decay and determined by taking the weighted average of all values obtained by fitting. The spectra were corrected by background subtraction. A plot of the decay curves for the selected γ rays as a function of time is shown in Fig. 4.30 on page 67. The obtained half-life of 1.222(8) s is in good agreement with the previously reported value of 1.224(3) s based on β-delayed neutron decay counting [Kra91].

The proposed decay scheme of ^{75}Cu (Fig. 4.28 and 4.29) contains 59 levels including 120 γ rays whose placements were made based on $\gamma\gamma$ coincidence measurements. The γ-ray intensities are based on the analysis of γ-ray singles spectrum with the exception of a few weaker transitions. For these γ rays, analysis of a β-gated spectrum or a background subtraction technique were used. For the former case the β-detection efficiencies were estimated using stronger γ rays de-exciting the same level or levels with about the same excitation energy. The obtained intensities are normalized relative to the 421-keV γ ray - the strongest transition observed in the decay - and corrected for summing effects. Most of the β-decay strength is concentrated up to $\sim$ 1100 keV and in the 3000-4000 keV range. All γ rays with relative intensities greater than 1% have been placed in the proposed decay scheme or assigned to another decay. A number of unresolved doublets have been observed that have a component from ^{75}Zn or ^{75}Ga β decay. These include the γ rays at 724, 855, 1552, 1982, 2217, 2222, 2350, 2635, and 2813 keV. The component of the intensity of these γ rays due to ^{75}Cu decay was determined using saturation, β-gated and $\gamma\gamma$ coincidence spectra.

The energy levels up to the 1144-keV level are established based on the following arguments. The 421-724-keV γ-ray sequence ordering is supported by the evidence that both γ rays are in coincidence with each other (Fig. 4.31) and the 421-keV transition is seen by many high-energy γ rays (Fig. 4.28 and 4.29) that in turn do not observe the 724-keV γ ray thus putting the 724-keV γ ray above the 421-keV γ ray, thus establishing the 1144-keV level. The 668-724-799-908-keV group was assigned to depopulate the same 1144-keV level because all of these transitions are seen by a 1760-keV γ ray (Fig. 4.31) and many other higher-energy γ rays and they are not in coincidence with each other (e.g. the 724- and 799-keV gates in Fig. 4.31). These transitions lead to additional levels at 236, 345, and 476 keV. The 1144-keV γ ray is dashed because its energy matches that for a cross-over transition to the ground state but it is not seen in coincidence with any other γ rays.

The γ rays at 193, 218, and 345 keV are observed by the 799-keV γ ray (Fig. 4.31) and numerous higher-energy γ rays that all see the same sequence of γ rays in their coincidence gates. These three

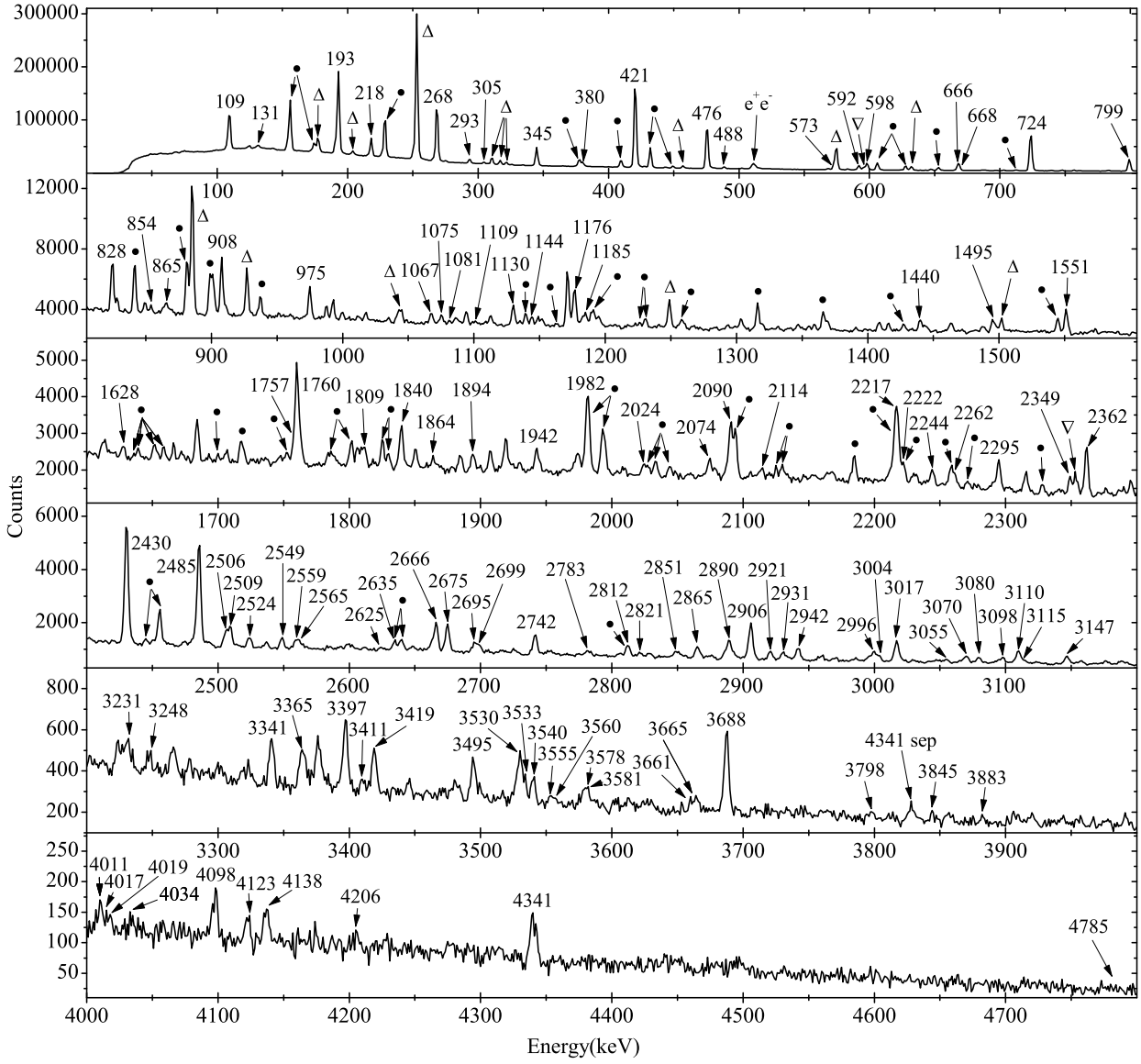

Figure 4.27: Saturation spectrum obtained in the LeRIBSS data run with a purified ^{75}Cu beam. The γ-ray peak, assigned to ^{75}Cu are indicated by their energy with single and double escape peaks marked as sep and dep, respectively. Other members of the two decay chains are indicated by symbols: ^{75}Zn(•), ^{75}Ga(△), ^{74}Ga(▽)

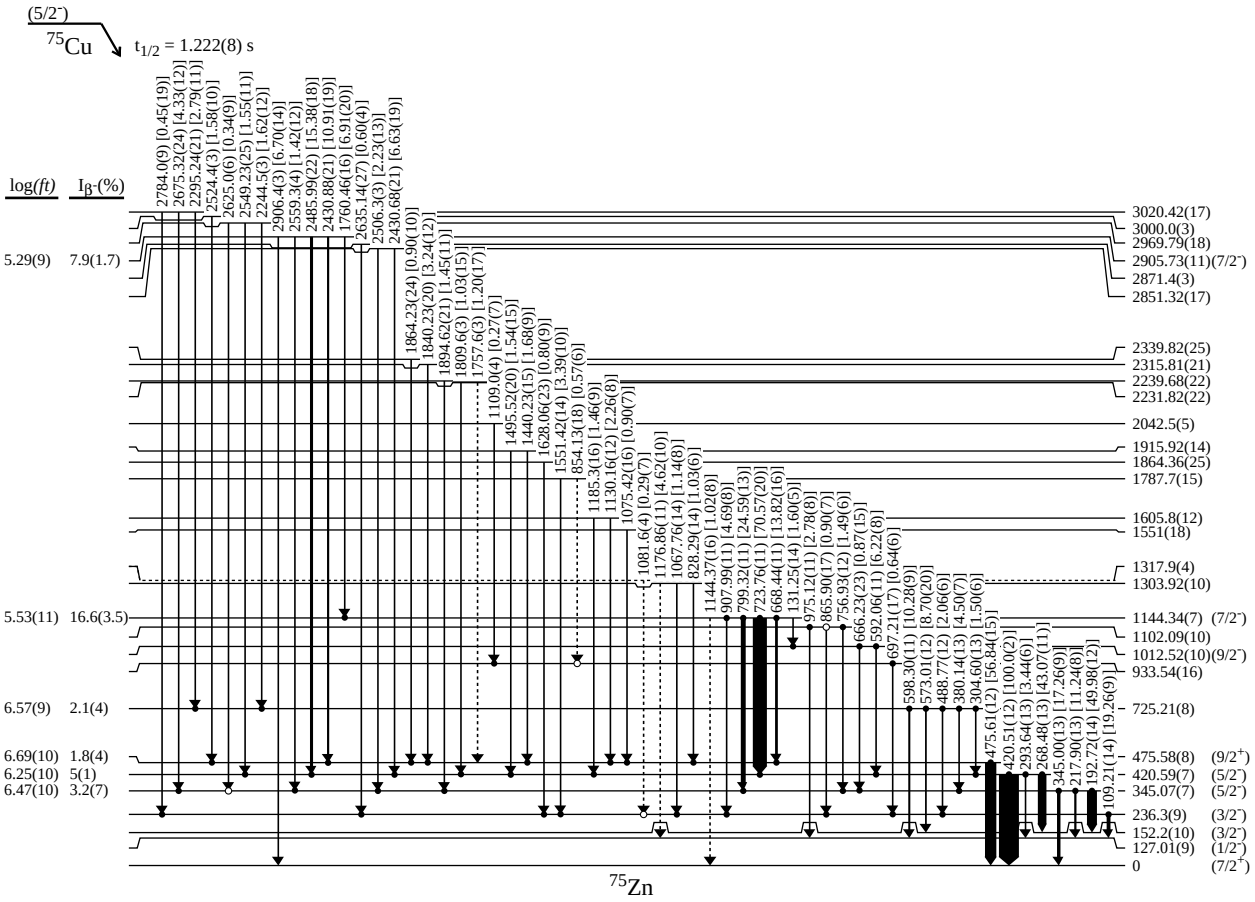

Figure 4.28: Part I of the proposed decay scheme for ^{75}Cu to excited states in ^{75}Zn showing low energy transitions. The relative intensities of the γ rays to the 421-keV transition are indicated in the figure. Filled circles indicate γ-γ coincidences seen both ways, whereas open circles indicate coincidences observed only from the upper transition. Transitions and levels without strong coincidence relationships and/or other linking transitions are indicated by dashed lines. The level feedings are based on an estimated absolute branching ratio of 19(4)% for the 421-keV transition, see text for details. Absolute β-decay feedings and $\log(ft)$ values are specified for some levels. The $\log(ft)$ values were calculated using mass values from Refs. [Rah07] and [Bar08].

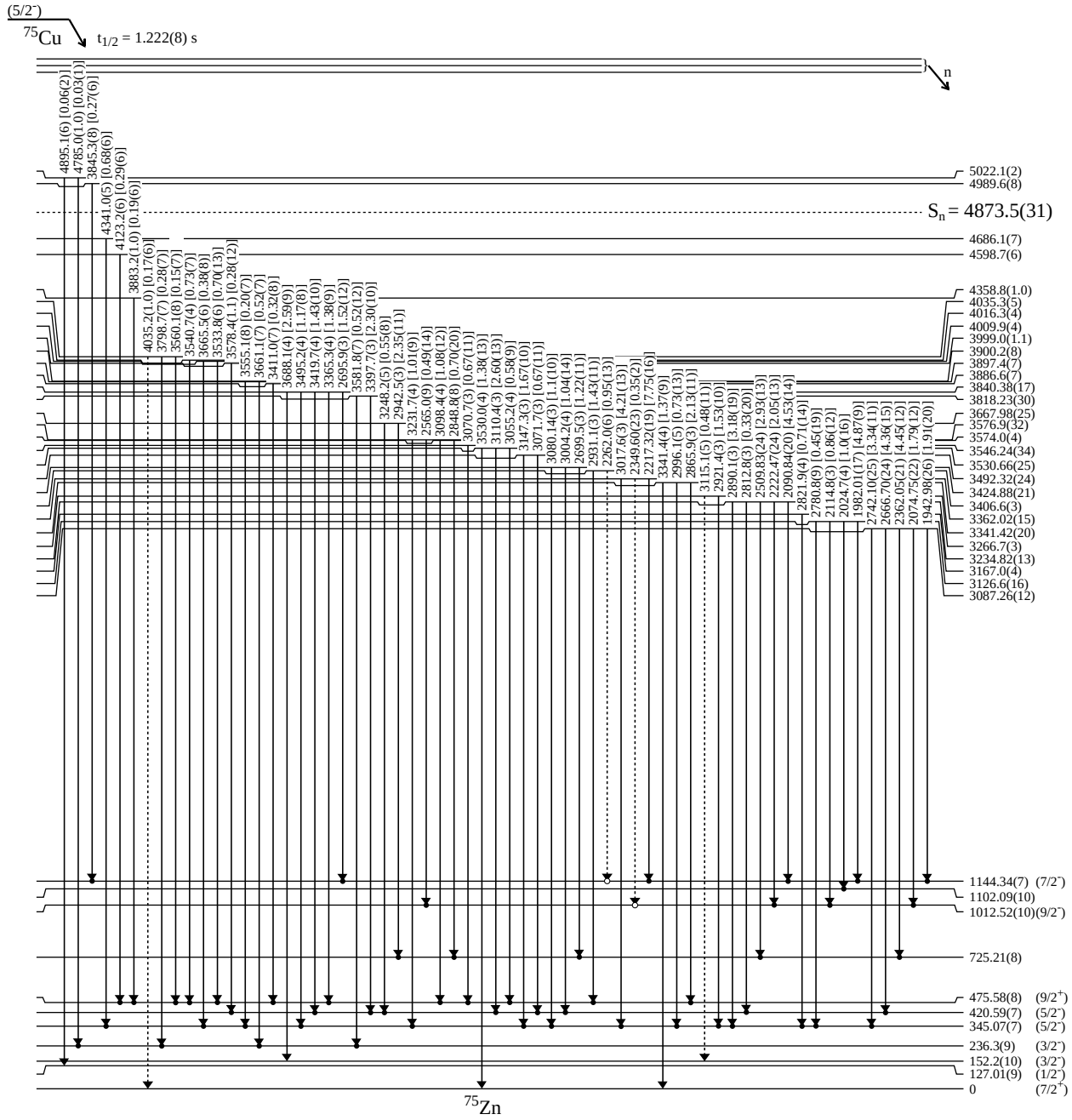

Figure 4.29: Part II of the proposed decay scheme for ^{75}Cu to excited states in ^{75}Zn showing high energy transitions. The relative intensities of the γ rays to the 421-keV transition are indicated in the figure. Filled circles indicate γ-γ coincidences seen both ways, whereas open circles indicate coincidences observed only from the upper transition. Transitions and levels without strong coincidence relationships and/or other linking transitions are indicated by dashed lines.

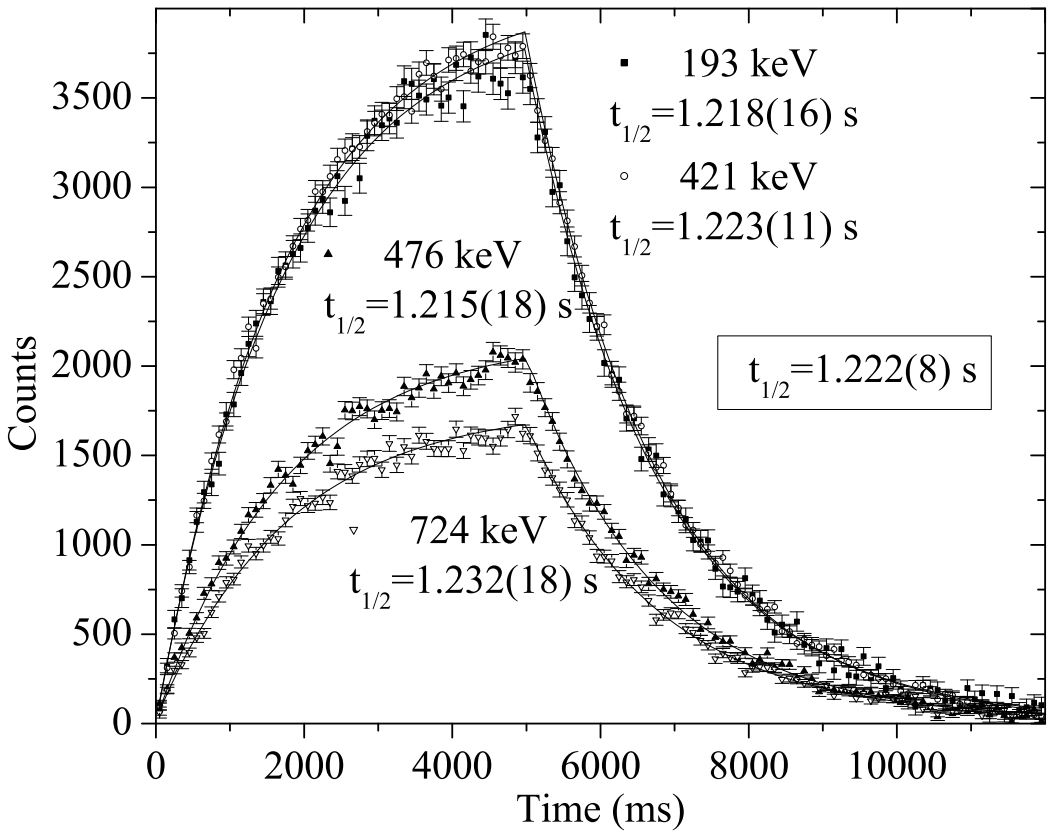

Figure 4.30: Half-life curves for γ rays depopulating the 193-, 421-, 476-, and 724-keV levels. Data were fit in both the growth and the decay portions of the curve, to optimize statistics, using a nonlinear least-squares fit routine. The average half-life value was determined from the half-live values for the 109-, 193-, 268-, 345-, 421-, 476-, 724-, and 799-keV transitions.

γ rays are not observed to be in coincidence with each other. Furthermore, the energy separation between these γ rays exactly matchers that of the 268-, 294-, and 421-keV γ rays observed in the 724-keV coincidence gate. Finally, this latter set of three γ rays are also not observed to be in coincidence with each other. Therefore, the 193-218-345 group de-exciting the 345-keV level and the 268-294-421 group de-exciting the 421-keV level establish levels at 127, 152, and 345 keV. In a search for γ rays at 127- and 152-keV, both singles and $\gamma\gamma$ coincidence spectra were investigated. However, no evidence for γ rays at these energies was observed suggesting that there is no direct link between these states and the ground state.

The 908-109 sequence is the third cascade originating from the 1144-keV level. This cascade fits in the decay scheme providing additional support for the existence of the 127-keV level. The order of the γ rays in this cascade is based on the large number of coincident transitions observed in the 109-keV gate while only the two γ rays at 109- and 1760-keV are observed in the 908-keV gate. This establishes the level at 236 keV.

Placement of the 476-keV transition was complicated by the fact that it is not in coincidence with any other major γ ray and the peak at 668 keV seen in the 476-keV coincidence gate (Fig. 4.31) is interpreted as being representative of two different γ rays with part of it being in coincidence with the 193-218-345 group. If the 668-keV peak represented only a single transition, the strong

coincidences with the 193-keV peak seen in Fig. 4.31 could only be accounted for if a third linking transition of about 130-keV energy depopulating the 476-keV state were present. A 131-keV transition does exist in the spectrum (Fig. 4.27) and it is observed to be in coincidence with a 666-keV γ ray. However, it is assigned to de-excite the 1144-keV state based on $\gamma\gamma$ coincidences with a 421-592 cascade. It could thus be concluded that the peak near 668-keV is in fact composed of two different γ rays at 666 and 668 keV. Coupling this result with numerous high-energy γ rays in the 476-keV coincidence gate and the presence of the 666-keV γ ray in the 193-keV gate (see Fig. 4.31) allows the definite placement of levels at 476- and 1013-keV in the decay scheme.

The assumption that four cascades – 908-109, 799-(193,218,345), 724-(268,294,421), and 668-476 – are in parallel is supported by the fact that no coincidences are observed between γ rays in one cascade and any other cascade from the 1144-keV level (Fig. 4.31).

It is apparent in Fig. 4.31 on the following page that the 489-keV γ transition is in coincidence with the 109-keV γ ray. From the coincidence relationships for the 489- and 598-keV γ rays with higher energy γ rays and the fact that the energy sum for the 489-109 cascade is equal to 598-keV suggests that the 489 and 109-keV coincident radiations are adjacent in the cascade and that the 598-keV γ ray represents the crossover transition. A similar argument holds for the 380-keV transition populating the 345-keV level and provides evidence for placement of the 573-keV γ ray. These cascades combine to establish the level at 725 keV.

The levels at 934 and 1102 keV are established by the strong coincidences between the 109-keV γ ray and γ rays at 697 and 866 keV (Fig. 4.31). The 697-keV γ ray also has a strong coincidence with an 1109-keV γ ray. However, the latter cannot be used in establishing the level at 934 keV due to lack of a cross-over transition from the 2042-keV state. Placement of the 1102-keV level is confirmed by the 757-keV γ ray observed in the 193-keV gate.

All levels in the decay scheme above 1144-keV are observed to decay only to states at or below this level. The levels are all established by $\gamma\gamma$ coincidence relationships observed in both the gate on the γ ray de-exciting the level and gates on the γ rays below this in the proposed decay scheme. Any γ rays feeding into the 236-keV level or above but which are not confirmed by coincidences being observed both ways are dashed in the decay scheme. A number of γ-ray transitions placed in the decay scheme populate the ground, 127-, and 152-keV states but are considered to be well established by their observed relative intensity being greater than 1% as well as a good energy match as a crossover transition. None of these γ rays are observed to be in coincidence with any of the γ rays placed in the lower portion of the decay scheme.

Three γ rays are observed to de-excite two levels (4990 and 5022 keV) above the neutron separation energy at $S_n = 4874(3)$ keV ([NNDC]). Both the 3845- and 4785-keV γ rays are established by convincing coincidence relations (see Fig. 4.32). The 4895-keV γ-ray placement is based on energy matching as a cross-over transition and lack of $\gamma\gamma$ coincidences even though it is more intense than the 4785-keV γ ray.

The establishment of two ^{75}Zn γ-decaying states above the neutron separation energy and a similar observation of three states in ^{77}Zn [Ily09] may have an effect on theoretical calculations of β-delayed neutron branching ratios in this nuclear mass range. Currently, the calculations are typically being done under the assumption of a two-way β-strength distribution - with a sharp cut above and below the neutron separation energy. The fact that we identified levels lying above the neutron separation energies which decay at least partially by γ emission, not entirely by β-delayed neutron emission, suggests that the previous assumption might not be valid and more comprehensive theoretical analysis of β-delayed neutron branching ratios is needed.

The absolute branching ratio of the 421-keV γ ray could not be directly determined in this experiment. A comparison to the known decay scheme for ^{75}Ga was not possible because of the unknown amount of primary gallium in the beam. In addition, we cannot use the published

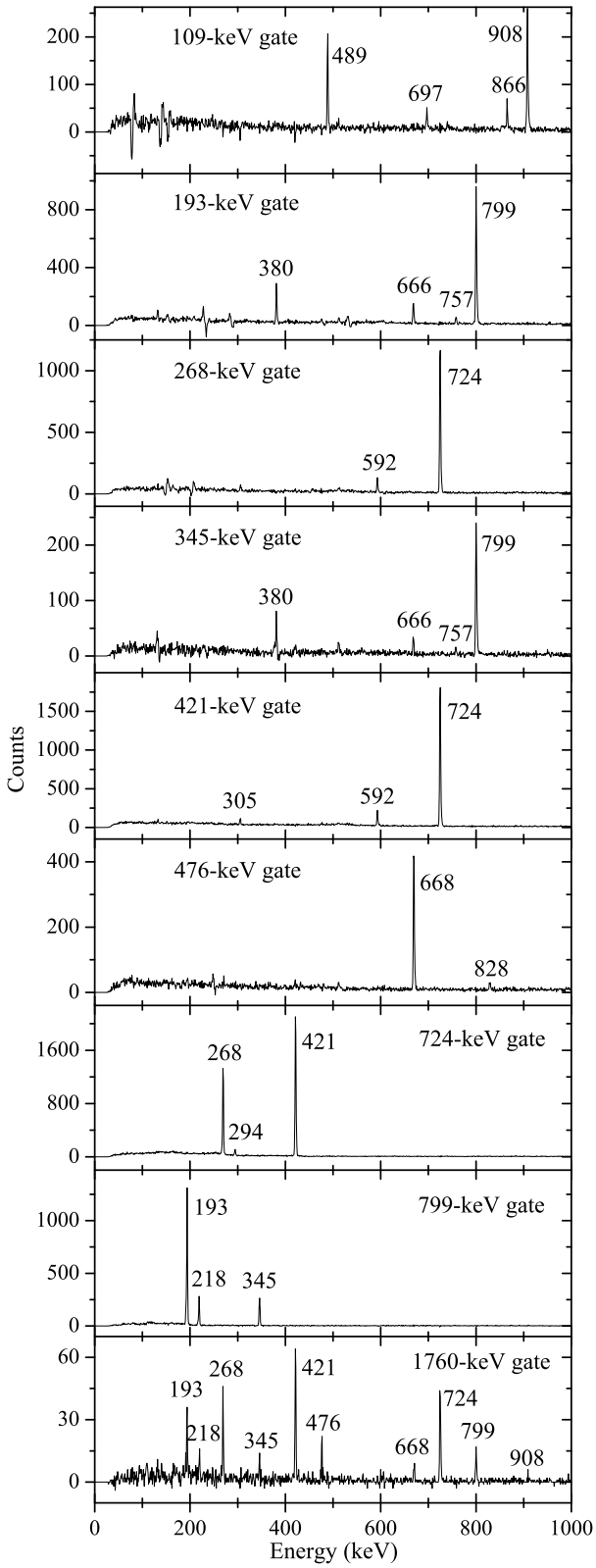

Figure 4.31: γ-ray spectra coincidence with the 109-, 193-, 268-, 345-, 421-, 476-, 724-, 799-, and 1760-keV transitions.

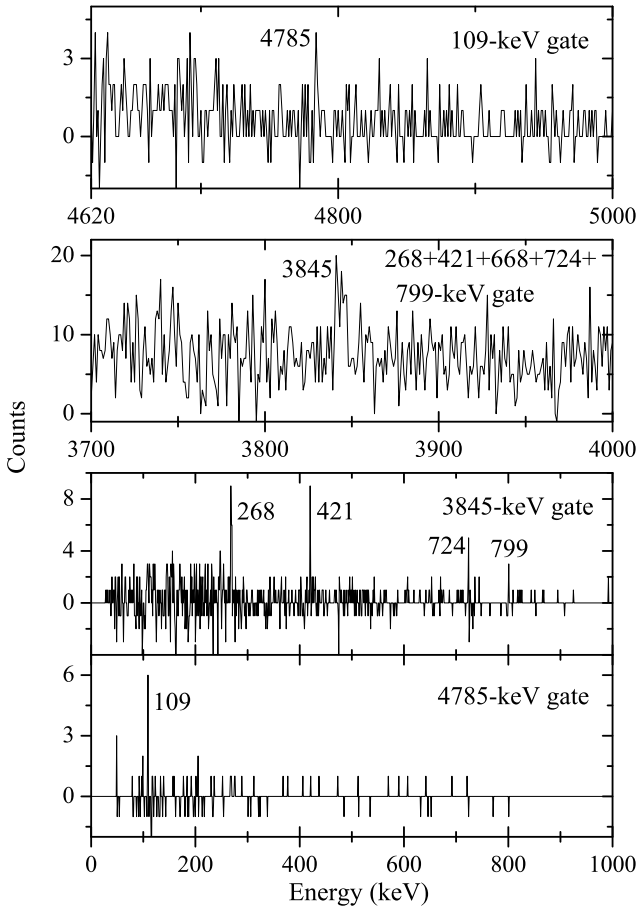

Figure 4.32: Portions of the γ-ray coincidence spectra for the 109-, 268+421+668+724+799-, 3845-, and 4785-keV transitions.

absolute branching ratio for ^{75}Zn decay since we do not know the effect of the feeding through the 127- and 152-keV levels on this value. However, a range of values can be given based on information available from the decay scheme obtained as described in the following paragraphs. Although we do not observe a transition between the 152- and 127-keV levels since this energy (25 keV) is below our energy threshold, we will assume this transition does exist as will be argued later. In addition, some of the arguments will be based upon spin/parity assignments which will be presented later.

First, we assume that we have observed all the γ-ray intensity from the decay and there is no direct feeding to the ground state, or 127- and 152-keV levels (Fig. 4.33(a)). This assumption is not completely correct as there should be some direct feeding to the ground state since this is a first forbidden transition (the $5/2^-$ ^{75}Cu^g to the $7/2^+$ ^{75}Zn^g), any direct feeding to the 127- and 152-keV levels cannot be measured, and any intensity from γ rays feeding into these states would result in an increase in the total β-decay intensity. Therefore, this assumption imposes the absolute upper limit since any missing feeding will reduce the value. Based on the published value of 96.5(6)% for the β-decay branching ratio [Ree85], we obtain an upper limit of 28.3(2)% for the absolute branching ratio of the 421-keV γ ray.

Second, we can refine the previous estimate by considering possible unobserved direct feeding. As mentioned above, the actual feeding will be lower since it is not unlikely that there exists some

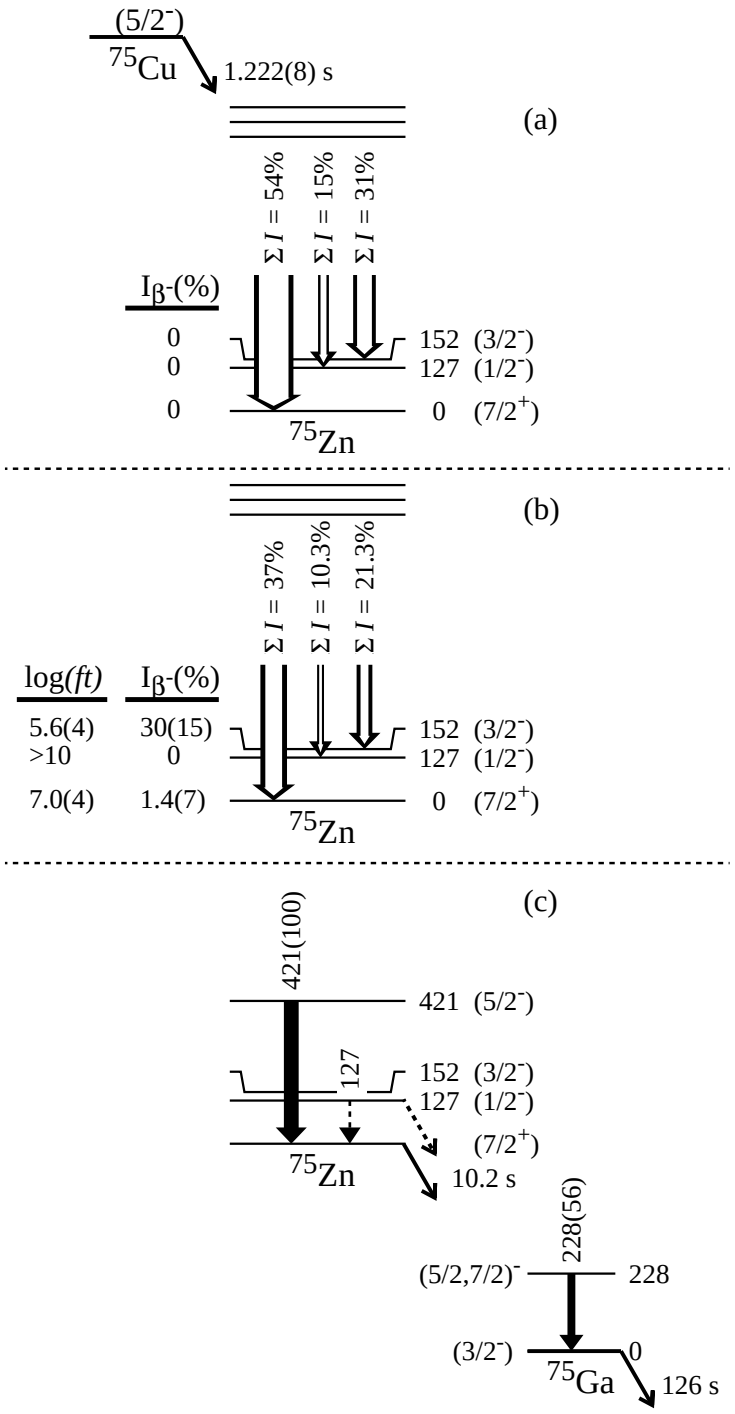

Figure 4.33: Different scenarios of β decay of ^{75}Cu to levels in ^{75}Zn used to determine the limits for the absolute branching ratio of the 421-keV γ ray transition. The sum relative γ-ray intensities (the actual value of 353 was normalized to 100%) to corresponding levels are represented by white arrows and absolute β intensities are shown traditionally on the left next to energy levels. (See text for details.)

unobserved branching to the ground state from the high energy states or unobserved direct feeding to the three lowest energy states in ^{75}Zn. Unobserved feeding from higher-lying states (above 2 MeV) is probably insignificant since it would likely feed through observed transitions and not go directly to one of the three lowest states. To determine the effect of the unobserved feeding to the three lowest states, we estimated this feeding based on the spin/parity assignments presented later. There should be no substantial feeding to the proposed $1/2^-$ isomeric state at 127 keV as it would require a second forbidden transition ($5/2^- \rightarrow 1/2^-$). If we then assume reasonable $\log(ft) = 5.6(4)$ for allowed feeding to a $3/2^-$ 152-keV state and 7.0(4) for first-forbidden feeding to the $7/2^+$ ground state, we would estimate the unobserved β feeding to be 30(15)% and 1.4(7)%, respectively (Fig. 4.33(b)). These values can be used to obtain a more realistic estimate of 19(4)% for the 421-keV absolute branching ratio.

Third, we can assume that there is an unobserved linking transition between the ground and the first excited states (Fig. 4.33(c)) and get an estimate on the absolute branching ratio of the 421-keV γ ray by direct comparison to γ rays from ^{75}Zn β decay. The basic assumption is that all the feeding goes through the ground state and the measured absolute branching ratio for the 228-keV γ ray from ^{75}Zn (28.9(14)%) [Eks86] can be used directly. The value obtained by this analysis is 49.8(25)% when considering the ^{75}Cu β-branch value of 96.5(6)%. This value which exceeds our previously established upper limit, indicates that the $1/2^-$ state has a significant β-decay branch thus confirming the existence of an isomeric state.

Finally, we assume a 100% β-decay branch from the $1/2^-$ isomeric state which directly feeds the ^{75}Zn ground state, keep the assumptions about direct feeding to the three lowest states, and again do the direct comparison between the 421- and 228-keV γ rays. The resulting absolute branching ratio for the 421-keV transition is 19(4)%. The agreement between this value and that obtained from the total intensity sum using the same assumptions about unobserved direct feeding suggests that a value of 19(4)% is a reasonable estimate. We chose to use this for the determination of the level feedings and $\log(ft)$ values shown in Fig. 4.28 on page 65.

The β-delayed neutron branching ratio of ^{75}Cu could not be determined from the ratio of corresponding γ-ray intensities. The problem is related to the difficulty in extracting meaningful values for both the β and βn branches (Fig. 4.34). As mentioned in the previous section, the unknown absolute branching ratio for the 228-keV transition in ^{75}Ga fed by β decay and ^{75}Ga in the beam make the $P_{\beta n}$ determination using the β branch impossible. In addition, our experimental setup did not allow us to measure directly the exact number of ^{75}Cu ions in the beam, so that a determination using only the βn branch is not possible. The presence of ^{74}Zn is confirmed by the 606-812-keV cascade but since the energies of the γ rays from the decay of ^{74}Zn are fairly low, their intensities could not be accurately determined due to a high background level. Therefore, we have used the previously reported value of 3.5(6)% [Ree85] since systematics in this region [Win09] indicate that this value is reasonable.

The arguments presented previously establish the primary low-energy level structure of ^{75}Zn. Based on the present level arrangement, it is now possible to make predictions concerning the spin-parity assignments for some of these states.

The ground state of ^{75}Zn was deduced in its β decay study [Eks86] based on the following arguments. It was found experimentally [Eks86] that the decay patterns of ^{75}Zn and ^{77}Zn are very similar with the maximum of the β-strength centered near 2.5 MeV in the gallium nuclei. $J^\pi = 7/2^+$ was assumed [Eks86] to be the ground state of ^{77}Zn similar to that of ^{77}Ge [Mit52]. Therefore, a J^π of $7/2^+$ has been adopted for the ground state of ^{75}Zn as well. Low-lying $7/2^+$ states in this area of the nuclear chart have been interpreted as being due to a $(g_{9/2})^3$ configuration rather than the $g_{7/2}$ single-particle state [Mih51]. A splitting between the ^{77}Ge^g, if assumed to be a $g_{7/2}$ single-particle state, and a $g_{9/2}$ second excited state would be too small to be compatible with

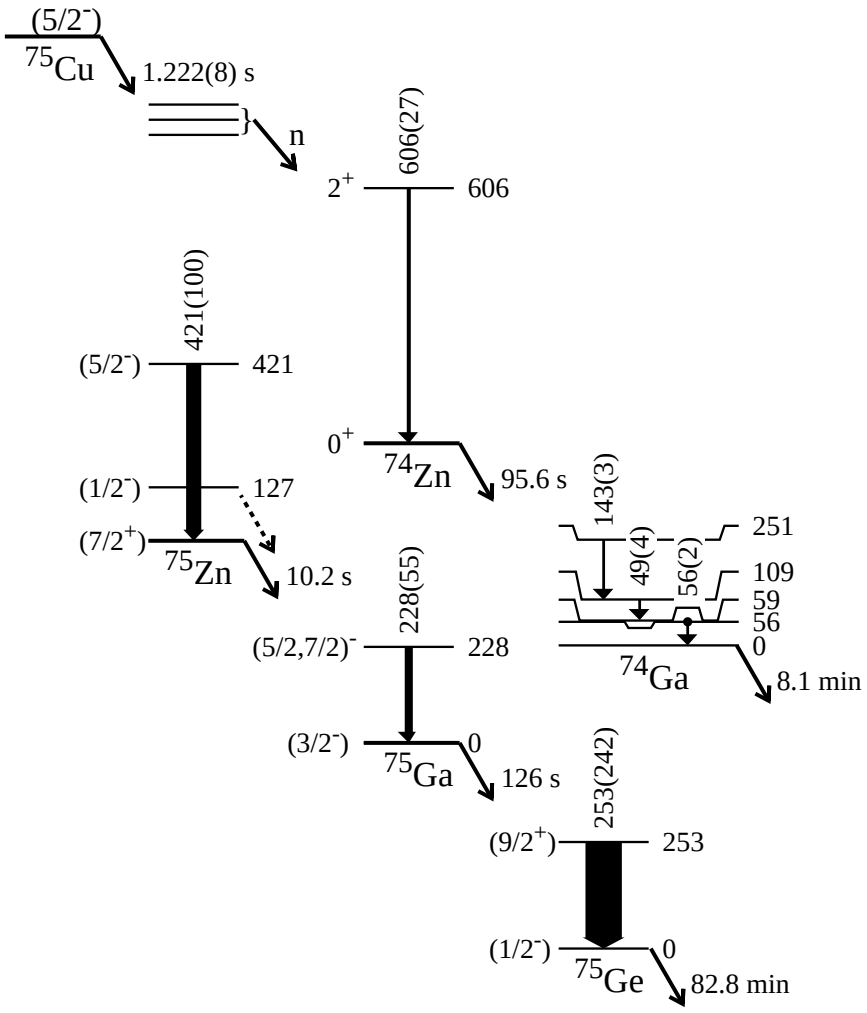

Figure 4.34: Subset of the decay schemes of ^{75}Cu and its daughter activities used to estimate the $P_{\beta n}$value. The intensities shown are relative to the 421-keV transition.

the much larger energy separation required by spin-orbit coupling [Har51]. Therefore, it seems likely that these levels can be thought of as arising from the coupling of an odd nucleon and a Coriolis-broken pair of nucleons all adding their spins together.

One particular feature of the ^{75}Zn structure is that there are two low-lying levels sitting close to each other at 127 and 152 keV which do not appear to have γ rays de-exciting them. For β decay to compete with an IT transition of 25 or 152 keV, a multipolarity of M2 as the lowest multipolarity exit channel is needed. This can only happen if $J^\pi = 11/2^-$, an improbable situation given the orbitals available. It is, therefore, unlikely that ^{75}Zn will have two β decaying isomers. Consequently, similar to other cases in this nuclear mass range, we have assumed that ^{75}Zn has a single β-decaying isomeric state. The assumption of a low-energy 25-keV highly converted $M1$ transition between the 152- and 127-keV levels seems quite reasonable. This energy is below our detection limit and additional specifically designed conversion electron measurements would be needed to confirm this suggestion.

From systematics, the first excited isomeric state at 127 keV could reasonably be assigned to

be $1/2^-$ since this type of isomerism is expected to occur (see Figs. 4.25 and 4.26). The reason why the isomeric state has not been observed previously is because it might predominantly feed directly the $3/2^-$ ^{75}Ga^g and thus cannot be seen among γ-ray transitions belonging to ^{75}Zn decay in a manner similar to that known in the β decay of ^{77}Zn [Ily09]. This conjecture is supported by the results of our absolute branching ratio estimate where this assumption was used. In this arrangement with $J^\pi = 7/2^+$ and $1/2^-$ being the ground and the first excited states, respectively, the allowed β transition from $1/2^-$ ^{75}Zn^m to the $J^\pi = 3/2^-$ ground state of ^{75}Ga would bypass the 228-keV transition in ^{75}Ga. The non-observation of a 127-keV γ ray can also be understood from the systematics (Fig. 4.26). For ^{79}Se and higher-Z $N = 45$ isotones, the $1/2^-$ isomer decays to the $7/2^+$ ground state by a 100% IT branch. At ^{77}Ge, the increase in the β-decay energy allows a competition between the two decay paths such that an 81% β-decay branch occurs [NNDC]. With the further increase in available β-decay energy at ^{75}Zn, it is reasonable to assume that the β-decay branch will reach nearly 100%. The Weisskopf estimate for a 127-keV E3 transition is 6.8 s, so an allowed β decay to low-spin negative parity states in ^{75}Ga should be the dominate decay path.

Based on the assignments of the spin/parity of the ground and isomeric states, we can make further spin/parity assignments for additional levels based on their decay patterns to these states (see Figs. 4.28, 4.29, as well as Table II in Ref. [Ily11]). These assignments will be based on a few simple assumptions. First, it is assumed that only γ rays with multipolarities of E1, M1/E2, or E2 will be observed. Any higher multipolarity transitions are improbable since a lower multipolarity transition should be possible to either the ground or isomeric state. This assumption will limit the spin/parity assignment for a number of levels to only a few possibilities. Second, we will assume that in general the dipole transitions will be stronger. This is not a firm requirement since the actual wave functions will determine the transition probability, but does provide some guidance. Third, additional insight is provided by considering the strength of the β-decay feeding to the level. The $\pi 1f_{5/2}$ ground state of ^{75}Cu will feed $3/2^-$, $5/2^-$, and $7/2^-$ states by allowed transitions, and $3/2^+$, $5/2^+$, and $7/2^+$ states by first forbidden transitions. Any feeding to a $9/2^+$ state will be a very weak first forbidden unique β decay. These last two assumptions will suggest a preferred assignment from the values specified by the first assumption.

The strongest γ ray in the decay links the 421-keV state to the $7/2^+$ ^{75}Zn ground state. This level also has a much weaker transition, 294 keV, to the $1/2^-$ isomeric state. This observation with a difference of three units of angular momentum and a change in parity requires one transition to be of E1 multipolarity while the other is of E2 multipolarity, and limits the spin/parity assignment to $3/2^+$ or $5/2^-$. The much greater intensity for the 421-keV γ ray favors it being the E1 transition in the pair. Therefore, we suggest a $J^\pi = 5/2^-$ for the 421-keV state. The apparent β-decay feeding to this level with $\log(ft) = 6.3(3)$ is consistent with either an allowed or first-forbidden decay. Arguments to firm up the assignment for this level will be presented later.

The 476-keV level de-excites by a single γ ray transition to the ground state. This single transition cannot put a strong limit on the spin/parity assignment. However, the lack of observed transitions to the isomeric state and the 421-keV level can be used to restrict the assignment. If the 421-keV level is $5/2^-$ then the spin/parity is restricted to $9/2^+$. However, if the 421-keV level is a $3/2^+$ state then $7/2^-$ and $9/2^-$ assignments are also possible. From systematics of the $N = 45$ isotones (Fig. 4.26) we expect to observe a low-lying $9/2^+$ state. The energy separation between this state and the $7/2^+$ ground state appears to be increasing in energy as Z decreases, so an energy separation of 476 keV is reasonable. No other observed state has a decay pattern which would suggest a $9/2^+$ assignment. Therefore, although based on the non-observation of transitions, we assume this assignment is $9/2^+$ and will consider this a firm assignment for later arguments.

The 1144-keV level is observed to de-excite by strong transitions to the 421- and 476-keV levels, a weak possible transition to the ground state, and no transition to the isomeric state. In

addition, it is observed to be the strongest directly fed state in β decay resulting in an apparent $\log(ft) = 5.6(4)$. Although not conclusive, this result is indicative of an allowed β decay which limits the spin/parity to $3/2^-$, $5/2^-$ and $7/2^-$. This assignment can further be restricted to $7/2^-$ by the lack of a transition to the isomeric state. A first-forbidden β decay to this state cannot be ruled out, but this would mean there are no states fed by allowed β decays. This value also restricts the assignment for the 421-keV level to $5/2^-$ as previously suggested. A $5/2^-$ assignment for the 421-keV level adds further support to a $9/2^+$ assignment for the 476-keV level since the two negative parity possibilities should have resulted in an observed transition to the 421-keV level.

The 2906-keV level also exhibits strong β feeding indicating an allowed transition which limits its spin/parity to $3/2^-$, $5/2^-$, and $7/2^-$. This level is observed to connect by γ-ray transitions to $5/2^-$, $7/2^\pm$, and $9/2^+$ levels which limits the assignment to $7/2^-$. This assignment is further justified by the observation that the strongest transition, 2486 keV, is to the $5/2^-$ 421-keV level indicating a strong M1 transition.

The 345-keV level has a decay pattern similar to the 421-keV level which restricts the spin/parity assignment to $3/2^+$ or $5/2^-$. The major difference is in the intensity of the decay pattern which suggests a difference in the structure of the states. The 218- and 345-keV transitions are of about equal intensity, while the 193-keV transition to the 152-keV level is the strongest. We might then assume that the 345- and 421-keV levels do not have the same spin/parity assignment. However, the 799-keV γ ray from the 1144-keV level requires a $5/2^-$ assignment. The observed β-decay feeding and $\log(ft)$ values are consistent with either allowed or first forbidden β decays, so no distinction based on this is possible. Yet, the nearly identical β-decay feeding to these states suggests that they must be fed by the same type of β decay lending support to the $5/2^-$ assignment for the 345-keV level. The hinderance of the E1 transition to the ground state would be an indication of significant differences in the structure of the two states.

A spin/parity assignment for the 152-keV level requires considering the transitions feeding it from the 345-, 421-, and 1144-keV levels as well as the lack of a transition to the ground state. The requirement of no feeding to the ground state limits the possible assignments to $1/2^-$ and $3/2^-$. This assignment is further restricted to be $3/2^-$ by the observed transition from the 1144-keV state. This assignment is also consistent with the $5/2^-$ assignments for the 345- and 421-keV levels which show strong E1 and M1/E2 transitions to the ground state and 152-keV level, respectively, and a weaker E2 transition to the isomeric state.

The 236-keV level has γ-ray transitions connecting it to $1/2^-$ and $7/2^-$ states. This observation restricts the spin/parity assignment to be $3/2^-$ or $5/2^-$. The weaker intensity of the 908-keV transition out of the 1144-keV level compared to the dipole transitions suggests that this might be of E2 multipolarity. In addition, the lack of observed transitions to the ground state or 152-keV level suggest that the 109-keV transition must be a dipole transition. Therefore, we favor a $3/2^-$ assignment for this state.

The 1013-keV level does not have any apparent β-decay feeding, has observed γ-ray transitions connecting it to $5/2^-$ and $7/2^-$ states, and no observed transitions to the $1/2^-$, $3/2^-$, $7/2^+$, and $9/2^+$ states. If we consider only the observed transitions, the lack of direct β feeding suggests a $9/2^-$ assignment, requiring a strong hinderance of the E1 transitions to the ground state and 476-keV level.

Similar arguments based on the observed γ ray decay patterns of the levels connected to by each level can be made. The results of this analysis, using the previously discussed spin/parity assignments, are presented in Table II of Ref. [Ily11]. In this analysis, only observed γ-ray transitions were considered. In addition, for levels above 1144 keV, direct feeding in the β decay requires allowed or first-forbidden β decays which limits the spin/partity assignments to $3/2^\pm$, $5/2^\pm$, and $7/2^\pm$. However, it is not possible to distinguish between these two modes of β decay. Only cases

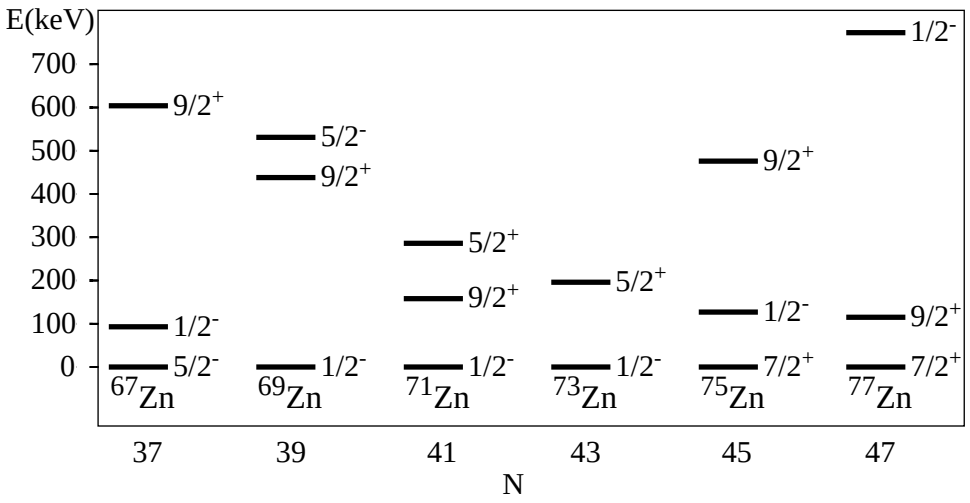

Figure 4.35: Low-energy level systematics of odd-A Z=30 zinc isotopes including the lowest $1/2^-$ and $9/2^+$ states in ^{75}Zn. Energy levels in zinc are taken from [Huh98], [Lin63], [Ehr67], and the present work. For discussion, see text.

which are limited to four or fewer possible assignments are shown in the table.

Identification of the proposed lowest $1/2^-$ and $9/2^+$ states in ^{75}Zn allows us to complete the systematics for evolution of these states up to N=47 in the odd-A zinc isotopes (Fig. 4.35). The energy of the $1/2^-$ isomer follows the expected trend for the zinc isotopes, but has a lower energy than would have been expected from the systematics of the odd-A N=45 isotopes (Fig. 4.26). Conversely, the $9/2^+$ state follows the expected trend from the N=45 isotopes, but is at a much higher energy than expected when comparing to this state in ^{77}Zn.

The observed structure of ^{75}Zn is similar to that of both the other zinc isotopes as well as the $N = 45$ isotones. However, there is a significantly larger number of low spin, negative parity states at low energy in ^{75}Zn when compared to these other nuclei. The question then arises as to the composition of these states. As a first step, consider the possible states which can arise from simple shell model arguments. The positive parity states come from the $(\nu g_{9/2})^3$ couplings. As mentioned previously, the ground state is understood to come from a three-quasiparticle configuration [Eks86], while the $9/2^+$ state is probably composed of both single-particle and three-quasiparticle configurations. The presence of negative parity states requires breaking the $\nu p_{1/2}$ pair, to produce states with a $(\nu g_{9/2})^2_J \otimes (\nu p_{1/2})^{-1}$ configuration. These states can occur at low energy due to the stronger coupling between nucleons in the $g_{9/2}$ orbital. The isomeric state can then be understood to come from the $J = 0$ coupling, while the $3/2^-$ and $5/2^-$ states could come from the $J = 2$ coupling. However, this concept cannot explain the number of $3/2^-$ and $5/2^-$ states observed or their energy. In a weak coupling approach, the two states from the $J = 2$ coupling should lie centered about the energy of the 2^+_1 in the adjacent even-even nuclei, which in this case is ~ 600 keV.

It does not seem likely that strong deformation is involved (see, e.g., [Huh98]) since either prolate or oblate deformation should result in a $5/2^+$ ground state. The occurrence of a three-quasiparticle state seems the reasonable explanation since our data are consistent with a $7/2^+$ ground state and not $9/2^+$.

It is evident that a complex interplay of effects is involved in the structure of the heavy zinc isotopes. It is possible that large-basis shell-model calculations (see, e.g., [Sie10]) could provide the answer. However, additional experimental work is needed to solidify the spin/parity assignments

for all nuclei in this region.

A more thorough study of the ^{75}Zn low-energy level structure might be useful. In particular, a specifically designed conversion electron measurement would be needed to confirm our suggestion for a low-energy highly converted transition supposedly linking the 152- and 127-keV states. The present work also indicates that a closer look at the structure of ^{73}Zn is needed.

4.2.5 Research in Progress: The $A=74$ β-decay Chain

The primary effort at the end of the project was analysis of $A = 74$ β-decay data (^{74}Cu $\rightarrow$ ^{74}Zn $\rightarrow$ ^{74}Ga $\rightarrow$ ^{74}Ge(stable)) taken in April 2012 at the HRIBF. This data was obtained as a part of the last series of experiments performed at the facility prior to its closure. The primary interest for this study lies in the total decay heat produced by the decay and its importance to nuclear reactors.

For any given decay, the known transitions and intensities can be used to generate a predicted total absorption spectroscopy (TAS) spectrum, i.e. the total decay heat. What has been found is that there is significant differences between the predicted and observed spectra. This is generally attributed to a large number of unobserved γ rays from higher-energy (> 3 MeV) states fed by Gamow-Teller transitions, i.e. the pandemonium effect. Hence, the purpose of the current study is to do the high-resolution compliment to the TAS measurement to determine the extent to which the unobserved states can be identified. Since feeding to these states can be very large even if the observed intensities of the γ grays is small, a significant shift in the β-decay feeding may be indicated resulting in a reinterpretation of the previous results. There were plans to also obtain TAS data for this decay chain, but that experiment has yet to be performed. Therefore, this high-resolution experiment is simply meant to increase our knowledge of the level structure fed by the decays, especially to weakly fed ($< 1\%$ β feeding) states at energies above 2 MeV.

The $A = 74$ β-decay chain has been studied extensively in the past. However, improvements in beam intensities and purity, as well as improved detection systems, allowed us to restudy these decays to determine if any information has been missed. For both ^{74}Cu and ^{74}Zn, we have placed a large number of previously unreported γ rays and established many new levels as indicated below. For ^{74}Ga decay, we had hoped to use a detailed knowledge for the decay to a well studied stable nucleus as a way to internally check the data set. However, during the analysis, we discovered significant problems with information in the NNDC database. Therefore, we have added ^{74}Ga β decay to our study in order to resolve the discrepancies which were observed.

To insure an unbiased result, the development of the level schemes is being done without consideration of the previously published results. This "from the ground up" approach was used to check the previous results for errors. At this time a number of new transitions have been identified leading to possible new states. Development of the decay schemes relied heavily on the $\gamma\gamma$ coincidence data. The main problem being encountered is the lack of cross-over transitions to firmly establish new states. Therefore, quantitative evidence is needed for the $\gamma\gamma$ coincidences in order to provide confidence in placements of new levels involving a single γ-ray transition. This has been accomplished by determining a statistical significance for each "observed" coincidence to establish our confidence in that perceived coincidence. The statistical significance was determined by fitting peak areas in both a peak plus background gate and an adjacent background gate. The background gate was adjusted to make sure that any obvious background lines in the spectra would exactly cancel out when subtracting areas. The difference in areas (Δ_A) of the two spectra were determined along with uncertainty (σ) in that difference. The statistical significance factor was then defined as $S = \Delta_A/\sigma$. If $S < 2$ the possible coincidence was ignored as being statistically insignificant. If $2 < S < 3.5$ the coincidence was considered a possible but not a definite coincidence, while $S > 3.5$

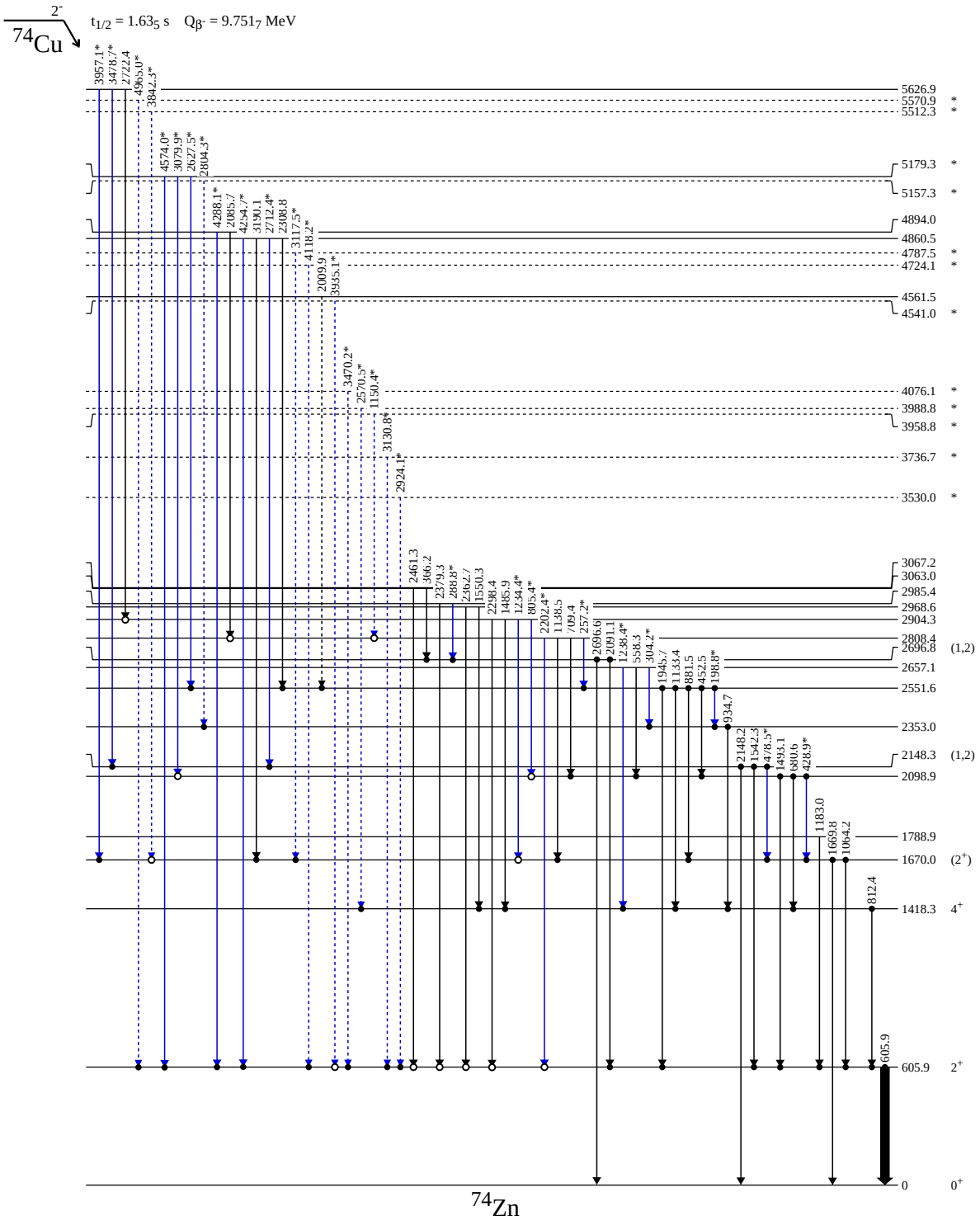

Figure 4.36: Preliminary decay scheme for ^{74}Cu. The half-life, Q_β, and spin/parity assignments are taken from the NNDC.[NNDC] Closed dots indicate firm coincidence relationships while open dots indicate a possible coincidence. The dashed levels indicate cases here a level is placed based on a single γ ray. New levels and γ rays are indicated by a *, with the γ rays also being color coded.

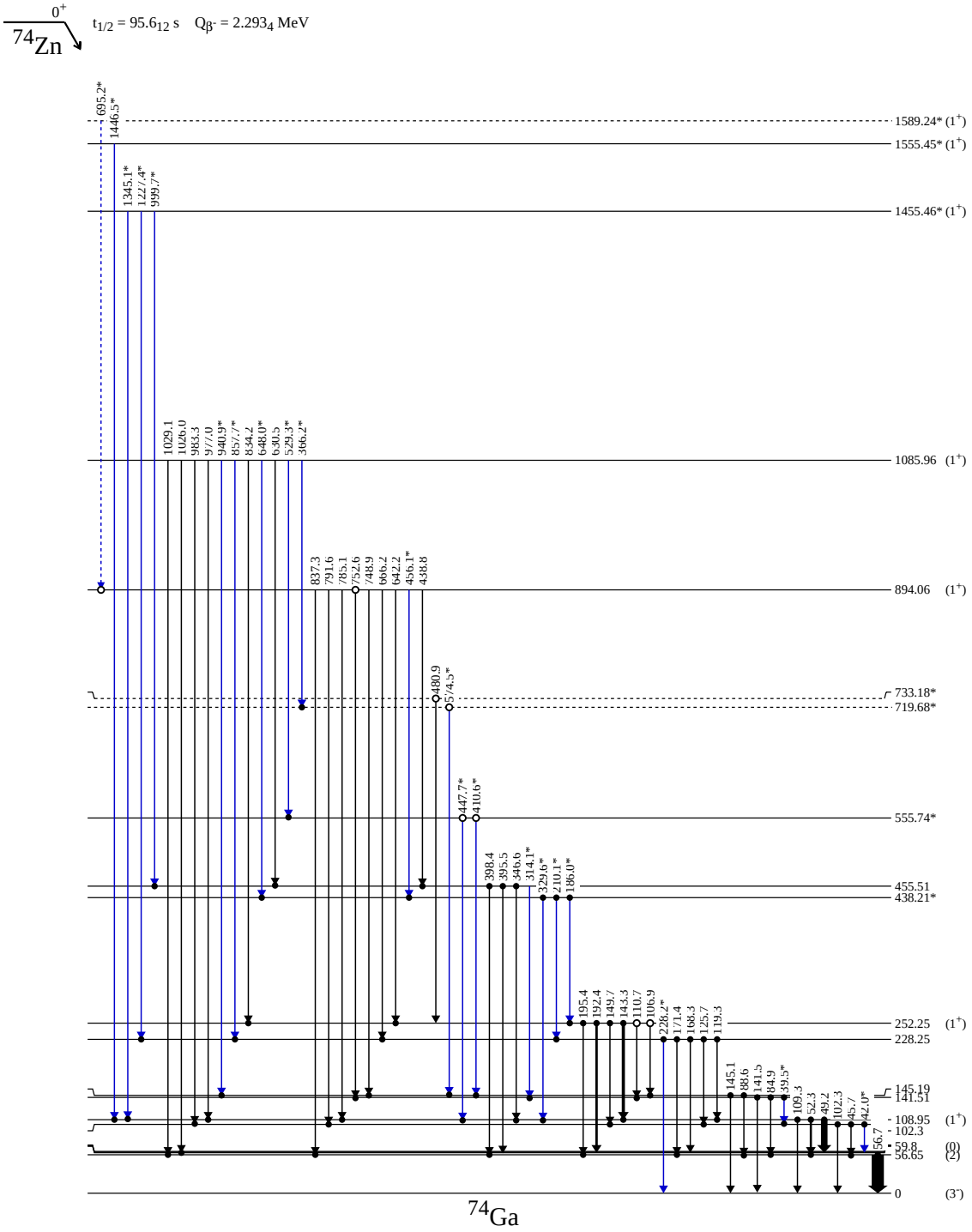

Figure 4.37: Preliminary decay scheme for ^{74}Zn. The half-life and Q_β are taken from the NNDC.[NNDC] The spin/parity assignments for he first three levels come from the NNDC while the designated (1^+) states are based on the current analysis. Closed dots indicate firm coincidence relationships while open dots indicate a possible coincidence. The dashed levels indicate cases here a level is placed based on a single de-exciting γ ray. New levels and γ rays are indicated by a *, with the γ rays also being color coded.

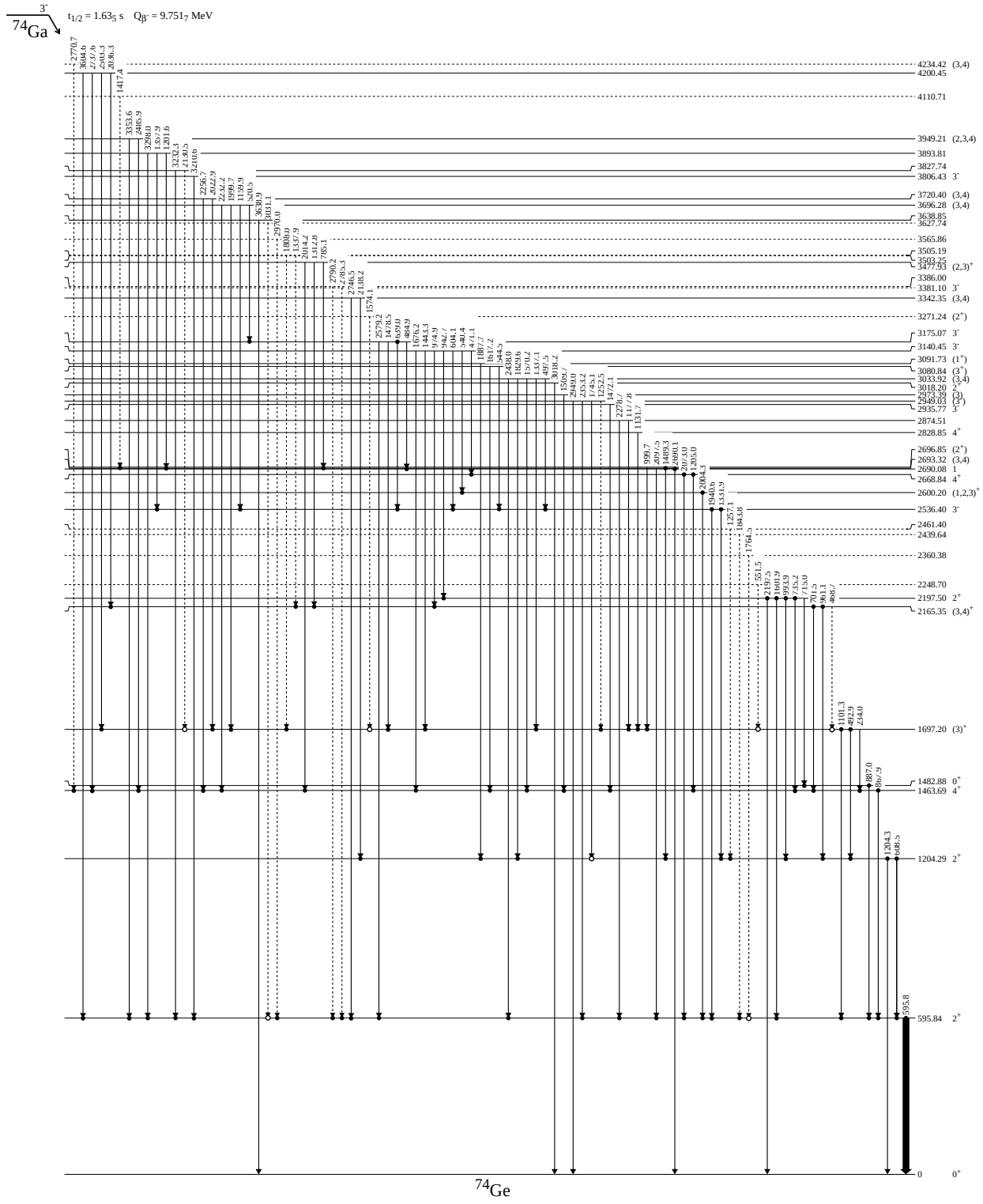

Figure 4.38: Preliminary decay scheme for ^{74}Ga. The half-life, Q_β, and spin/parity assignments are taken from the NNDC.[NNDC] Closed dots indicate firm coincidence relationships while open dots indicate a possible coincidence. The dashed levels and transitions are for cases which are still to be confirmed.

was considered a definite coincidence. This method has been necessary to avoid incorrect placements based on assumptions about coincidence results where incomplete background subtraction can give erroneous results. In addition, we have established a method by which to use the coincidence data to extract γ-ray intensities in cases where an unresolved doublet is observed in the γ-ray singles spectrum.

The preliminary decay scheme for ^{74}Cu is shown in Fig. 4.36 on page 78. This decay scheme includes 29 new γ rays and 12 new levels beyond those observed in previous studies.[NNDC] The decay pattern is what would be expected for this type of decay. The states below $\approx$3 MeV should be positive parity states fed by first-forbidden β decaysor through γ-ray cascades from above, while the states above this energy are primarily negative parity states fed by allowed β decays. These later states depopulate by E1 transitions to the positive parity states. The lack of obvious transitions from any negative parity state directly to the ground state calls into question the 2^- assignment for the ^{74}Cu ground state since an allowed β decay to a 1^- state should have resulted in a ground state transition. Given the controversial nature of this conjecture, we are continuing to search for any possible case where a negative parity state decays to both the ground and first excited states. What is abundantly clear in the decay scheme is a shift of the observed β-decay feeding from states below 3 MeV to states above 3 MeV. This includes a significant reduction in the observed direct feeding to the 2_1^+ state. The current limit for the observed transitions feeding the 606-keV level is an intensity of about 0.3% relative to the 606-keV transition as compared to a limit of about 0.9% in the previous studies. Although the current results are not definitive, they do point out the effect of pandemonium on on this system.[Har77]

The preliminary decay scheme for ^{74}Zn is shown in Fig. 4.37 on page 79. This decay scheme includes 21 new γ rays and 7 new levels beyond those observed in previous studies.[NNDC] Four of the 7 new levels are well established by multiple de-exciting γ rays. Above 800 keV we expect only 1^+ states to be observed due to strong allowed β-decay feeding. The states below 800 keV are a mix of both positive and negative parity states. The 57-keV state shows stronger intensity de-exciting the level than feeding it by observed transition. However, the 3-keV IT transition can account for all the missing feeding and would not require additional direct β-decay feeding to the 60-keV isomeric state. The 109- and 252-keV states both show apparent strong feeding suggesting these to be 1^+ states. However, the observed ground state transition would preclude this assignment for the former. No definitive statement can be made about the other states based solely on β-decay feeding. The γ rays de-exciting the 894- and 1086-keV levels might provide the best insight into the lower-lying states since both connect to essentially all the states below 500 keV with the exception of the ground state. (There is the possibility of an 894-keV γ ray, but more evidence needs to be obtained to support its placement.) These states will be connected to the lower-lying negative parity states by E1 transitions thus putting an upper limit of 2^- for all possible negative parity states except the ground state. The M1/E2 transitions to positive parity states will limit these states to spins between 0 and 3. If the the ground state is 3^- as proposed, then any positive parity state connecting to it will need to have a spin of 2^+ or 3^+ since a 4^+ state is not allowed. Hence, the possible spin/parity assignments for states below 300 keV are $0^\pm$, $1^\pm$, $2^\pm$, and 3^+. What we need to do still is to go through the decay pattern in more detail to see if the assignments to specific states can be reduced further. There are two unique features of the decay scheme. First, the large number of possible 1^+ states. Second, the occurrence of several pairs of close states. Understanding so many 1^+ states are observed and why the pairs of states occur could provide significant insight into the structure of this odd-odd nucleus. A simple shell-model picture would place the 31^{st} proton in either the $\pi p_{3/2}$ or $\pi f_{5/2}$ while the 43^{rd} neutron would go into the $\nu g_{9/2}$ orbital. (The two proton orbitals are nearly degenerate in this region.) Coupling of these states gives only the expected 2^- and 3^- state. However, strong pairing in the $\nu g_{9/2}$ orbital will lead to preferred occupation of the

$\nu p_{1/2}$ orbital leading to 1^+ and a 2^+ state from $(\pi p_{3/2})^1 \otimes (\nu p_{1/2})^1$ configuration. Obtaining a spin 0 state will probably require a $(\pi f_{5/2})^1 \otimes (\nu f_{5/2})^1$ configuration, but such a state would not be expected at low energy. The inclusion of four particle couplings might help in this situation, but it must go beyond simply coupling to the excited state configurations of the adjacent even-even nuclei. Obviously a theoretical understanding of this nuclide will require extensive and detailed calculations.

The preliminary decay scheme for ^{74}Ga is shown in Fig. 4.38 on page 80. This decay scheme contains 91 γ rays placed with 47 levels. Since ^{74}Ga β decays to stable ^{74}Ge, we believed the decay would have been well studied and would provide a good internal check for the data analysis. What we discovered was that the two previous β-decay measurements of ^{74}Ga were fraught with inconsistencies.[Cam71, Tay75] Although the two experiments agreed on most of the observed γ rays, the placement of these transitions into a decay scheme disagreed significantly. This lead to numerous double placements and erroneous levels being assigned within the ENSDF database.[NNDC] The problem arose due to the lack of $\gamma\gamma$ coincidence information being obtained in the two experiments. In our measurement we had good data for $\gamma\gamma$ coincidences despite the fact that the MTC cycles used in the experiment were never optimized for this decay. So far we have modified the placement of 21 γ raysobserved in the two previous studies. We have been able to confirm 24 levels identified in the two previous studies plus three levels proposed by the NNDC evaluators based on (n, γ) measurements and γ rays reported in the previous β-decay measurements. We have also added 13 levels to the β-decay scheme which have been observed in other types of measurements as well as propose 9 new levels which need further confirmation to establish our confidence in these levels. (Seven of the later cases involve a single γ-ray transition.) Finally, we we have removed 5 erroneous levels and have a further 3 levels for which we need to confirm our changed placement of a γ ray in order to fully reject. It is unclear if any of these modifications have repercussions on other experimental results, however the results do point out the need to recheck some of the older data included in the ENSDF database.

The $A=74$ decay-chain data is being analyzed by three graduate students who had no previous knowledge of β-decay spectroscopy. This has slowed the analysis and preparation of final publications. Consequently, the research was not completed prior to the end of the grant. However, the analysis of the data is continuing and will be completed within the coming months resulting in three publications.

4.3 ADN Systematics

One graduate student had been working on concepts related to α clustering prior to started graduate school at MSU. The student was seeking an understanding of why certain elements have no stable isotope. His concept was to look at the ground state of a nucleus to be composed of a number of α clusters onto which deuterons and neutrons bind. After giving some direction to the project, the student started working on his own time on a study of ground-state mass systematics using his α clustering model. Once he had developed the model sufficiently for it to appear viable, the student asked and was given permission to use part of his time on the grant working on his model. We now refer to the model as α-Deuteron-Neutron (ADN) Systematics. The complete scope of this project exceeds what can be placed in the report, so the following is a brief synopsis of what has been accomplished. A first article based on the research is in final review and will be submitted for publication soon.

The guiding hypothesis of the study is: *The ground state of a nucleus with multiple numbers of protons and neutrons will rearrange until all protons are bound with equal numbers of neutrons in α clusters in an $N = Z$ core, due to the strong binding of the α cluster. Any odd proton remaining will pair with a neutron, forming a deuteron, or otherwise follow a decay mode to convert to a neutron. Any remaining neutrons will then couple to the $N = Z$ core.* The initial study has focussed on even-Z nuclei which will all have an α-cluster core onto which excess neutrons ($n_e = N - Z$) are added. Systematic trends were then sought by observing the trend in the binding energy (BE) as a function of n_e for each isotopic chain. A neutron pairing effect was compensated for in a consistent manner for each isotopic chain. Observations of the binding energy trends showed the data could be reasonably fit using a quadratic function of the form

$$BE(n_e) = a_0 + a_1 \cdot n_e + a_2 \cdot n_e^2 \tag{4.1}$$

where each fit parameter represents a physical characteristic or interaction among the nucleons. Dimensional analysis of each coefficient provided a first general interpretation of the each fit parameters. The constant term, a_0, has units of keV and is an intercept where $n_e = 0$ so it must be the total core binding energy. The linear coefficient, a_1, has units of keV/n_e and so should represent an interaction energy between excess neutrons and the α-cluster core. The third coefficient, a_2 has units keV/n_e^2. In many areas of physics, multiplying terms usually is the result of two physical quantities interacting directly, e.g. m^2 for two masses interacting in the law of universal gravitation and q^2 for interacting charges in Coulomb's law. Here, this then represents two neutrons interacting, and a_2 will inform the effect pairing has between the two excess neutrons and the core. There is no reason why the fit parameters would be the same for different elements, but it was expected that they would be smoothly varying functions of the number of α clusters (n_α) in the core.

In order to identify the proper coefficients for a given α-cluster core and isotopic chain, a series of iterative weighted least-squares fits to the experimental binding energies in the AME2012 evaluation[AME12] was performed. Each parameter was found to vary uniquely as a function of core size (n_α). These results are presented as functions of n_α, though the results can be equally shown as functions of Z without loss of information. The least-squares fitting procedure was performed multiple times, in an effort to refine the parameter values due to strong correlations between the fit parameters. A first run of the fitting allowed all three parameters to vary freely, and revealed trends for each parameter. Subsequent iterations involved fixing one or more parameters to the n_α trend and refining the fit for the free parameter(s). Iterations were continued until the fitting stabilized. It was then possible to provide some interpretation to the fit parameters.

The detail analysis revealed some interesting trends. First, an odd-even effect as a function of n_e was was observed. It was found that the data could be brought into alignment by applying the

function

$$BE_{align} = 1747.9 - 22.730\, n_e \tag{4.2}$$

Once the data was aligned it reveal that for each isotonic chain there was a kink occurs at magic neutron numbers. The curvature parameters a_2 defining the data trends on either side of the magic kink generally are very close or almost identical. The linear term a_1 distinctly reflects a slope that reduces after the kink. The constant term, a_0, is higher in the range above the kink and should have the same value as the magic-N nuclide's binding energy. Since it has been deemed that the a_0 represents a core binding energy, the lower-n_e range will be referred to as "near-core" and its a_0 will be the true $N=Z$ binding energy. The range above the kink will be referred to as an "inflated-core", reflecting the inflation of the $N=Z$ core with excess neutrons up to the magic N. These a_0 values will provide a fixed value in the inflated-core ranges when performing the least-squares fitting in later iterations.

The a_2 term was the first to be fixed. When the even-n_e trends and odd-n_e trends were treated separately, it was difficult to discern any distinctive behavior of the a_2 parameter as a function of n_α for cores of $n_\alpha \leq 20$. This problem was exacerbated by some correlation effects that resulted from the 3-parameter fits. The values varied around a possibly linear fit of the a_2 trend, and so the first few iterations assumed a linear fit for a_2 as a function of n_α. When the neutron pairing effect was considered, many of these variances were reduced and it became apparent that a decaying exponential function would yield a better fit of the collected a_2 values. Alternating between iterative fits with fixed a_0 and freely-varying a_2 and vice-versa further refined these results, until a set of values that could be fitted with an inverted decaying exponential function. The functional form is given by

$$a_2(n_\alpha) = -69.81(74) - 881(55) * e^{-0.1371(57)*n_\alpha} \tag{4.3}$$

in keV/n_e^2. This function should be interpreted as a reduction of the binding interaction between paired excess neutrons and the $N=Z$ core. In other words, when adding an excess neutron to a set of *in situ* odd-numbers of excess neutrons surrounding the core, the new neutron will pair with the unpaired *in situ* neutron, and the newly formed pair will be less bound to the $N=Z$ core, according to Equation 4.3. This effect occurs regardless of how many existing n_e are in the nucleus, but the effect itself diminishes with the increasing size of the core. While the pairing behavior is well documented, the reduction of the pair's interaction with the core is new physics. Because this quality reduces the interaction without dissolving it altogether, it cannot be called dissociation. Instead it will be referred to this as "pairing minu-sociation", from the Latin *minua* which means "diminish".

The a_0 term, represents the binding energy of the $N=Z$ core. Within this energy resides information about the nature of the nuclear interactions and structure among the protons and neutrons for $N=Z$ nuclides. Up to two values for a_0 may exist for a given isotope chain for any $N=Z$ core: the near-core and the inflated-core binding energies. Note that a_0 can be determined for all isotopic chains even though the $N=Z$ nuclide may be unbound since the values come from the fit of binding energy given by Equation 4.1. The inflated-core a_0 values show a smooth trend as a function of n_α when grouped according to the neutron magic number shell of their core. I.e., below $n_\alpha = 10$, a smooth trend is observed for the $N=20$ core, *etc.* These smooth trends allow a quadratic fit in n_α to determine the a_0 parameter. The functional form chosen is then

$$a_0(n_\alpha) = a_{0,0} + a_{0,1} n_\alpha + a_{0,2} n_\alpha^2 \tag{4.4}$$

It was discovered that the curvature term follows a smooth trend given by

$$a_{0,2}(Z) = -574 - 4446 e^{-0.0329Z} \tag{4.5}$$

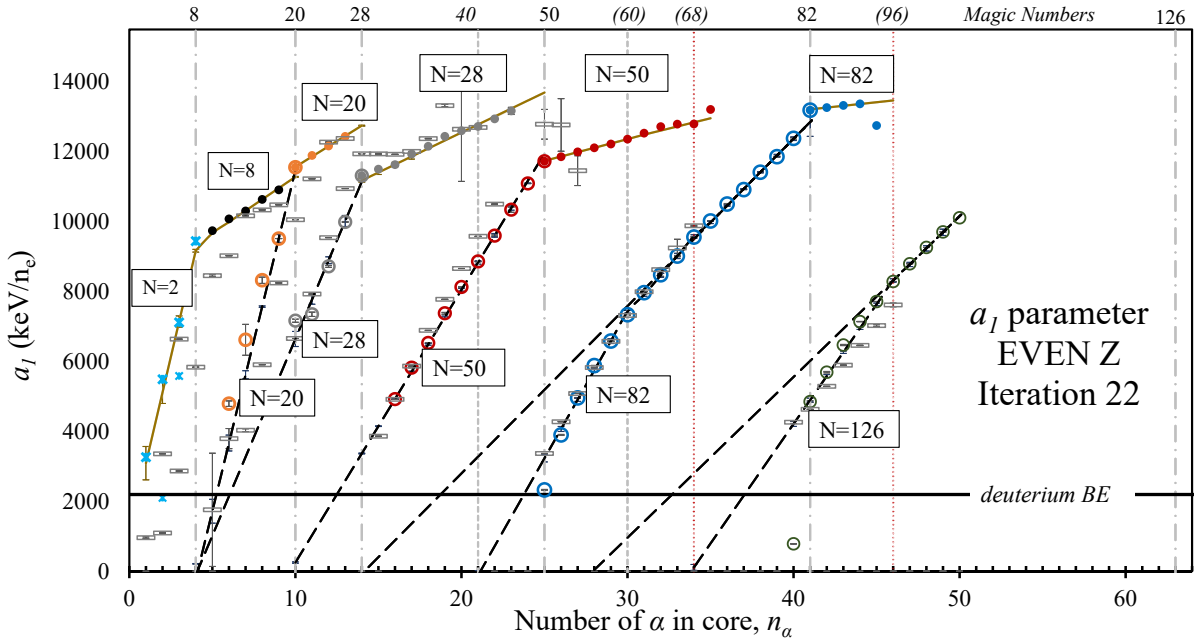

Figure 4.39: The a_1 fit parameter for the near-core (solid data) and the inflated-core (open data). The solid and dashed lines represent linear fits which are included to help guide the eye. The empty horizontal bars represent direct BE(Core+1n_e)-BE(Core) values, to confirm the a_1 behaviors were being properly identified.

By applying the curvatures as fixed parameter and allowing the $a_{0,0}$ and $a_{0,1}$ to vary freely it was found that the curves for $N=20$, 28, and 50 appear to converge at $n_\alpha = 4$ while neither the $N=82$ nor the $N=126$ trend to the same point. This may suggest that the lower-N inflated cores are more closely linked somehow to the 4α core, while the heavier inflated cores are less directly tied to this low-Z core. For the near-core binding energies, the a_0 values follow a generally smooth trend, but actually require a more detailed analysis. It was discovered that a simple fit to the trend resulted in unacceptable deviation between calculated and measured binding energies. Hence, a simple polynomial function is not a reasonable description of the binding energy of the $N=Z$ core. It is thus necessary to examine the a_0 values with a more unorthodox approach. The analysis assumes that since the core is composed of α clusters that we should be able to specify masses using the α mass (m_α) as a reference unit. The mass defect (Δ_α) would then be written as

$$\Delta_\alpha = m_{core} - n_\alpha m_\alpha \tag{4.6}$$

where m_{core} is the mass of the $N=Z$ core which comes from a_0. The result of this novel approach is a trend that strongly suggests symmetry around $n_\alpha = 25$ ($Z=50$). Because of the near-symmetry, the decision was made to fully symmetrize the range of near-core a_0 values around $n_\alpha = 25$ up to $n_\alpha = 48$. Modifications were made the to the weighting of the data points to insure the symmetry. It was very clear that the near-core a_0 mass defect values do not follow a simple smooth function and hints at the structure of the nucleus. Further analysis of these data for insights will require the removal of Coulomb interactions which are beyond the scope of the current study. Nevertheless, the importance of the symmetrization process cannot be understated as it provided a significant refinement of the large n_α a_2 fit parameters and contributed to the reduction of correlations effects.

Interpretation of a_1 was more difficult because determining the proper trends required first

establishing the other two parameters due strong correlation effects. However, once a_0 and a_2 could be specified and fixed in a consistent manner as a function of n_α, it was possible to redo the fitting procedure to extract the a_1 values shown in Fig. 4.39 on the previous page. In short ranges, these data appear to be linear. Also note that the extrapolation of the inflated-core fits appear to go to zero binding energy around magic numbers of neutrons, indicated with grey vertical dot-dash (strongly magic) and small-dot (weakly magic) lines. Notice that the near-core data reflect strong binding between the excess neutron and the core ($\sim$10–14 MeV), and consistently stronger than for the inflated-core. In addition, there is a smooth increase in binding energy as a function of increasing core size. If viewed in short ranges of n_α, these data appear to be linear in nature. A linear fit was performed on each obvious short range to gauge the linearity, with reasonable results. The linearity of these fits gives an important insight into the possible physics governing the n_e-core interaction as well, if a connection between the binding energy and the elusive nuclear force can be drawn. By comparison to a $1/r^2$ force such as the electrostatic force with a distended central charged object, it is possible to see that the binding energy per nucleon should be a linear function of the core size. There are two important physics principles that are suggested by this relationship. The first that the interaction between the an excess neutron and the core is a conservative, $1/r^2$ force, and may be similar in form to the electric and gravitational force laws. Second, the slope of the binding energy per nucleon as a function of core size must contain within it the universal constant for the strong interaction which is symmetric with the universal constants ε_0 and G. Further, the progressive shallowing of the general slopes also indicates an inverse-radius relationship. The calculation of these important values will be pursued in future work.

It is important to be able to predict masses with uncertainties below 500 keV. The ADN systematics have successfully accomplished this for a small majority of the even-Z nuclides which have been measured at least one time. Further refinement of these formulae is quite feasible by adding a higher-order term to the fit function. Deeper analysis of the a_0 terms will focus on illuminating inter-cluster qualities, and further study of a_1 will seek out the universal constant that is symmetric with G (gravitation) and ε_0 (electric). Once these have been done, the next stage will be to use these refined values to empirically derive the Coulomb effect for p-rich nuclides. This process will also be performed for the odd-Z nuclei.

Bibliography

[AME12] G. Audi, M. Wang, A. H. Wapstra, F. G. Kondev, M. MacCormick, X. Xu, and B. Pfeiffer, Chin. Phys. C**36**, 1287 (2012).

[Ang07b] G. de Angelis, Prog. Nucl. Part. Phys. **59**, 409 (2007).

[Aud03] G. Audi, O. Bersillon, J. Blachot, and A. H. Wapstra, Nucl. Phys. **A729**, 3 (2003).

[Bal93] D. P. Balamuth, U. J. Hüttmeier, and J. W. Arrison, Phys. Rev. C**48**, 2648 (1993).

[Bar08] S. Baruah, G. Audi, K. Blaum, M. Dworschak, S. George, C. Guénaut, U. Hager, F. Herfurth, A. Herlert, A. Kellerbauer, H.-J. Kluge, D. Lunney, H. Schatz, L. Schweikhard, C. Yazidjian, Phys. Rev. Lett. **101**, 262501 (2008).

[Bau07] T. Baumann, A. M. Amthor, D. Bazin, B. A. Brown, C. M. Folden III, A. Gade, T. N. Ginter, M. Hausmann, M. Matos, D. J. Morrissey, M. Portillo, A. Schiller, B. M. Sherrill, A. Stolz, O. B. Tarasov, and M. Thoennessen, Nature **449**, 1022 (2007).

[B^2FH] E. M. Burbidge, G. R. Burbidge, W. A. Fowler, and F. Hoyle, Rev. Mod. Phys. **29**, 547 (1957).

[Bor96] I. N. Borzov, S. A. Fayans, E. Krömer, and D. Zawischa, Z.Phys A**355**, 117 (1996).

[Bor05] I. N. Borzov, Phys. Rev. C**71**, 065801 (2005).

[Bur54] S. B. Burson, W. C. Jordan and J. M. Le Blanc, Phys. Rev. **96**, 1555 (1954).

[Cam71] D. C. Camp, D. R. Fielder, and B. P. Foster, Nucl. Phys. A**163**, 145 (1971).

[Cam01] J. A. Cameron and B. Singh, Nucl. Data Sheets **92**, 783 (2001).

[Dan02] A. Dangelo, Prog. Nucl. Energy **41**, 1 (2002).

[Dar09] I.G. Darby, R.K. Grzywacz, J.C. Batchelder, C.R. Bingham, L. Cartegni, C.J. Gross, M. Hjorth-Jensen, D.T. Joss, S.N. Liddick, W. Nazarewicz, S. Padgett, R.D. Page, T. Papenbrock, M.M. Rajabali, J. Rotureau, and K.P. Rykaczewski, presented at the ENAM 2008 Conf., Ryn, Poland, Sept. 2008, and submitted to Nature (2010).

[Dob07] J. Dobaczewski, N. Michel, W. Nazarewicz, M. Płoszajczak, and J. Rotureau, Prog. Part. Nucl. Phys. **59**, 432 (2007).

[Dom03] Zs. Dombrádi, D. Sohler, O. Sorlin, F. Azaiez, F. Nowacki, M. Stanoiu, Yu.-E. Penionzhkevich, J. Timár, F. Amorini, D. Baiborodin, A. Bauchet, F. Becker, M. Belleguic, C. Borcea, C. Bourgeois, Z. Dlouhy, C. Donzaud, J. Duprat, Z. Elekes, D. Guillemaud-Mueller, F. Ibrahim, M. Lewitowicz, M. J. Lopez, R. Lucas, S.M. Lukyanov, V. Maslov, C. Moore, J. Mrazek, M. G. Saint-Laurent, F. Sarazin, J.A. Scarpaci, G. Sletten, C. Stodel, M. Taylor, C. Theisen, and G. Voltolini, Nucl. Phys. A**727**, 195 (2003).

[Duf86] J. P. Dufour, R. Del Moral, A. Fleury, F. Hubert, D. Jean, M. S. Pravikoff, H. Delagrange, H. Geissel, and K. -H. Schmidt, Z. Phys. A**324**, 487 (1986).

[Ehr67] D. von Ehrenstein, J. P. Schiffer, Phys. Rev. **164**, 1374 (1967).

[Eks86] B.Ekström, B. Fogelberg, P. Hoff, E. Lund, and A. Sangariyavanish, Phys.Scr. **34**, 614 (1986)

[Fla08] K. Flanagan, in Contr. to 5^{th} Int. Conf. ENAM'08, Sept. 2008, Ryn, Poland.

[Fla09] K.T. Flanagan, P. Vingerhoets, M. Avgoulea, J. Billowes, M.L. Bissell, K. Blaum, B. Cheal, M. De Rydt, V.N. Fedosseev, D.H. Forest, Ch. Geppert, U. Köster, M. Kowalska, J. Krämer, K.-L. Kratz, A. Krieger, E. Mané, B.A. Marsh, T. Materna, L. Mathieu, P.L. Molkanov, R. Neugart, G. Neyens, W. Nörtershäuser, M.D. Seliverstov, O. Serot, M. Schug, M.A. Sjoedin, J.R. Stone, N.J. Stone, H.H. Stroke, G. Tungate, D.T. Yordanov and Yu.M. Volkov, Phys. Rev. Lett. **103**, 142501 (2009).

[For00] B. Fornal, R. Broda, W. Królas, T. Pawłat, J. Wrzesiński, D. Bazzacco, S. Lunardi, C.Rossi Alvarez, G. Viesti, G. de Angelis, M. Cinausero, D. Napoli, J. Gerl, E. Caurier, F. Nowacki, Eur. Phys. J. A**7**, 147 (2000).

[Gad06] A. Gade, B. A. Brown, D. Bazin, C. M. Campbell, J. A. Church, D. C. Dinca, J. Enders, T. Glasmacher, M. Horoi, Z. Hu, K. W. Kemper, W. F. Mueller, T. Otsuka, L. A. Riley, B. T. Roeder, T. Suzuki, J. R. Terry, K. L. Yurkewicz, and H. Zwahlen, Phys. Rev. C**74**, 034322 (2006).

[Gau06] L. Gaudefroy, O. Sorlin, D. Beaumel, Y. Blumenfeld, Z. Dombrádi, S. Fortier, S. Franchoo, M. Gélin, J. Gibelin, S. Grévy, F. Hammache, F. Ibrahim, K. W. Kemper, K.-L. Kratz, S. M. Lukyanov, C. Monrozeau, L. Nalpas, F. Nowacki, A. N. Ostrowski, T. Otsuka, Yu.-E. Penionzhkevich, J. Piekarewicz, E. C. Pollacco, P. Roussel-Chomaz, E. Rich, J. A. Scarpaci, M. G. St. Laurent, D. Sohler, M. Stanoiu, T. Suzuki, E. Tryggestad, and D. Verney, Phys. Rev. Lett. **97**, 092501 (2006).

[Gau08] L. Gaudefroy, O. Sorlin, F. Nowacki, D. Beaumel, Y. Blumenfeld, Z. Dombrádi, S. Fortier, S. Franchoo, S. Grévy, F. Hammache, K. W. Kemper, K. L. Kratz, M. G. St. Laurent, S. M. Lukyanov, L. Nalpas, A. N. Ostrowski, Yu.-E. Penionzhkevich, E. C. Pollacco, P. Roussel, P. Roussel-Chomaz, D. Sohler, M. Stanoiu, and E. Tryggesta, Phys. Rev. C**78**, 034307 (2008).

[Gol51] M. Goldhaber and A.W. Sanyar, Phys. Rev. **83**, 906 (1951).

[Gre03] S. Grévy, J. Mrázeka, J. C. Angélique, P. Baumann, C. Borcea, A. Buta, G. Canchel, W. Catford, S. Courtin, J. M. Daugas, F. De Oliveira, P. Dessagne, Z. Dlouhý, A. Knipper, K. L. Kratz, F. R. Lecolley, J. L. Lecouey, G. Lehrsenneau, M. Lewitowicz, E. Liénard, S. Lukyanov, F. Maréchal, C. Miehé, F. Negoita, N. A. Orr, D. Pantelica, Y. Penionzhkevich, J. Péter, B. Pfeiffer, S. Pietri, E. Poirier, O. Sorlin, M. Stanoiu, O. Stodel, and C. Timis, Nucl. Phys. A**722**, C424 (2003).

[Gre04] S. Grévy, J.C. Angélique, P. Baumann, C. Borcea, A. Buta, G. Canchel, W.N. Catford, S. Courtin, J.M. Daugas, F. de Oliveira, P. Dessagne, Z. Dlouhy, A. Knipper, K.L. Kratz, F.R. Lecolley, J.L. Lecouey, G. Lehrsenneau, M. Lewitowicz, E. Liénard, S. Lukyanov, F. Maréchal, C. Miehé, J. Mrazek, F. Negoita, N.A. Orr, D. Pantelica, Y.

Penionzhkevich, J. Péter, B. Pfeiffer, S. Pietri, E. Poirier, O. Sorlin, M. Stanoiu, I. Stefan, C. Stodel, C. Timis, Phys. Lett. **B594**, 252 (2004).

[Gro05] C. J. Gross, K. P. Rykaczewski, D. Shapira, J. A. Winger, J. C. Batchelder, C. R. Bingham, R. K. Grzywacz, P. A. Hausladen, W. Królas, C. Mazzocchi, A. Piechaczek, and E. F. Zganjar, Eur. Phys. J. A**25**, **S01**, 115 (2005)

[Gro09] C.J. Gross, J.A. Winger, S.V. Ilyushkin, K.P. Rykaczewski, S.N. Liddick, I.G. Darby, R.K. Grzywacz, C.R. Bingham, D. Shapira, C. Mazzocchi, S. Padgett, M.M. Rajabali, L. Cartegni, E.F. Zganjar, A. Piechaczek, J.C. Batchelder, J.H. Hamilton, C.T. Goodin, A. Korgul, and W. Królas, Acta Phys. Pol., B **40**, 447 (2009).

[Grz03] R. Grzywacz, Nucl. Instr. Meth. Phys. Res. B **204**, 649 (2003).

[Gud00] W. Gudowski, Nucl. Phys. A**663**, 169c (2000).

[Hak08] J. Hakala, S. Rahaman, V.-V. Elomaa, T. Eronen, U. Hager, A. Jokinen, A.Kankainen, I. D. Moore, H. Penttilä, S. Rinta-Antila, J. Rissanen, A. Saastamoinen, T. Sonoda, C. Weber, and J. Äystö, Phys. Rev. Lett. **101**, 052502 (2008).

[Har51] J. A. Harvey, Phys. Rev. **81**, 353 (1951).

[Har77] J.C. Hardy, L.C. Carraz, B. Jonson, and P.G. Hansen, Phys. Lett. B**71**, 307 (1977).

[Hil88] J.C. Hill, J.A. Winger, F.K. Wohn, R.L. Gill, A. Piotrowski, X. Ji, and B.H. Wildenthal, AIP Conf. Proc. **164**, 375 (American Institute of Physics, New York, 1988).

[Hof81] P. Hoff and B. Fogleberg, Nucl. Phys. **A368**, 210 (1981).

[Huc81] A. Huck, G. Klotz, A. Knipper, C. Miehé, C. Richard-Serre, and G. Walter, in *Proceedings of the* 4^{th} *International Conference on Nuclei Far from Stability*, Helsingor, Denmark, edited by P. G. Hansen and O. B. Nielsen, CERN Report No. 81-09 (1981), Vol. 2, p. 378.

[Huh98] M. Huhta, P. F. Mantica, D. W. Anthony, P. A. Lofy, J. I. Prisciandaro, R. M. Ronningen, M. Steiner, and W. B. Walters, Phys. Rev. C**58**, 3187 (1998).

[Ily09] S.V. Ilyushkin, J.A. Winger, C.J. Gross, K.P. Rykaczewski, J.C. Batchelder, L. Cartegni, I.G. Darby, C. Goodin, R. Grzywacz, J.H. Hamilton, A. Korgul, W. Królas, S.N. Liddick, C. Mazzocchi, S. Padgett, A. Piechaczek, M.M. Rajabali, D. Shapira, and E.F. Zganjar, Phys. Rev. C**80**, 054304 (2009).

[Ily11] S.V. Ilyushkin, J.A. Winger, K.P. Rykaczewski, C.J. Gross, J.C. Batchelder, L. Cartegni, I.G. Darby, R. Grzywacz, J.H. Hamilton, A. Korgul, W. Królas, S.N. Liddick, C. Mazzocchi, T. Mendez, S. Padgett, M.M. Rajabali, D. Shapira, D.W. Stracener, and E.F. Zganjar, Phys. Rev. C**83**, 014322 (2011).

[Jan07] R. V. F. Janssens, Nature **435**, 897 (2005).

[Ji89] X. Ji and B. H. Wildenthal, Phys. Rev. C**39**, 701 (1989).

[Kar08] M. Karny, K.P. Rykaczewski, R.K. Grzywacz, J.C. Batchelder, C.R. Bingham, C. Goodin, C.J. Gross, J.H. Hamilton, A. Korgul, W. Królas, S.N. Liddick, K. Li, K.H. Maier, C. Mazzocchi, A. Piechaczek, K. Rykaczewski, D. Schapira, D. Simpson, M.N. Tantawy, J.A. Winger, C.H. Yu, E.F. Zganjar, N. Nikolov, J. Dobaczewski, A.T. Kruppa, W. Nazarewicz, and M.V. Stoitsov, Phys. Lett. B**664**, 52 (2008).

[Klo72] G. Klotz, J. P. Gonidec, P. Baumann, and G. Walter, Nucl. Phys. **A197**, 229 (1972).

[Kra91] K.-L. Kratz, H. Gabelmann, P. Möller, B. Pfeiffer, H. L. Ravn, A.Wöhr, and the ISOLDE Collaboration, Z. Phys. A**340**, 419 (1991).

[Kra00] K.-L. Kratz, B. Pfeiffer, F.-K. Thielemann, and W. B. Walters, Hyperfine Interact. **129**, 185 (2000).

[Kra06] K.-L. Kratz in presentation at the *HRIBF Workshop – Nuclear Measurements for Astrophysics*, Oak Ridge, TN, October 23–24, 2006. Presentation available on-line at http://www.phy.ornl.gov/workshops/astrophys/.

[Kra07] K.-L. Kratz, K. Farouqi, and B. Pfeiffer, Prog. Nucl. Part. Phys. **59**, 147 (2007).

[Koe03] U. Köster, priv. comm., HRIBF Decay Spectroscopy Workshop, Oak Ridge, Aug. 2003 (unpublished).

[Leb09] M. Lebois, D. Verney, F. Ibrahim, S. Essabaa, F. Azaiez, M. Cheikh Mhamed, E. Cottereau, P. V. Cuong, M. Ferraton, K. Flanagan, S. Franchoo, D. Guillemaud-Mueller, F. Hammache, C. Lau, F. Le Blanc, J.-F. Le Du, J. Libert, B. Mouginot, C. Petrache, B. Roussière, L. Sagui, N. de Séréville, I. Stefan, and B. Tastet, Phys. Rev. C**80** 044308 (2009).

[Lew89] M. Lewitowicz, Yu. E. Penionzhkevich, A. G. Artukh, A. M. Kalinin, V. V. Kamanin, S. M. Luyanov, N. H. Chau, A. C. Mueller, D. Guillemaud-Mueller, R. Anne, D. Bazin, C. Détraz, D. Guerreau. M. G. Saint-Laurent, V. Borrel, J. C. Jacmart, F. Pougheon, A. Richard, and W. D. Schmidt-Ott, Nucl. Phys. **A496**, 477 (1989).

[Lin63] E. K. Lin, B. L. Cohen, Phys. Rev. **132**, 2632 (1963).

[Lis90] C. J. Lister, P. J. Ennis, A. A. Chishti, B. J. Varley, W. Gelletly, H. G. Price, and A. N. James, Phys. Rev. C**42**, R1191 (1990).

[Lis04] A. F. Lisetskiy, B. A. Brown, M. Horoi, and H. Grawe, Phys. Rev. C**70**, 044314 (2004).

[Lu13] F. Lu, Jenny Lee, M. B. Tsang, D. Bazin, D. Coupland, V. Henzl, D. Henzlova, M. Kilburn, W. G. Lynch, A. M. Rogers, A. Sanetullaev, Z. Y. Sun, M. Youngs, R. J. Charity, L. G. Sobotka, M. Famiano, S. Hudan, M. Horoi, and Y. L. Ye, Phys. Rev. C**88**, 017604 (2013).

[Lun80] E. Lund, P. Hoff, K. Aleklett, O. Glomset, and G. Rudstam, Z. Phys. A**294**, 233 (1980).

[Mah92] J. P. Maharana, Y. K. Gambhir, J. A. Sheikh, P. Ring, Phys. Rev. C**46**, R1163 (1992).

[Mar99] F. Maréchal, T. Suomijärvi, Y. Blumenfeld, A. Azhari, D. Bazin, J. A. Brown, P. D. Cottle, M. Fauerbach, T. Glasmacher, S. E. Hirzebruch, J. K. Jewell, J. H. Kelley, K. W. Kemper, P. F. Mantica, D. J. Morrissey, L. A. Riley, J. A. Scarpaci, H. Scheit, and M. Steiner, Phys. Rev. C**60**, 064623 (1999).

[Men10] D. Mengoni, J. J. Valiente-Dobón, A. Gadea, S. Lunardi, S. M. Lenzi, R. Broda, A. Dewald, T. Pissulla, L. J. Angus, S. Aydin, D. Bazzacco, G. Benzoni, P. G. Bizzeti, A. M. Bizzeti-Sona, P. Boutachkov, L. Corradi, F. Crespi, G. de Angelis, E. Farnea, E. Fioretto, A. Goergen, M. Gorska, A. Gottardo, E. Grodner, A. M. Howard, W. Królas, S. Leoni, P. Mason, D. Montanari, G. Montagnoli, D. R. Napoli, A. Obertelli, R. Orlandi, T. Pawłat, G. Pollarolo, F. Recchia, A. Algora, B. Rubio, E. Sahin, F. Scarlassara, R. Silvestri, J. F. Smith, A. M. Stefanini, D. Steppenbeck, S. Szilner, C. A. Ur, P. T. Wady, and J. Wrzesiński, Phys. Rev. C**82**, 024308 (2010).

[Mic06] S. Michimasa, S. Shimoura, H. Iwasaki, A. Tamaki, S. Ota, N. Aoi, H. Baba, N. Iwasa, S. Kanno, S. Kubono, K. Kurita, A. Kurokawa, T. Minemura, T. Motobayashi, M. Notani, H. J. Ong, A. Saito, H. Sakurai, E. Takeshita, S. Takeuchi, Y. Yanagisawa, A. Yoshida, Phys. Lett. B **638**, 146 (2006).

[Mih51] J. W. Mihelich, M. Goldhaber, and E. Wilson, Phys. Rev. **82**, 972 (1951).

[Mit52] A. C. G. Mitchell and A. B. Smith, Phys. Rev. **85**, 152 (1952).

[Mol97] P. Möller, J. R. Nix, and K. -L. Kratz, At. Data Nucl. Data Tables **66**, 131 (1997).

[Mor02] A. C. Morton, P. F. Mantica, B. A. Brown, A. D. Davies, D. E. Groh, P. T. Hosmer, S. N. Liddick, J. I. Prisciandaro, H. Schatz, M. Steiner, and A. Stolz, Phys. Lett. B**544**, 274 (2002).

[Mue93] A. Mueller and B. M. Sherrill, Ann. Rev. Nucl. Part. Sci. **43**, 529 (1993).

[Nuc10a] *Technology Roadmap, Nuclear Energy*, International Energy Agency, 2010 (http://www.iea.org/papers/2010/nuclear_roadmap.pdf).

[Nuc10b] *Nuclear Energy Research and Development Roadmap*, Report to Congress, U.S. Department of Energy, 2010 (http://www.ne.doe.gov/pdfFiles/NuclearEnergy_Roadmap_Final.pdf).

[Nuc10c] *ENERGY FOR THE FUTURE, The Nuclear Option*, a position paper of the European Physical Society, Nuclear Physics Division, 2010 (http://nuclear.epsdivisions.org/reports/eps-position-paper-energy-for-the-future)

[NNDC] ENDSF Database at the National Nuclear Data Center (http://www.nndc.bnl.gov).

[Num01] S. Nummela, P. Baumann, E. Caurier, P. Dessagne, A. Jokinen, A. Knipper, G. Le Scornet, C. Miehé, F. Nowacki, M. Oinonen, Z. Radivojevic, M. Ramdhane, G. Walter, and J. Äystö, Phys. Rev. C**63**, 044316 (2001).

[Oll03] J. Ollier, R. Chapman, X. Liang, M. Labiche, K.-M. Spohr, M. Davison, G. de Angelis, M. Axiotis, T. Kröll, D. R. Napoli, T. Martinez, D. Bazzacco, E. Farnea, S. Lunardi, and A. G. Smith, Phys. Rev. C**67**, 024302 (2003).

[Omt91] J.P. Omtvedt, P. Hoff, M. Hellström, L. Spanier, and B. Fogelberg, Z. Phys. A**338**, 241 (1991).

[Ots01] T. Otsuka, R. Fujimoto, Y. Utsuno, B. A. Brown, M. Honma, and T. Mizusaki, Phys. Rev. Lett. **87**, 082502 (2001).

[Ots05] T. Otsuka, T. Suzuki, R. Fujimoto, H. Grawe, and Y. Akaishi, Phys. Rev. Lett. **95**, 232502 (2005).

[Ots09] T. Otsuka, T. Suzuki, M. Honma, Y. Utsuno, N. Tsunoda, K. Tsukiyama, and M. Hjorth-Jensen, Phys. Rev. Lett. **104**, 012501 (2010).

[Ots10] T. Otsuka, T. Suzuki, M. Honma, Y. Utsuno, N. Tsunoda, K. Tsukiyama, and M. Hjorth-Jensen, Phys. Rev. Lett. **104**, 012501 (2010).

[Pat09] N. Patronis, H. De Witte, M. Gorska, M. Huyse, K. Kruglov, D. Pauwels, K. Van de Vel, P. Van Duppen, J. Van Roosbroeck, J. -C. Thomas, S. Franchoo, J. Cederkall, V. N. Fedoseyev, H. Fynbo, U. Georg, O. Jonsson, U. Köster, T. Materna, L. Mathieu, O. Serot, L. Weissman, W. F. Mueller, V. I. Mishin and D. Fedorov, Phys. Rev. C**80**, 034307 (2009).

[Per03] O. Perru, F. Ibrahim, O. Bajeat, C. Bourgeois, F. Clapier, E. Cottereau, C. Donzaud, M. Ducourtieux, S. Gales, D. Guillemaud-Mueller, C. Lau, H. Lefort, F. Le Blanc, A.C. Mueller, J. Obert, N. Pauwels, J.C. Potier, F. Pougheon, J. Proust, B. Roussiere, J. Sauvage, O. Sorlin, and D. Verney, Phys. Atomic Nuclei **66**, 1421 (2003).

[Per04] D. Verney, F. Ibrahim, O. Perru, O. Bajeat, C. Bourgeois, F. Clapier, E. Cottereau, C. Donzaud, S. Du, M. Ducourtieux, S. Essabaa, S. Gales, L. Gaudefroy, D. Guillemaud-Mueller, F. Hammache, F. Hosni, C. Lau, H. Lefort, F. Le Blanc, A.C. Mueller, N. Pauwels, J.C. Potier, F. Pougheon, J. Proust, B. Roussiere, J. Sauvage, and O. Sorlin, Braz. J. Phys. **34**, 979 (2004).

[Per06] O. Perru, D. Verney, F. Ibrahim, O. Bajeat, C. Bourgeois, F. Clapier, E. Cottereau, C. Donzaud, S. Du, M. Ducourtieux, S. Essabaa, S. Gales, D. Guillemaud-Mueller, O. Hubert, C. Lau, H. Lefort, F. Le Blanc, A.C. Mueller, J. Obert, N. Pauwels, J.C. Potier, F. Pougheon, J. Proust, B. Roussiere, J. Sauvage, and O. Sorlin, Eur. Phys. J. A**28**, 307 (2006).

[Pfe02] B. Pfeiffer, K.-L. Kratz, and P. Möller, Prog. Nucl. Energy, **41**, 39 (2002).

[Rah07] S. Rahaman, J. Hakala, V.-V. Elomaa, T. Eronen, U. Hager, A. Jokinen, A. Kankainen, I. D. Moore, H. Penttil, S. Rinta-Antila, J. Rissanen, A. Saastamoinen, C. Weber and J. Äystö, Eur. Phys. J. A**34**, 2007.

[Ree85] P. L. Reeder, R. A. Warner, R. M. Liebsch, R. L. Gill, A. Piotrowski, Phys. Rev. C**31**, 1029 (1985).

[Rei99] P.G. Reinhard, D.J. Dean, W. Nazarewicz, J. Dobaczewski, J.A. Maruhn, and M.R. Strayer, Phys. Rev. C**60**, 014316 (1999).

[Ret97] J. Retamosa, E. Caurier, F. Nowacki, and A. Poves, Phys. Rev. C**55**, 1266 (1997).

[Rud93] G. Rudstam, K. Aleklett, and L. Sihver, Atom. Data Nucl. Data Tab. **53**, 1 (1993).

[Run83] E. Runte, W.-D. Schmidt-Ott, P. Tidemand-Petersson, R. Kirchner, O. Klepper, W. Kurcewicz, E. Roeckl, N. Kaffrell, P. Peuser, K. Rykaczewski, M. Bernas, P. Dessagne, M. Langevin, Nucl. Phys. **A399**, 163 (1983).

[Run85] E. Runte, K. L. Gippert, W.-D. Schmidt-Ott, P. Tidemand-Petersson, L. Ziegeler, R. Kirchner, O. Klepper, P. O. Larsson, E. Roeckl, D. Schardt, N. Kaffrell, P. Peuser, M. Bernas, P. Dessagne, M. Langevin and K. Rykaczewski, Nucl. Phys. **A441**, 237 (1985).

[Ryd10] M. De Rydt, J. M. Daugas, F. de Oliveira Santos, L. Gaudefroy, S. Grévy, D. Kameda, V. Kumar, R. Lozeva, T. J. Mertzimekis, P. Morel, T. Nagatomo, G. Neyens, L. Perrot, O. Sorlin, C. Stödel, J. C. Thomas, N. Vermeulen, and P. Vingerhoets, Phys. Rev. **81**, 034308 (2010).

[Sar00] F. Sarazin, H. Savajols, W. Mittig, F. Nowacki, N. A. Orr, Z. Ren, P. Roussel-Chomaz, G. Auger, D. Baiborodin, A. V. Belozyorov, C. Borcea, E. Caurier, Z. Dlouhý, A. Gillibert, A. S. Lalleman, M. Lewitowicz, S. M. Lukyanov, R. de Oliveira, Y. E. Penionzhkevich, D. Ridikas, H. Sakuraï, O. Tarasov, and A. de Vismes, Phys. Rev. Lett. **84**, 5062 (2000).

[1] Sch96 H. Scheit, T. Glasmacher, B. A. Brown, J. A. Brown, P. D. Cottle, P. G. Hansen, R. Harkewicz, M. Hellstrom, R. W. Ibbotson, J. K. Jewell, K. W. Kemper, D. J. Morrissey, M. Steiner, P. Thirolf, and M. Thoennessen, Phys. Rev. Lett. **77**, 3967 (1996).

[Sch04] J. P. Schiffer, S. J. Freeman, J. A. Caggiano, C. Deibel, A. Heinz, C.-L. Jiang, R. Lewis, A. Parikh, P. D. Parker, K. E. Rehm, S. Sinha, and J. S. Thomas, Phys. Rev. Lett. **92**, 162501 (2004).

[Sha00] D. Shapira, T. A. Lewis, and L. D. Hulett, Nucl. Instr. Meth. Phys. Res. A **454**, 409 (2000).

[Sie10] K. Sieja and F. Nowacki, Phys. Rev. C**81**, 061303 (2010).

[Smi08] M. Smith, M. Brodeur, T. Brunner, S. Ettenauer, A. Lapierre, R. Ringle, V.L. Ryjkov, F. Ames, P. Bricault, G.W.F. Drake, P. Delheij, D. Lunney, F. Sarazin, and J. Dilling, Phys. Rev. Lett. **101**, 202501 (2008).

[Sor93] O. Sorlin, D. Guillemaud-Mueller, A. C. Mueller, V. Borrel, S. Dogny, F. Pougheon, K.-L. Kratz, H. Gabelmann, B. Pfeiffer, A. Wöhr, W. Ziegert, Yu. E. Penionzhkevich, S. M. Lukyanov, V. S. Salamatin, R. Anne, C. Borcea, L. K. Fifield, M. Lewitowicz, M. G. Saint-Laurent, D. Bazin, C. Détraz, F.-K. Thielemann, and W. Hillebrandt, Phys. Rev. C**47**, 2941 (1993).

[Sor95] O. Sorlin, D. Guillemaud-Mueller, R. Anne, L. Axelsson, D. Bazin, W. Böhmer, V. Borrel, Y. Jading, H. Keller, K. -L. Kratz, M. Lewitowicz, S. M. Lukyanov, T. Mehren, A. C. Mueller, Yu. E. Penionzhkevich, F. Pougheon, M. G. Saint-Laurent, V. S. Salamatin, S. Shoedder, A. Wöhr, Nucl. Phys. **A583**, 763 (1995).

[Sor04] O. Sorlin, Zs. Dombrádi, D. Sohler, F. Azaiez, J. Timár, Yu.-E. Penionzhkevich, F. Amorini, D. Baiborodin, A. Bauchet, F. Becker, M. Belleguic, C. Borcea, C. Bourgeois, Z. Dlouhy, C. Donzaud, J. Duprat, L. Gaudefroy, D. Guillemaud-Mueller, F. Ibrahim, M. J. Lopez, R. Lucas, S. M. Lukyanov, V. Maslov, J. Mrazek, C. Moore,

F. Nowacki, F. Pougheon, M. G. Saint-Laurent, F. Sarazin, J. A. Scarpaci, G. Sletten, M. Stanoiu, C. Stodel, M. Taylor, and Ch. Theisen, Eur. Phys. J. A**22**, 173 (2004).

[Str12] S. R. Stroberg, A. Gade, T. Baugher, D. Bazin, B. A. Brown, J. M. Cook, T. Glasmacher, G. F. Grinyer, S. McDaniel, A. Ratkiewicz, and D. Weisshaar, Phys. Rev. C**86**, 024321 (2012).

[Tan92] I. Tanihata, D.Hirata, T.Kobayashi, S.Shimoura, K.Sugimoto, and H.Toki, Phys. Lett. **B289**, 261 (1992).

[Tay75] H. W. Taylor, R. L. Schulte, P. J. Tivin, and H. Ing, Can. J. Phys. **53**, 107 (1975).

[Thi07] F.-K. Thielemann, C. Fröhlich, R. Hirschi, M. Liebendörfer, I. Dillmann, D. Mocelj, T. Rauscher, G. Martinez-Pinedo, K. Langanke, K. Farouqi, K.-L. Kratz, B. Pfeiffer, I. Panov, D. K. Nadyozhin, S. Blinnikov, E. Bravo, W. R. Hix, P. Höflich, and N. T. Zinner, Prog. Nucl. Part. Phys. **59** 74 (2007).

[Tho05] J. S. Thomas, D. W. Bardayan, J. C. Blackmon, J. A. Cizewski, U. Greife, C. J. Gross, M. S. Johnson, K. L. Jones, R. L. Kozub, J. F. Liang, R. J. Livesay, Z. Ma, B. H. Moazen, C. D. Nesaraja, D. Shapira, and M. S. Smith, Phys. Rev. C**71**, 021302 (2005).

[Tho07] J. S. Thomas, G. Arbanas, D. W. Bardayan, J. C. Blackmon, J. A. Cizewski, D. J. Dean, R. P. Fitzgerald, U. Greife, C. J. Gross, M. S. Johnson, K. L. Jones, R. L. Kozub, J. F. Liang, R. J. Livesay, Z. Ma, B. H. Moazen, C. D. Nesaraja, D. Shapira, M. S. Smith, and D. W. Visser, Phys. Rev. C**76**, 044302 (2007).

[Urb07] W. Urban, T. Rząca-Urban, J. L. Durell, A. G. Smith, and I. Ahmad, Phys. Rev. C**70**, 057308 (2007).

[Van05] J. Van Roosbroeck, H. De Witte, M. Gorska, M. Huyse, K. Kruglov, D. Pauwels, J.-Ch. Thomas, K. Van de Vel, P. Van Duppen, S. Franchoo, J. Cederkall, V. N. Fedoseyev, H. Fynbo, U. Georg, O. Jonsson, U. Köster, L. Weissman, W. F. Mueller, V. I. Mishin, D. Fedorov, A. De Maesschalck, N. A. Smirnova, and K. Heyde, Phys. Rev. C**71**, 054307 (2005).

[Van07] J. Van de Walle, F. Aksouh, F. Ames, T. Behrens, V. Bildstein, A. Blazhev, J. Cederkäll, E. Clément, T. E. Cocolios, T. Davinson, P. Delahaye, J. Eberth, A. Ekström, D. V. Fedorov, V. N. Fedosseev, L. M. Fraile, S. Franchoo, R. Gernhauser, G. Georgiev, D. Habs, K. Heyde, G. Huber, M. Huyse, F. Ibrahim, O. Ivanov, J. Iwanicki, J. Jolie, O. Kester, U. Köster, T. Kröll, R. Krücken, M. Lauer, A. F. Lisetskiy, R. Lutter, B. A. Marsh, P. Mayet, O. Niedermaier, T. Nilsson, M. Pantea, O. Perru, R. Raabe, P. Reiter, M. Sawicka, H. Scheit, G. Schrieder, D. Schwalm, M. D. Seliverstov, T. Sieber, G. Sletten, N. Smirnova, M. Stanoiu, I. Stefanescu, J.-C. Thomas, J. J. Valiente-Dobón, P. Van Duppen, D. Verney, D. Voulot, N. Warr, D. Weisshaar, F. Wenander, B. H. Wolf, and M. Zielińska, Phys. Rev. Lett. **99**, 142501 (2007).

[Ver07] D. Verney, F. Ibrahim, C. Bourgeois, S. Essabaa, S. Galès, L. Gaudefroy, D. Guillemaud-Mueller, F. Hammache, C. Lau, F. Le Blanc, A. C. Mueller, O. Perru, F. Pougheon, B. Roussière, J. Sauvage, and O. Sorlin, Phy. Rev C**76**, 054312 (2007).

[Vos81] B. Vosicki, T. Bjornstad, L. C. Carraz, J. Heinemeier, and H. L. Ravn, Nucl. Instrum. Methods **186**, 307 (1981).

[War86] R. A. Warner and P. L. Reeder, Radiat. Eff. **94**, 27 (1986).

[War89] E. K. Warburton and J. A. Becker, Phys. Rev. C**39**, 1535 (1989).

[War91] E. K. Warburton, Phys. Rev. C**44**, 268 (1991).

[War04] D. Warner, Nature **430**,517 (2004).

[Win88] J. A. Winger, J. C. Hill, F. K. Wohn, R. L. Gill, X. Ji, B. H. Wildenthal, Phys. Rev. C**38**, 285 (1988).

[Win89] J. A. Winger, J. C. Hill, F. K. Wohn, and D. S. Brenner, Phys. Rev. C**40**, 1061 (1989).

[Win90] J. A. Winger, J. C. Hill, F. K. Wohn, E. K. Warburton, R. L. Gill, A. Piotrowski, R. B. Schuhmann, and D. S. Brenner, Phys. Rev. C**42**, 954 (1990).

[Win98] J. A. Winger, H. H. Yousif, W. C. Ma, V. Ravikumar, W. Lui, S. K. Phillips, R. B. Piercey, P. F. Mantica, B. Pritychenko, R. M. Ronningen, and M. Steiner, in *Proceedings of the Second International Conference on Exotic Nuclei and Atomic Masses*, Bel Aire, MI (1998), B. M. Sherrill, D. J. Morrissey, C. N. Davids Eds. , AIP Conference Proceedings 455, AIP Press, New York, 606 (1998).

[Win01] J. A. Winger, P. F. Mantica, R. M. Ronningen, and M. A. Caprio, Phys. Rev. C**64**, 064318 (2001).

[Win06] J. A. Winger, P. F. Mantica, and R. M. Ronningen, Phys. Rev. C**73**, 044318 (2006).

[Win08] J.A. Winger, S.V. Ilyushkin, C.J. Gross, K.P. Rykaczewski, and D. Shapira, R. Grzywacz, S.N. Liddick, S. Padgett, and M.M. Rajabali, J.C. Batchelder, A. Korgul, W. Królas, C. Mazzocchi, A. Piechaczek and E.F. Zganjar, C. Goodin and J.H. Hamilton, in *Proceedings of the Fourth International Conference on Fission and Properties of Neutron-Rich Nuclei*, Sanibel Island, FL, USA, pp. 663 (2008).

[Win09] J.A. Winger, , S.V. Ilyushkin, K.P. Rykaczewski, C.J. Gross, J.C. Batchelder, C. Goodin, R. Grzywacz, J.H. Hamilton, A. Korgul, W. Królas, S.N. Liddick, C. Mazzocchi, S. Padgett, A. Piechaczek, M.M. Rajabali, D. Shapira, E.F. Zganjar, and I.N. Borzov, Phys. Rev. Lett. **102**, 142502 (2009).

[Win10] J. A. Winger, K. P. Rykaczewski, C. J. Gross, R. Grzywacz, J. C. Batchelder, C. Goodin, J. H. Hamilton, S. V. Ilyushkin, A. Korgul, W. Królas, S. N. Liddick, C. Mazzocchi, S. Padgett, A. Piechaczek, M. M. Rajabali, D. Shapira, E. F. Zganjar, and J. Dobaczewski, Phys. Rev. C**81**, 044303 (2010).

[Woo86] C. L. Woods, Nucl. Phys. **A451**, 413 (1986).

[WPEC] *Assessment of Fission Product Decay Data for Decay Heat Calulations: A report by the Working Party on International Evaluation Co-operation of the Nuclear Energy Agency Nuclear Science Committee*, Nuclear Science, NEA/WPEC-25, NEA No. 6284, (NEA OECD, Paris, 2007)
(http://www.oecd-nea.org/science/wpec/volume25/volume25.pdf).

[Yoh76] W. A. Yoh, S. E. Darden and S. Sen, Nucl. Phys. **A263**, 419 (1976).

[Zal08] M. Zalewski, J. Dobaczewski, W. Satula, and T.R. Werner, Phys. Rev. C**77**, 024316 (2008).

[Zie09] M. Zielińska, A. Görgen, E. Clément, J.-P. Delaroche, M. Girod, W. Korten, A. Bürger, W. Catford, C. Dossat, J. Iwanicki, J. Libert, J. Ljungvall, P. J. Napiorkowski, A. Obertelli, D. Piętak, R. Rodrguez-Guzmán, G. Sletten, J. Srebrny, Ch. Theisen, and K. Wrzosek, Phys. Rev. C**80**, 014317 (2009).

Appendix A

Acronyms

A1200	Projectile fragmentation separator at the NSCL prior to CCF upgrade
A1900	Projectile fragmentation separator at the NSCL after the CCF upgrade
ADN	α-Deuteron-Neutron Systematics
β_{eff}	β-particle detection efficiency
CARDS	Clarion Array for Radioactive Decay Spectroscopy
CCF	Coupled Cyclotron Facility at the NSCL
CERN	European Center for Nuclear Research in Geneva, Switzerland
DEP	Double Escape Peak observed in γ-ray spectra
DF3	Density Functional 3 interaction
GT	Gamow-Teller β-decay transition
GCM	Geometrical Collective Model
HFB	Hartree-Fock-Bogoliubov Method
HPGe	Hyper-Pure Ge detector for γ-ray spectroscopy
HRIBF	Holifield Radioactive Ion Beam Facility at Oak Ridge National Laboratory
IC	Ion Chamber detector
ISOL	Isotope Separation On-Line
ISOLDE	On-line isotope mass separator at CERN
LeRIBSS	Low-energy Radioactive Ion Beam Spectroscopy Station at the HRIBF
MCP	Multi-Channel Plate detector
MSU	Mississippi State University
MTAS	Modulated Total Absorption Spectrometer at the HRIBF
MTC	Moving Tape Collector
NSCL	National Superconducting Cyclotron Laboratory at Michigan State University
ORIC	Oak Ridge Isochronous Cyclotron
ORNL	Oak Ridge National Laboratory
PARRNe	ISOL system used by the ALTO facility at IPN-Orsay
P_β	Probability for β decay within the mass chain (P_β= 1 - $P_{\beta n}$)
$P_{\beta n}$	Probability for β-decay neutron emission
PID	Particle Identification
PT	Pass Through mode utilizing an IC at the HRIBF
Q_β	Ground state to ground state energy difference available for β decay
Q_{eff}	Effective Q value for feeding through a specific excited state

RO	Ranging Out method using selective separation in an IC at the HRIBF
SCALE	A comprehensive modeling and simulation suite for nuclear safety analysis and design
SEP	Single Escape Peak observed in γ-ray spectra
S_n	Neutron separation energy
SPE	Single-Particle Energy
TAS	Total Absorption Spectroscopy
UNIRIB	University Radioactive Ion Beam Consortium